

DSE - Advanced Wingsuit

Design a next generation wingsuit to improve the safety of flying while keeping the thrilling aspects of the sport

M.E.J. Beekman	1506676	K. van Giessen	4092384
B.L.K. Delrue	4001583	F. Hartvelt	1353942
N.T. Drenthe	4049977	Mazin Inaad Mohamed	1356909
J.M.P. Flick	1533916	J. Michielssen	4111877
T.F.L. Gheysens	4102932	V.L.J. Somers	4105885

Final Report

Design Synthesis Exercise

Table of contents

I	Problem statement	1
1	Introduction	2
2	Wingsuit basics	3
2.1	Wingsuit structure	3
2.2	Operating regime	3
2.3	Basic flight observations	3
3	Accidents	4
II	Research	6
4	Survey	7
4.1	Discipline	7
4.2	Experiences	7
4.3	Human	7
4.4	Safety	8
4.5	Gear	8
5	Wind tunnel Test	9
5.1	Assumptions	9
5.2	Construction and set-up	10
5.3	Test plan	11
5.4	Data analysis and test results	12
5.5	Test conclusions and recommendations	16
6	Analytical analysis	18
6.1	Know and quantify the basic aerodynamic aspects	18
6.2	Construct simple geometrical models of the wingsuit	22
6.3	Compute 2D aerodynamic properties of the geometrical models	23
6.4	Compute 3D aerodynamic properties of the geometrical models	28
6.5	Discussion of results	33
7	Numerical Analysis	35
7.1	Overview	35
7.2	Obtain 2D and 3D models of the wingsuit	36
7.3	Compute aerodynamic properties of the 2D models	37
7.4	Compute aerodynamic properties of the 3D models	37
7.5	Verify and validate the model	38
8	Performance	41
8.1	Flight characteristics	41
8.2	Flight envelope	42

III	Conclusions	43
9	Conclusions	44
9.1	Current wingsuit operation	44
9.2	Current wingsuit knowledge	44
9.3	Dangerous aspects and situations in wingsuiting	45
IV	Recommendations	46
10	Physics of Concepts	47
10.1	Anti-slip	47
10.2	Swiss pouch	47
10.3	Quick-release	49
10.4	Shoulder reinforcement	50
10.5	Turbulator and vortex generator	51
10.6	Passive flap & stall warning	53
10.7	Droop	56
10.8	Air tunnels & wing connection	57
10.9	Integrated GoPro	59
11	Aerodynamic Characteristics	61
11.1	Basic wingsuit	61
11.2	Vortex generators	61
11.3	Passive flap	61
11.4	Leading edge droop	62
11.5	Air tunnels & wing connection	63
11.6	Numerical concept analysis	70
12	Structural Characteristics	75
12.1	Inflatable cells	75
12.2	Shoulder reinforcement	75
12.3	Passive flap	77
12.4	Droop leading edge	79
13	Material Characteristics	80
13.1	Fabric	80
13.2	Foam	80
13.3	Aluminum	80
13.4	Carbon fiber-epoxy	81
13.5	Mylar	81
14	Stability & Control	82
14.1	Current wingsuits	82
14.2	Effects of concepts	82
15	Configuration / Layout	84
16	Sensitivity Analysis	85
16.1	Selection of main parameters	85
16.2	Sensitivity of the general improvements	85
16.3	Sensitivity analysis of safety concept specifics	86
16.4	Sensitivity analysis of wingsuit characteristics	86
17	Requirements Compliance Matrix and Feasibility Analysis	87
17.1	Compliance matrix	87
17.2	Feasibility analysis	87

18 Future research	91
18.1 Future project research	91
18.2 New project options	91
Appendices	
V Project Deliverables	i
A Project Log	ii
A.1 Project Plan	ii
A.2 Baseline Review	ii
A.3 Mid-Term Review	ii
A.4 Flying Squirrel concept	iii
B Functional Flow Diagram	v
C Functional Breakdown Structure	vii
D Resource Allocation	viii
D.1 Human resources	viii
D.2 Technical resources	ix
E Technical Risk Assessment	xi
E.1 Risks	xi
E.2 Risk map	xii
F Market Analysis and Product Introduction	xiii
F.1 Market analysis	xiii
F.2 Market scenarios	xvi
F.3 Production target and buildup strategy	xvi
G H/W - S/W block diagram	xvii
H Electrical block diagram	xviii
I Data Handling Block Diagram	xviii
J Manufacturing & Production	xviii
K Sustainable Development Strategy	xix
K.1 Sustainability of wingsuit design	xix
K.2 Sustainability of the advanced wingsuit design	xxi
L Project Design & Development Logic	xxii
M Project Gantt Chart	xxiii
N Cost Breakdown Structure	xxiv
N.1 Material cost	xxiv
N.2 Other direct cost	xxv
O Return On Investment	xxvi
O.1 Market data	xxvi
O.2 Cost and sales balances	xxvii
P Operations and Logistic Concept Description	xxviii
P.1 Operational concept description	xxviii
P.2 Logistic concept description	xxviii

Q RAMS	xxx
VI Results	xxxii
R Analytical Simulation - 2D results	xxxii
R.1 JavaFoil	xxxii
R.2 XFLR5	xxxiii
S Analytical Simulation - 3D results	xxxiv
S.1 JavaFoil	xxxiv
S.2 XFLR5	xxxv
S.3 Impact of droop concept	xxxvi
T Validation	xxxvii
U Numerical Analysis - Results	xxxix
U.1 Basic wingsuit - 2D results	xxxix
U.2 Basic wingsuit - 3D CFD results	xl
V Numerical verification	xlii
W MATLAB CODE	xliv
W.1 Shoulder reinforcement	xliv

Nomenclature

Symbol	Description
AL	Aluminum
AOA	Angle Of Attack
BOC	Bottom Of Container
CFD	Computational Fluid Dynamics
c.g.	Center of gravity
DSE	Design Synthesis Exercise
DOT	Design Option Tree
FBD	Free Body Diagram
FBS	Functional Breakdown Structure
FFD	Functional Flow Diagram
FR	Final Review
HR	Human Resources
H/W	HardWare
IMU	Inertial Measurement Unit
L/D	Lift over Drag ratio, or glide ratio
LLT	(nonlinear) Lifting Line Theory
MTBF	Mean Time Between Failures
MTR	Mid-term Review
OCD	Operational Concept Description
ODC	Other Direct Costs
OJF	Open Jet Facility
PAPI	Precision Approach Path Indicator
PC	Pilot Chute
PVC	Polyvinyl Chloride
ROI	Return On Investment
S/W	Software
SWOT	Strength Weakness Opportunity Threat
T.L.	Transition Lower
T.U.	Transition Upper
VG	Vortex Generator
VLM	Vortex Lattice Method
Vmin	Minimum velocity
WBS	Work Breakdown Structure
WFD	Work Flow Diagram

List of symbols

Symbol	Description	Unit
AR	Aspect Ratio	[-]
b	Span	[m]
C_{l_α}	$C_l - \alpha$ slope	$[\frac{1}{rad}]$
C_{L_α}	$C_L - \alpha$ slope	$[\frac{1}{rad}]$
C_l	Lift coefficient (2D)	[-]
C_L	Lift coefficient (3D)	[-]
C_d	Drag coefficient (2D)	[-]
C_D	Drag coefficient (3D)	[-]
C_{D_0}	Zero drag coefficient (3D)	[-]
C_y	Lift/y coefficient (2D)	[-]
c	Chord	[m]
D	Drag	[N]
F_y	Lift/y force (2D)	[N]
g	Gravitational constant	$9.81 [\frac{m}{s^2}]$
L	Lift	[N]
L_{char}	Characteristic length	[m]
P_a	Power available	$[\frac{N \cdot m}{s}]$
P_r	Power required	$[\frac{N \cdot m}{s}]$
S	Area	$[m^2]$
t	Time	[s]
T	Thrust	[N]
V	Velocity	$[\frac{m}{s}]$
\wedge	Sweep	[°]
W	Weight	[N]
α	Angle of attack	[°]
β	Prandtl-Glauert compressibility factor	[-]
γ	Flight path angle	[°]
δ	Deflection angle	[°]
θ	Pitch or attitude angle	[°]
η	Airfoil efficiency	[-]
ρ	Density	$[\frac{kg}{m^3}]$
μ	Dynamic viscosity	$[\frac{Ns}{m^2}]$

Acknowledgements

During the DSE, the group has received a lot of help from external people, who we would like to thank for their contribution.

A special thanks goes out to our tutor Ronald van Gent who inspired us to keep thinking outside the box and motivated us to pursue our ideas, especially when they seemed difficult to accomplish. Also his help in the wind tunnel and with the flight test are greatly appreciated. Furthermore, our coaches Theo Michelis and Ricardo Balbino Dos Santos Pereira were of great help when technical questions arose, which we could ask during their frequent visits, and the extra helping hands during the wind tunnel test and computational routines were very well appreciated.

At the beginning of the project, we had no experience in the field of wingsuit flying. The help from Coen van Disberg en Jarno Cordia has been tremendous. The willingness to answer all our questions, the possibility to borrow some suits and even the opportunity to place them in a wind tunnel has really helped us a lot. Also the input from the other wingsuiters who filled in the survey was valuable during the requirement analysis. During our contact with external clients, Jacco Hoekstra was of great assistance during the formal parts of this contact.

Last but not least we would like to thank the people who helped us during our wind tunnel experiment. Nando Timmer, who was critical about our test set-up, forced us to make sure that no one would get hurt. We thank him for the confidence to let us continue the experiment. We would also like to thank Leo Veldhuis and Marios Kotsonis for their pragmatic approach and their problem-solving attitude that made this experiment possible. Finally, we would like to thank Nico van Beek for operating the wind tunnel.

Preface

This is the final report of a Design Synthesis Exercise (DSE) at the Aerospace Engineering faculty of the Delft University of Technology. For the DSE, a group of ten students works for eleven weeks on a certain subject in the final weeks of their bachelor. This is the fourth and final report of the group developing an advanced wingsuit. The goal of this project is to reduce the fatalities of wingsuiting by inventing new concepts to improve the safety.

Prior knowledge of this report is established in the Project plan (the first report where the project is organized) the Baseline review (where the subject is researched and the requirements are defined) and the Midterm review. The Midterm report deals with the conceptual design of the advanced wingsuit. In this report the detail design of the advanced wingsuit is presented.

This project took place under the supervision of Ir. R.N.H.W. van Gent and two coaches Ir. R. B. Santos Pereira and Ir. T. Michelis.

Summary

This report is the fourth and last report and covers the worked out details of all the concepts on the ‘safety’ suit, which were mentioned in the mid-term report.

The one, the problem statement, explains the general ideas behind wingsuiting and its dangers. First, it is stated that a wingsuit is a special suit with extra surface between arms and legs, which makes it possible to generate lift whilst falling towards the earth. This can be done by jumping out of a plane, called skydiving, or by jumping from a high building, antenna, span (bridge) or earth (cliff). These are all part of BASE jumping. Second, it is discussed that the number of fatal accidents is increasing and is rather high: 13 fatalities in 2012 from the 4000 wingsuiters in total. These fatal accidents are mainly caused by not pulling the parachute or a collision of the wingsuiter with an external object.

At the moment, no basic information about the aerodynamic properties of wingsuits is known. Therefore the basic characteristics are obtained in this report. First, a survey is set up to get a better understanding of wingsuiting and its corresponding problems. This survey is filled in by 62 wingsuiters, of whom 21 are BASE wingsuiters. From this survey it was clear that the exit and parachute opening phase were the most dangerous phases. Dangerous situations also occurred by slipping at the exit, bad canopy deployment and due to poor pilot chute reachability. Furthermore empirical data is gathered from a test in the Open Jet Facility of the TU Delft, where two wingsuiters ‘fly’ a total of three suits at different angles of attack and different flow velocities up to $30m \cdot s^{-1}$. Tufts and smoke are used for visualization, and high-definition cameras are used to record all tests. At all angles of attack, reversed flow is visible behind the rig and at the outlet of the re-energizing tube of the leg wing. Disturbed flow is also found around the seams of the wingsuit which connect the separate lifting surfaces.

Next, the analytical calculations show that the Reynolds numbers for wingsuiting are within a range of $1.63 \cdot 10^6$ and $5.44 \cdot 10^6$. Five airfoil shapes are created and evaluated in 2D and 3D with JavaFoil and XFLR5 on, among others, the stall angle and $C_{l_{max}}$. Of these airfoils, airfoil 1 and airfoil 2 continued to the numerical analysis. In the numerical analysis they were evaluated in 2D. A 3D simulation was done with a CATIA model of a Vampire 4 wingsuit. Finally the programs were verified and validated using existing aerodynamic airfoil data.

From these parts, some conclusions can be drawn for a current wingsuit. When the conclusions are drawn, some solutions, concepts to increase the safety of a wingsuit, are designed. Some of the main concepts incorporated in the advanced wingsuit are: anti-slip soles for a safer exit, a quick-release system to release the arm wings for canopy flight and shoulder reinforcements to reduce loads on the wingsuiter during flight. To increase the aerodynamic performance and safety several concepts are added to cope with separation and delay stall. Vortex generators, droop, a passive flap and air tunnels delay stall and increase the angle of attack of the maximum C_L and thus enlarge the flight envelope. Also, a wing connection is incorporated to ensure simultaneous inflation during the exit phase and to prevent deflation of one of the arm wings during flight. Furthermore, to increase the safety of canopy opening, the Swiss pouch is chosen. In this canopy release system the pilot chute is stored at the wingtip such that the wingsuiter does not need to close his wings to pull the PC. Also, deployment is more likely to stay out of the burble. As an extra fun function for filming flights, the GoPro is integrated in the helmet. In the end, the concepts are combined with the aerodynamic knowledge, discovered during this project, in order to have the most optimal design.

Part I

Problem statement

1

Introduction

Similar to other stories about aviation, this story starts with the famous tale of Icarus. The Greek son of the master craftsman Daedalus dreamt of human flight and used feathers and wax to build his own set of wings; his own personal wingsuit. Ever since, men have tried to imitate bird flight with various constructions, some more successful than others.

The first recorded attempt of a construction similar to present wingsuits dates back to 1930, when Rex. G. Finney used a sailcloth between his legs to increase horizontal movement and maneuverability during skydiving [1]. After these jumps and tests, the wingsuits were further developed, but wingsuit flying kept an underground image, feared by many, but loved by skydivers who still felt nothing came closer to their long desired imitation of bird flight. During the 1990's the first wingsuits were created with a significant increase in stability and controllability, thereby enabling broader employment. Companies were set up and the community of wingsuit flyers grew. The first commercial company was founded in 1999 [2] and currently there are at least six companies [3][4][5] active in the wingsuit business. Nowadays the sport of wingsuit flying is certainly not underground anymore. The development of lightweight cameras accompanied by the possibility of worldwide distribution of the footage over Internet, has created a lot of publicity.

Sadly enough the tale of Icarus ended badly, but the ever prolonging desire of bird flight imitation still inspires many to push the boundaries of human ability.

This report will consist of four main parts. In the first part an introduction on the concept of wingsuiting, along with its associated risks and a problem definition will be provided. The second part will constitute an in depth analysis of wingsuit characteristics, consisting of an interview and survey among wingsuit flyers, a wind tunnel test, analytical and numerical models and a performance description. Part three is an overview of the most important conclusions about current wingsuits and their inherent shortcomings. Finally, in part four, the recommended concepts for the solutions to the problems mentioned in part three will be presented, along with their physical characteristics.

2

Wingsuit basics

To provide the reader with a starting point to better comprehend the subjects discussed in this report, this chapter will include a description of the basics of wingsuits and their operation.

2.1 Wingsuit structure

A wingsuit is a type of jumpsuit that is designed to make the user glide while falling. It is in essence a regular jumpsuit, with added fabric (wings) between the sleeves and trouser trunks, and between the two trouser trunks themselves. These extra pieces of fabric are hollow, and at high speed they are inflated by an inlet also known as a ram-air inlet. These inlets keep the wings pressurized, which makes them stiff when flying. This enables them to reach an aerodynamic shape and provide the wearer with a significant glide angle when airborne. The wingsuiter also wears a parachute, that is attached to the body with straps, similar to those used in a climbing harness, around the shoulders and legs. This parachute is not integrated into the wingsuit, but is a separate entity. The straps are fed through holes in the wingsuit so that they are exposed near the wearer's chest. This allows for easy access during flight. The parachute is deployed using a pilot chute, which is a small parachute stowed in a pouch on the underside of the parachute container. This pouch is fittingly called a Bottom of Container (BOC). The entire parachute system itself is also referred to as a "rig".

2.2 Operating regime

There are two ways to achieve the free fall necessary to operate a wingsuit:

- **Skydiving** Skydiving equates to jumping out of a flying aircraft at a high altitude in order to glide with the wingsuit, after which the parachute is deployed. After jumping, the suit is inflated quickly because of the high initial forward speed of the aircraft. Generally a smaller type of parachute is used in combination with an emergency chute to free the rig. The emergency chute has a pressure sensor built in, so it can deploy itself if the wearer becomes unconscious during flight.
- **BASE jumping** BASE is an acronym for "Buildings, Antennas, Spans and Earth", the latter referring to naturally high objects such as cliffs and mountaintops. A BASE jump is a jump with a parachute, performed from any one of these objects. The ascent is often done by hiking up. After the jump, the wingsuiter needs to gain sufficient speed to inflate the wingsuit. This is why inflation occurs later than during skydives. Therefore, wingsuits are almost exclusively flown from "Earth" objects, as these are high enough up to gain this speed necessary for inflation. Also, the parachute used in BASE jumping is larger than the one used for skydiving, and contains no reserve chute.

2.3 Basic flight observations

There are a number of basic observations to be made about the flight of a wingsuit. First of all, due to the low amount of attached flow on the back (top) of the wingsuit, a lower pressure region is formed there. In jargon, this is called a "burble".

There are also two different ways to perform a gliding flight in a wingsuit at maximum performance. Maximizing the ratio of speed forward to speed down, called the glide ratio, is one way. Maximizing the free fall time is another. Larger surface wingsuits tend to have a higher performance, but an even greater factor in performance flying are the abilities of the wingsuiter. A rough average for the glide ratio of a wingsuit is about 2.5 meters forward for 1 meter down, which constitutes a glide ratio of 2.5. To fly at lower performance, wingsuiters fold their wings backwards which results in a glide ratio of around 1.5.

3

Accidents

Besides the fun and the 'flying like a bird' feeling, there is a downside. There are significant risks associated with wingsuit flying and it is one of the sports with the highest fatality rates. Of the original 75 pioneers, also called Birdmen, 72 died while testing their new wingsuit designs [6]. Even since the further development of wingsuiting and founding of official wingsuiting companies selling today's more refined and 'safer' wingsuits, the fatality rate keeps increasing. Especially BASE wingsuiting is extremely dangerous and almost all wingsuit accidents are BASE related. Fatal accidents from wingsuit BASE jumps have increased from 3 accidents in 2002 to 13 in 2012 [7], see Figure 3.1. Moreover, since the start of this project three fatalities have been added to that list already. These casualty rates might seem small at first sight, however, their impact on the relatively small wingsuiting community, around 4000 people, is immense. Therefore in this project will be focused on BASE wingsuiting.

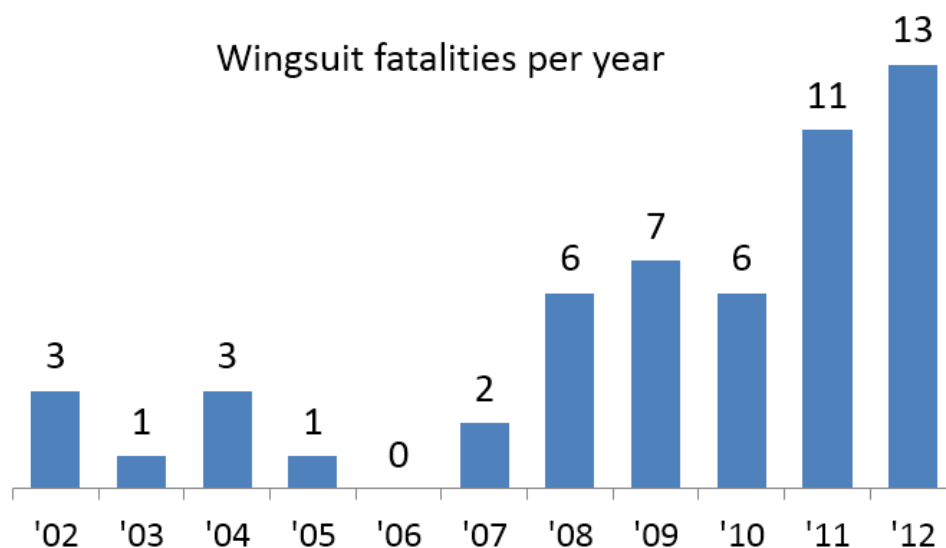


Figure 3.1: Wingsuit fatalities per year

So wingsuiting is extremely dangerous, but what exactly makes it so dangerous? What is the main cause of these fatalities? To be able to come up with an answer for this, the statistics of BASE fatal accidents are visualized in Figure 3.2 and an overview is given in Table 3.1 [8]. As can be seen no pull and strike of the body are the main causes of the accidents. But also small things as exit slip can be a cause. This emphasizes the fact that currently only one small coincidence or manoeuvre going wrong can be the difference between life and death.



Figure 3.2: BASE fatalities

Table 3.1: Cause of BASE fatalities

Cause of fatality	Percentage [%]
No Pull	38
Strike (Body)	30
Strike (Canopy)	9.5
Off-Heading Opening	8
Line Twist	8
Exit Slip	3
Drowning	3
Electrocution	0.5

Hence, wingsuiting is a sport with a high danger aspect and at the moment the realistic chance of accidents is part of the deal. However, the adrenaline kick, close resemblance to bird flying and extraordinary possibilities keep people inspiring to jump. Therefore, when tackling this problem and decreasing the number of fatalities, the fun aspect is not allowed to fall in name of safety. Therefore the following mission statement was defined:

“Design a next generation wingsuit to improve the safety of flying while keeping the thrilling aspects of the sport.”

Part II
Research

4

Survey

For the Design Synthesis Exercise 'Design of a Next Generation Wingsuit', a survey [9] has been held. This survey has been set up to get into contact with wingsuiters and obtain the necessary practical knowledge about the operation and corresponding safety issues.

The survey has been placed on dropzone.com, a popular forum for wingsuiters, and has been sent directly to a few wingsuiters the group already had contact with. The survey covers five question categories: Discipline, Experiences, Human, Safety and Gear.

The survey has been filled in by 62 wingsuiters, both from skydiving and BASE. This large response made it possible to exclude the skydiving responses since the focus of this project has been on BASE wingsuiting. The contact information of the participants is known by the project group but will not be shared with third parties.

Below the most important conclusions of the survey are presented.

4.1 Discipline

The questions in this section are based on the discipline of the wingsuiters and the number of flights they have performed so far.

From the wingsuiters who filled in the survey, 21 of them are BASE wingsuiters. Since BASE wingsuiting is the main objective of the project, only these results were used. Furthermore, it could be seen that the wingsuiters who filled in the survey were experienced jumpers since they made 220 BASE wingsuit jumps on average.

4.2 Experiences

The experiences section was set up to get a better idea of the dangers in BASE wingsuiting. This is done by asking whether they have already witnessed or been into a wingsuit accident and to describe the situation.

From the results it was seen that around 70% of the wingsuiters has already witnessed or been into a wingsuit accident. These accidents were both due to human errors and the current wingsuit design. One of the aspects of the current wingsuit design which causes some accidents is the large wing surface. This large wing surface creates a burble behind the wingsuiter, makes it difficult to grab the pilot chute and it takes more time to inflate. Furthermore, the pilot chute is located on a difficult location since it takes a while to grab the chute and bring it into the free stream while both wings are closed. Finally the wingsuiters explained that it is easy to get into a spin when performing radical maneuvers or after an unstable exit.

4.3 Human

The human part of the survey was based on the human experiences when flying a wingsuit. This means that the questions were based on the forces needed to fly a wingsuit and how comfortable a wingsuit is during flight.

From the survey results, it was seen that the force needed to fly a wingsuit depends on the line the wingsuiter wants to fly. This means that the force is high when the wingsuiter wants to fly at high performance for the whole flight but the forces are easy to handle if maximum performance is not needed for a certain line. Furthermore it was stated that a wingsuiter is exhausted after performing eight wingsuit jumps a day.

4.4 Safety

The safety section focuses on the most dangerous phases of a wingsuit flight and what makes these phases so dangerous.

From the survey it could be easily seen that the exit phase and the parachute deployment phase were most dangerous. The most dangerous aspects of the exit phase are slipping away before jumping, unstable exit jump and an asymmetric wing inflation which causes a spin. The second most dangerous phase is the moment when the parachute opens. First a line twist was stated as a big problem. Next it could be seen that it was hard to reach for the pilot chute since the large wings could cover the boc. Finally, the burble was said to be a big problem since the parachute could stay in the burble. When this happens the parachute is not able to deploy.

4.5 Gear

In the last section the gear of a wingsuit is treated. In this section the questions posed were about the weight of a wingsuit, the current deployment system and the opportunities of using fixed structures in wingsuits.

From these results it was seen that the weight of a wingsuit was not a problem for current wingsuiters. Furthermore it was seen that all the wingsuiters wanted zippers for rigging their wingsuit while a quarter of the wingsuiters would not be interested in using a different deployment system for landing. Finally it was seen that most wingsuiters, 80%, think a rigid structure would not eliminate the benefits of wingsuiting.

5

Wind tunnel Test

One of the options to reduce the knowledge gap is to use the Open Jet facility (OJF) for a flow visualization experiment. During this test the airflow of a flying wingsuit can be visualized. In this chapter the wind tunnel test is described, results are discussed and a conclusion is drawn.

5.1 Assumptions

Since a wind tunnel does not represent real life situations several assumptions are made and different corrections need to be taken into account. But since this is a qualitative experiment the influence of these effects can not be taken into account to correct the obtained quantitative results. However, with these stated assumptions in mind, the results are interpreted more critically.

Boundary layer interaction

Boundary layer interaction is caused by the boundary layer of the platform on which the construction is built. This boundary layer interacts with the wingsuit and can thus influence the flow around the wingsuit.

Turbulence intensity

The amount of turbulence in the wind tunnel will not be exactly the same as in a real free-fall situation.

Construction interaction

The construction that is built to sustain the wingsuiter interacts a lot with the flow. Also, because of the asymmetry of the construction (the pole used for camera mounting), the flow on the right wing will be different than the flow on the left wing.

Buoyancy

Buoyancy is an additional drag force that results from a decrease in static pressure along the test section due to the boundary layer at the walls, this influences the freestream velocity and the measurements of the pitot tube, since the pitot tube is mounted on the side wall of the tunnel.[10]

Non-uniform velocity field

The OJF has a squared cross-section of 8.12 m^2 , the flow that comes out of the wind tunnel is however not uniform, both the direction and the velocity of the incoming air may vary throughout the cross-section. It may be possible that the flow at the sides is slower than in the middle of the cross-section, due to boundary interaction.

Steady flow conditions

Two other deviations from reality are the unsteadiness of the flow in real life and the occurrence of side winds. In real flight, wingsuits do not fly steady most of the time, especially during BASE jumping. In the wind tunnel, no side winds are present.

Solid blockage

As final deviation, solid blockage has to be taken into account. Since the wingsuit is fixed above the table, the area between the wingsuiter and the table will be acting like a contraction. This phenomenon will result in an increased pressure and reduced airspeed or an increased airspeed and reduced air pressure below the wingsuiter. This effect has to be taken into account when analyzing the flow over the wingsuit.

During the wind tunnel test the Reynolds number varies between approximately $2.44 \cdot 10^6$ and $3.18 \cdot 10^6$. During normal flight the Reynolds number varies between $1.63 \cdot 10^6$ and $5.44 \cdot 10^6$, which is calculated in Chapter 6. When comparing both situations one can see that the wind tunnel Reynolds numbers are within the region of the real Reynolds numbers. Since there is not a large difference, it can be assumed that the Reynolds numbers from the wind tunnel test do not have to be scaled.

5.2 Construction and set-up

The construction for the wind tunnel, as can be seen in Figure 5.1, consists of a frame constructed on a platform. The rear of the frame is sturdily supported by the construction while giving the frame the freedom to hinge around this point. The front of the frame is connected to the frame of the wind tunnel outlet with cords. By varying the tension in the cord the angle of attack can be adjusted. The pilot can now lie down on the frame with his knees just below the rear end of the frame such that the leg inlet will not be blocked by the construction. He is fixed to the frame at the front of the frame and fixed to the platform with the aid of parachute lines. At the rear end of the construction an extra bar is attached as a camera mount. Two other cameras are also mounted in different locations, but cannot be seen in Figure 5.1. Next to these mounted cameras a couple of handheld cameras are used as well to capture as much as possible of the wind tunnel test.



Figure 5.1: The structure used during the wind tunnel testing

As preparation for the wingsuit, tufts are attached to them the day before the wind tunnel test. The positioning of the tufts can be seen in Figure 5.2. Two different wingsuits are used for the tests; the Phantom 3 wingsuit (seen on the left), which is a beginner/intermediate suit, and the Vampire 5 prototype wingsuit (seen on the right) which is a more expert level wingsuit. Also, the Viper wingsuit was used for extra flow visualization.



Figure 5.2: The wingsuit with tufts

5.3 Test plan

A combination of tufts and a smoke probe are used to see how the airflow behaves around the wingsuit. Three wingsuits are used both with and without a rig. A small number of angles of attack are tested with differing wingsuits by manufacturer Phoenix-Fly, and varying wingsuit configurations. The tests are summarized in Table 5.1

Table 5.1: Summary of the 6 different tests conducted in the wind tunnel

Nr.	Angle of Attack[°]	Tufts	Smoke	Wingsuit	Miscellaneous
1	low	✗	✗	Vampire 5	Feasibility test with Jarno
2	20	✓	✓	Vampire 5	Jarno with parachute rig attached
3	21	✓	✓	Vampire 5	Jarno with parachute rig attached
4	24	✓	✓	Vampire 5	Jarno without parachute rig
5	27	✓	✓	Phantom 3	Coen with parachute rig attached
6	24	✗	✗	Viper	Conclusion test

Before starting the tests the angles of attack can be pre-determined. This is done using basic trigonometry as shown in Figure 5.3. Since the height of the front part of the construction is variable, the angle of attack can be calculated quite easily.

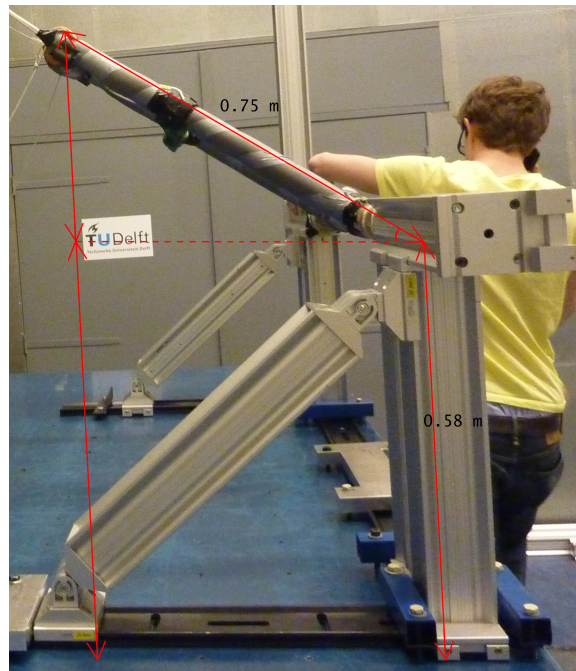


Figure 5.3: Pre-determining the angle of attack

5.4 Data analysis and test results

Since only qualitative data is obtained from the experiment, the analysis of the data is done by looking into all the footage of the cameras for every test. Using this footage different sketches of the flow patterns are made and the results can be seen in Figures 5.5 - 5.7. Since the flow patterns do not vary much between the different tests, only two sketches for the Vampire 5 and one sketch for the Phantom 3 are made. From the footage two main flows can be discerned, attached flow and separated flow. The attached flow is represented by the green lines while the separated flow is represented by the red lines.

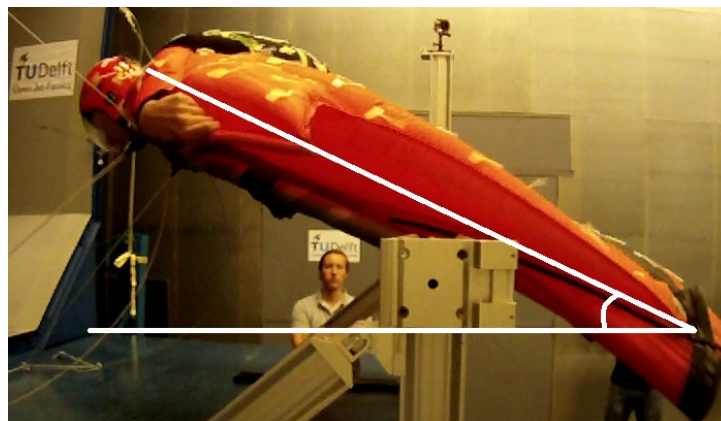


Figure 5.4: Angle of attack during the wind tunnel testing

One of the main issues when analyzing the data is the determination of the angle of attack. The angle of attack varies along the span of the wingsuit and since the human body is not entirely rigid over time, the angle of attack also varies with time. Before starting the tests the angles of attack are calculated as mentioned earlier. After the tests, the angle of attack is checked using snapshots of the footage and this is compared to the initial calculated value. A snapshot of how this is done is shown in Figure 5.4. With the help of this figure, it can be determined that in this case the angle of attack is approximately 24° .

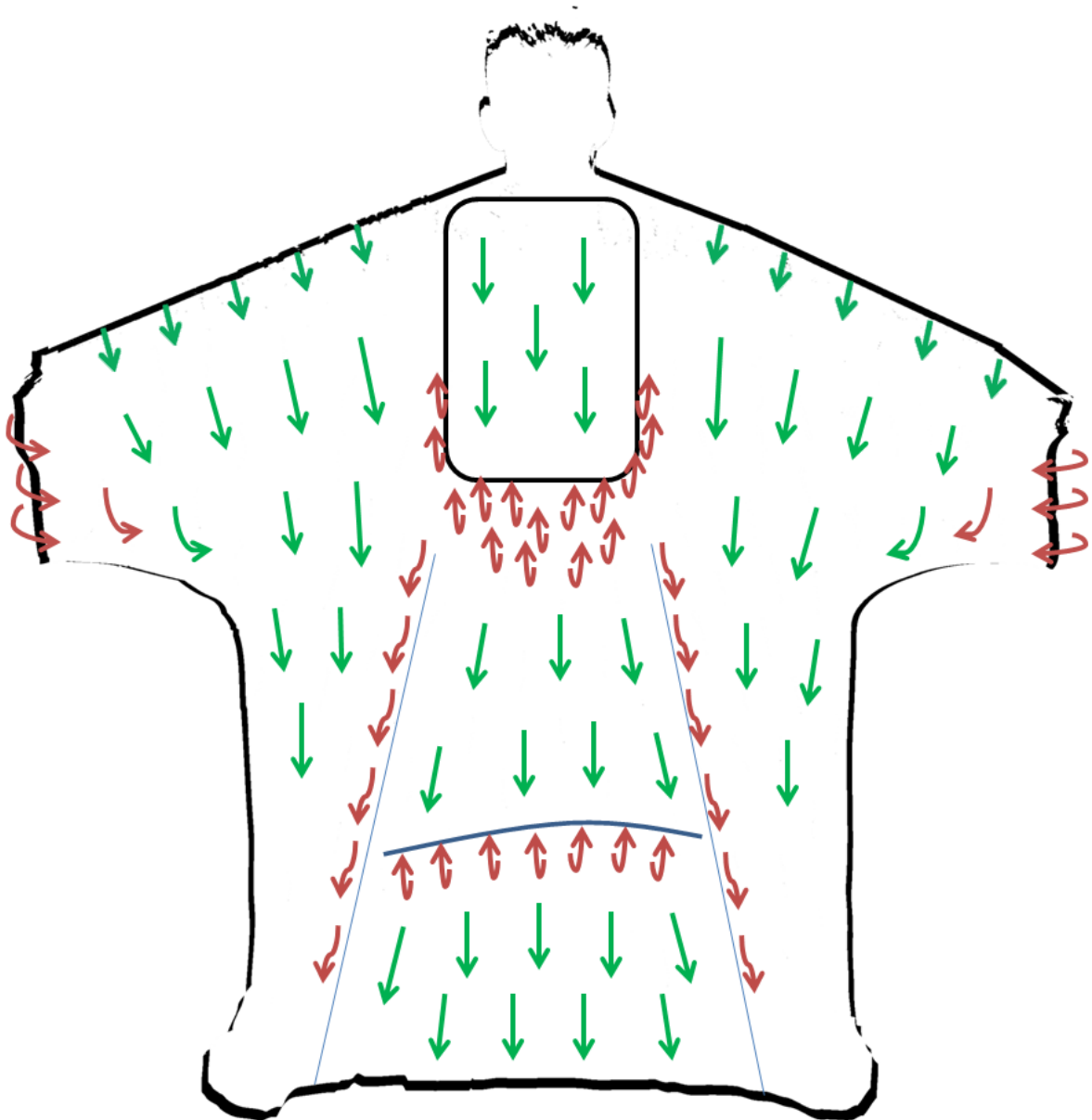


Figure 5.5: Flow pattern on the Vampire 5 wingsuit at an angle of attack of 24° .

In Figure 5.5, the flow is laminar at the leading edge and becomes turbulent immediately after the leading edge. Tip vortices and cross flow are present on the arm wings. As can be seen, the main cause of separation is the rig with the parachute attached. Also the seams between the different inflated parts of the suit causes a very disturbed flow. Another point of attention is the part of the leg wing where the hole is located. Despite the hole in the suit, immediately after the opening, reversed flow occurs. During the test, the wingtips are very prone to separation, depending on the posture and attitude of the wingsuiter.

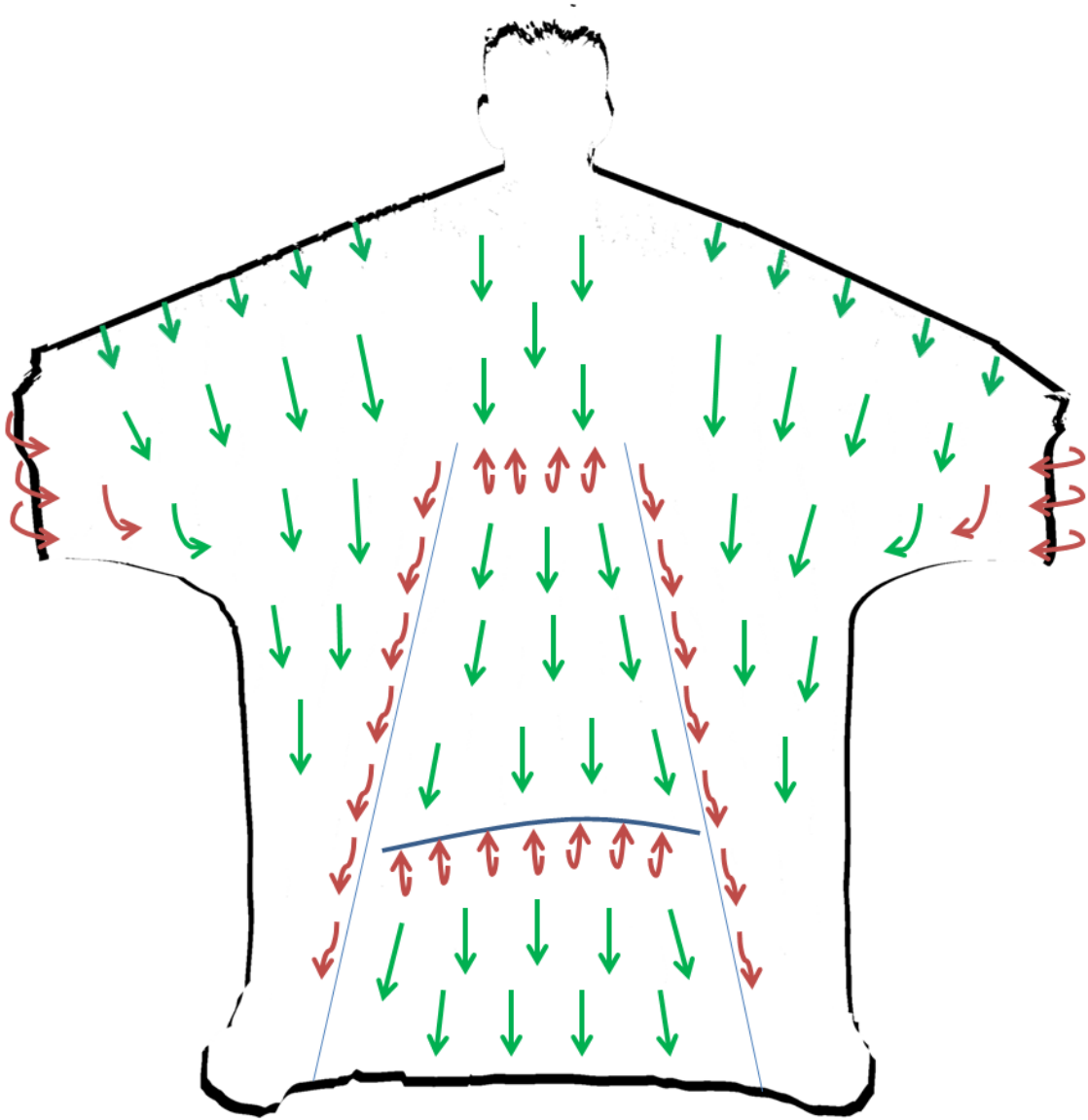


Figure 5.6: Flow pattern on the Vampire 5 wingsuit without parachute at an angle of attack of 24° .

Figure 5.6 shows exactly the same situation as Figure 5.5, but the parachute has been detached from the rig. It is quite obvious that there is a major improvement in the airflow on the back. There is however still some separation along the seams and on the back due to irregularities.

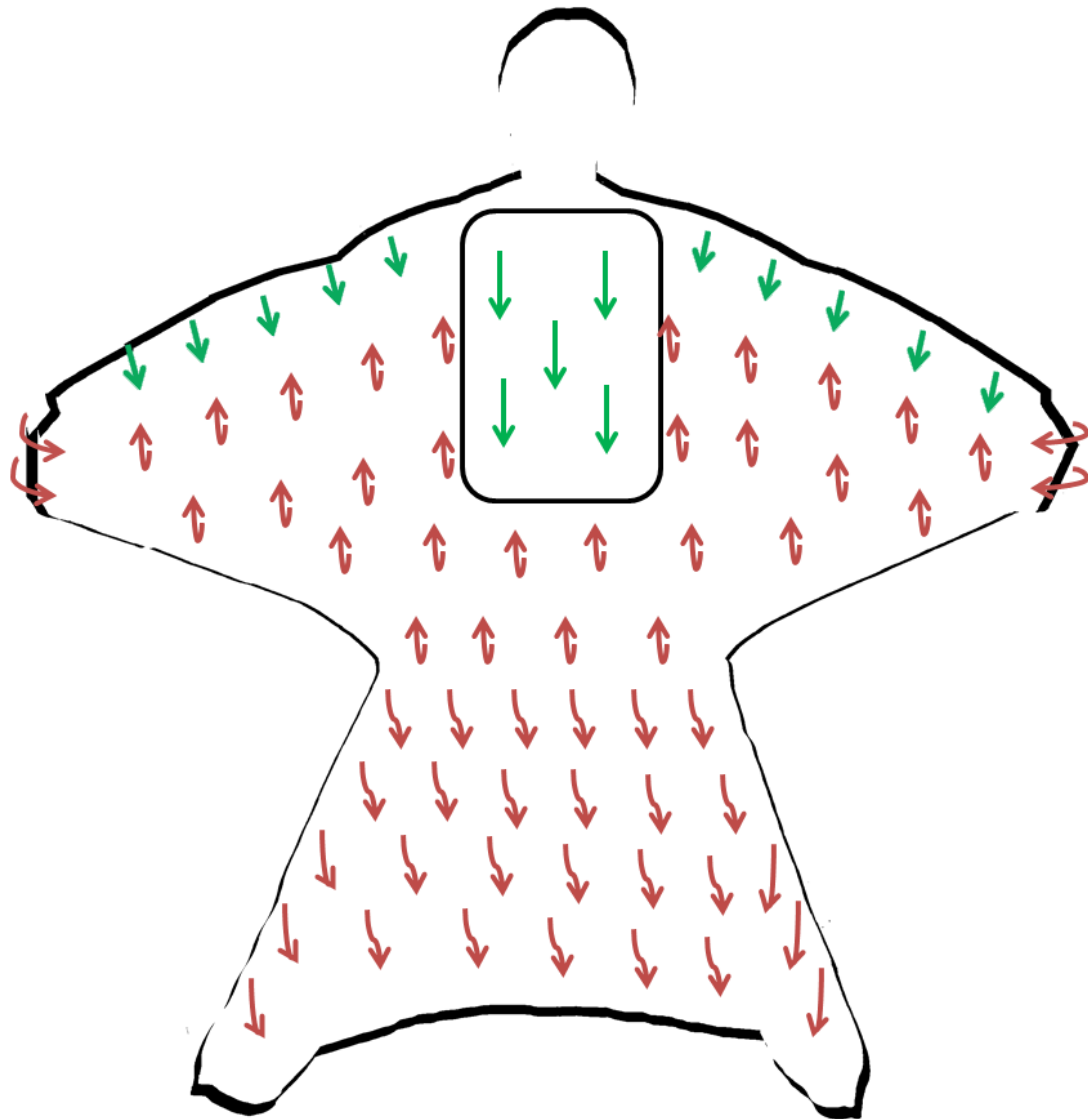


Figure 5.7: Flow pattern on the Phantom 3 wingsuit at an angle of attack of 27° .

Figure 5.7 shows the flow pattern on the Phantom 3 wingsuit, which has a worse performance than the Vampire 5 wingsuit. The Phantom 3 has a lot of separated flow on the arm wings and behind the parachute. The airflow over the leg wing is also detached. It should be stressed that the Phantom 3 was tested at an angle of attack of 27° and that this might also be a reason for the worse results.

During the analysis of the data, an important discovery was made about the leading edge and its influence on the flow. At high speeds the leading edge is indented and does not have its intended shape. Due to this phenomenon, a second leading edge is created which results in leading edge separation and thus a more separated flow over the wings. The effect of a bad leading edge on the airflow can be seen in Figure 5.8.

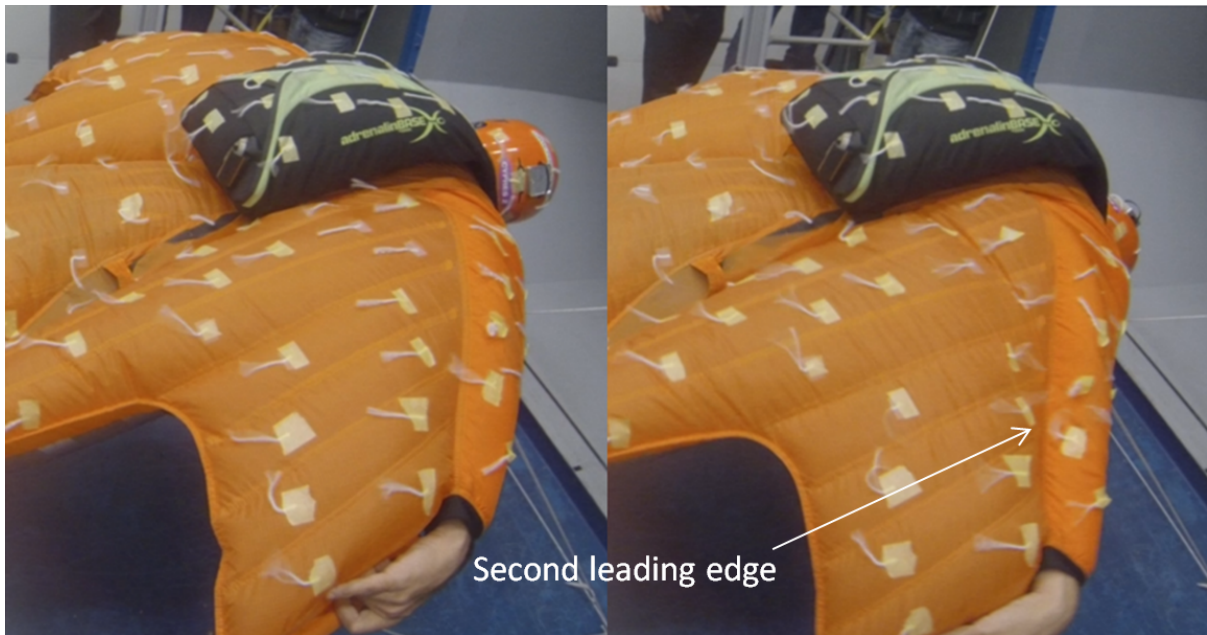


Figure 5.8: Flow pattern with a smooth leading edge compared to a second leading edge

Figure 5.9 shows the Viper wingsuit in the wind tunnel. Since this is a new wingsuit, no tufts are attached to it and as a result, the flow cannot be evaluated. Nevertheless, it can be seen that the Viper also has a dented, or double leading edge. Due to this it can be concluded that the flow near the second leading edge will be separated as was the case in Figure 5.8.



Figure 5.9: Leading edge of the Viper at an angle of attack of 24° .

5.5 Test conclusions and recommendations

The most important conclusion of the experiment is the large influence of the body positioning of the wingsuiter. By changing the position of the arms, core or legs, the wingsuiter can easily decrease the aerodynamic performance of his wingsuit without knowing. Another major factor for the flow pattern is the shape of the leading edge. Because this leading edge consists of very soft foam it is often dented into a bad shape. This causes very early separation of the flow and surely needs to be avoided in any

wingsuit design. The tip vortices at the arm wings are clearly visible. This suggests that the positioning and the shape of the pilot's hands is important to consider in any detailed design. Another conclusion about the wing tips is that they are very prone to separation and the airflow can only remain attached if the wingsuiter flies with an optimal arm positioning. As expected, a lot of separated flow were seen in the region behind and beside the parachute. Without the parachute, the separation was reduced a lot. There was still some separation, but this is due to the fact that the wingsuits are not designed to fly without a parachute. At the start of the lower leg wing, there is an inlet in the suit where flow can travel from under the suit to the upper side. This should energize the flow and delay separation on the leg wing. Since the airflow over the lower leg wing did not separate, this method could be a working principle. However, the area right after the hole has reversed flow. This is most likely caused by leading edge stall on the leg wing. This can be seen in Figure 5.10. After the leading edge stall, the airflow attaches again to the surface. The influence of the flow that comes from the upper surface of the upper leg wing could contribute to the reattachment.

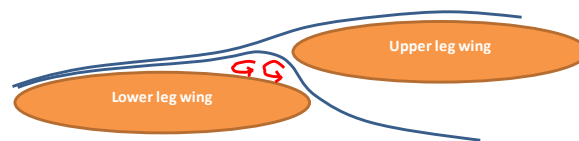


Figure 5.10: Flow pattern in the proximity of the hole in the wingsuit

From the wind tunnel test two conclusions can be drawn and recommendations for the detailed design can be made. First the bad leading edge can be seen as an important aspect to look at. Since the performance foam is one of the concepts which are implemented into the final design, the bad leading edge can be solved by adjusting this concept. A stiffer material and a larger performance foam area can already be the solution to this problem. Secondly it can be concluded that the backpack should be changed to increase the aerodynamic performance over the back of the wingsuiter. This problem can be solved by connecting the edges of the backpack to the wingsuit, resulting in a smooth transition from backpack to suit.

6

Analytical analysis

In order to get a basic understanding of the aerodynamic properties of a wingsuit, an analytical analysis is performed. Hereby, the lift and drag coefficients of a 2D and 3D wingsuit model, which represents the Vampire 5 from Phoenix Fly, are calculated. Finally, the results will be used to verify the numerical model. In this chapter, the analytical method and results are showed in the following five sections:

6.1: Know and quantify the basic aerodynamic aspects

- Reynolds number
- Angle of attack range
- Reference wing

6.2: Construct simple geometrical models of the wingsuit

- Shape of the airfoils
- Position of the airfoils
- Size of the airfoils

6.3: Compute 2D aerodynamic properties of the geometrical models

- Calculation methods
- Lift and drag coefficients of simplified models

6.4: Compute 3D aerodynamic properties of the geometrical models

- Calculation methods
- Lift and drag coefficients of simplified models

6.5: Discussion of results

- Validation of calculation methods
- Conclusion and recommendations

6.1 Know and quantify the basic aerodynamic aspects

In order to construct a basic model of a wingsuit, the aerodynamic properties of the flow need to be known. The Reynolds number and angle of attack range are important parameters.

Reynolds number

The Reynolds number is a similarity parameter which enables the comparison of flow fields between two different operation environments.[11] The Reynolds number gives the ratio between the inertial force and the viscous force:

$$Re = \frac{\text{Inertial force}}{\text{Viscous force}} \quad (6.1)$$

Using the momentum equation this can be rewritten as:

$$Re = \frac{\rho \cdot v \cdot L_{char}}{\mu} \quad (6.2)$$

Both the density and the dynamic viscosity depend on the flight altitude as with higher altitude the density and dynamic viscosity decrease. Altitudes from 1000[m] (typical canopy deployment) until 4000[m] (typical exit height)[12] have been used in combination with a speed range of 100 - 200km · h⁻¹, or 27.78 - 55.55m · s⁻¹. For the characteristic length, the wingsuit is considered to be a single flying wing with taper, as can be seen in Figure 6.1 . The characteristic length is then chosen to be the chord of the airfoil, which is 1.15m at the tip and 1.50m at the root. The Reynolds tool from [11] then produces the corresponding Reynolds numbers for standard atmospheric conditions.

Minimum Reynolds number: 1.63·10⁶ (h=4000m, v=27.78m · s⁻¹, l=1.15m)

Maximum Reynolds number: 5.44·10⁶ (h=1000m, v=55.55m · s⁻¹, l=1.50m)

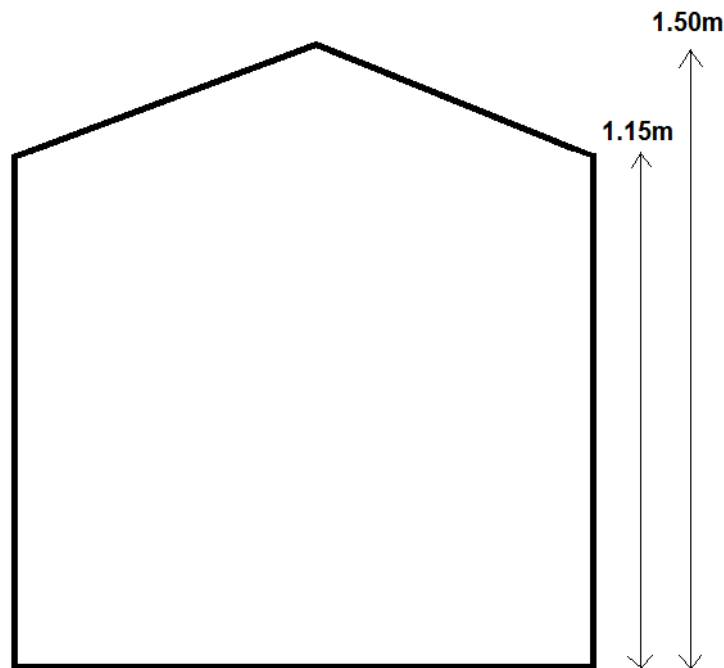


Figure 6.1: Single flying wing with taper

Angle of attack range

Wingsuits are operated at high angles of attack, with respect to the inflow, mostly higher than 20°[13]. The measurements from [13] show a linear relation between the angle of attack and the lift coefficient until approximately 18°, which shows that stall has not yet occurred. A wind tunnel test has been performed with a 6ft wingsuiter model [14][14] which shows a linear regression that even stretches until 32°. Although these references give no definite answer to the question what angles of attacks are used in actual operation, the approximation of a range from 20° until 40° seems justified.

6.1.1 Create a reference wing as a baseline for the calculations

In order to have an idea about the maximum performance of a wingsuit, a reference wing is created. This reference wing consists of a single airfoil which would be the ideal situation for a wingsuiter. Since this situation is ideal, the reference wing properties can be set to be the upper limits of a wingsuit.

To create a reference wing, first some parameters of the wingsuiter have to be determined. These parameters are the thickness, camber and chord of the airfoil and the span of the wing. To keep the model simple, the airfoil chosen was one of the basic NACA 4-series. The sizes of an average human

American male, from CATIA, were used to further define the parameters. This American male is chosen since 1.7[m] is around the average length of a man over the world.

Dimensions

To make sure that every calculation is done using the same lengths, the dimensions of the average human American male, from CATIA, are used. In Figure 6.2 all the dimensions of this person are shown. It has to be taken into account when using the dimensions that these lengths are from a person who is standing straight. When a person is wingsuiting his total height is 10cm lower since he opens his legs. This results in a total height (from shoulder to toe) of 1339mm.

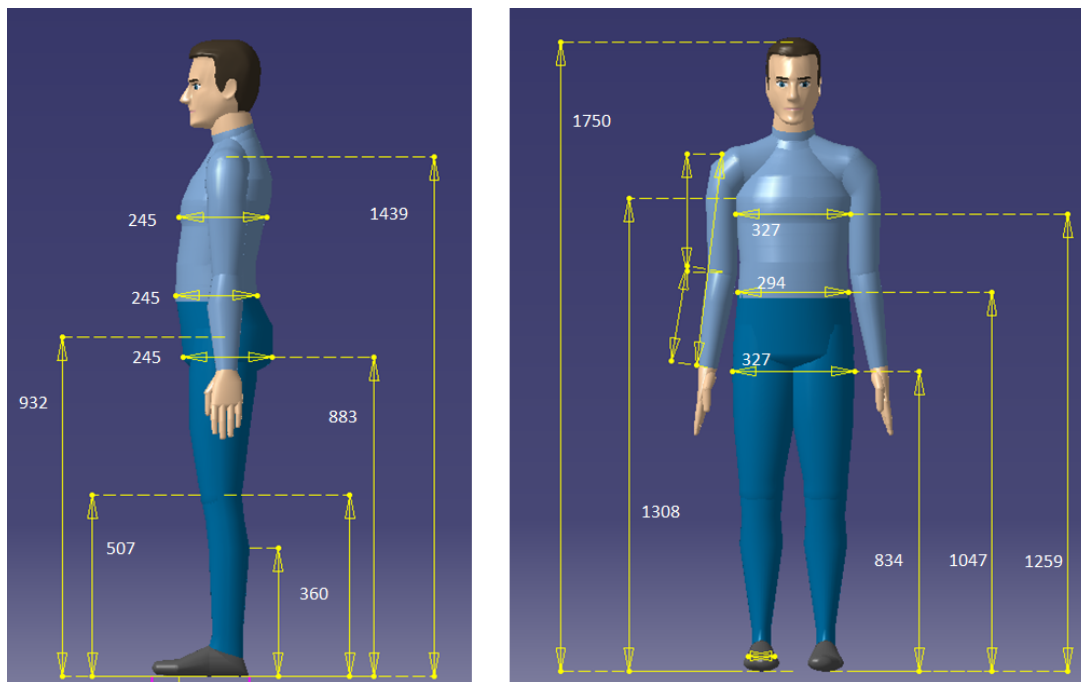


Figure 6.2: Dimensions of the human American male CATIA person in millimeter

Thickness of the airfoil

Based on photos from the wind tunnel tests, the thickest part of the wing of the Vampire 5 was estimated to be at the chest of the wingsuiter. The NACA 4 series has its thickest point at 30% from the leading edge[15]. An average American male has a chest depth of 243.2mm, the maximum chest depth is measured to be at 200mm from the top of his shoulders.

$$x/c \text{ of the chest} = \frac{200}{1339} = 14.9\%$$

$$t/c \text{ of the chest} = \frac{243.2}{1339} = 18.2\%$$

With these data points a NACA 0020 airfoil was found to have the correct thickness (Figure 6.3).

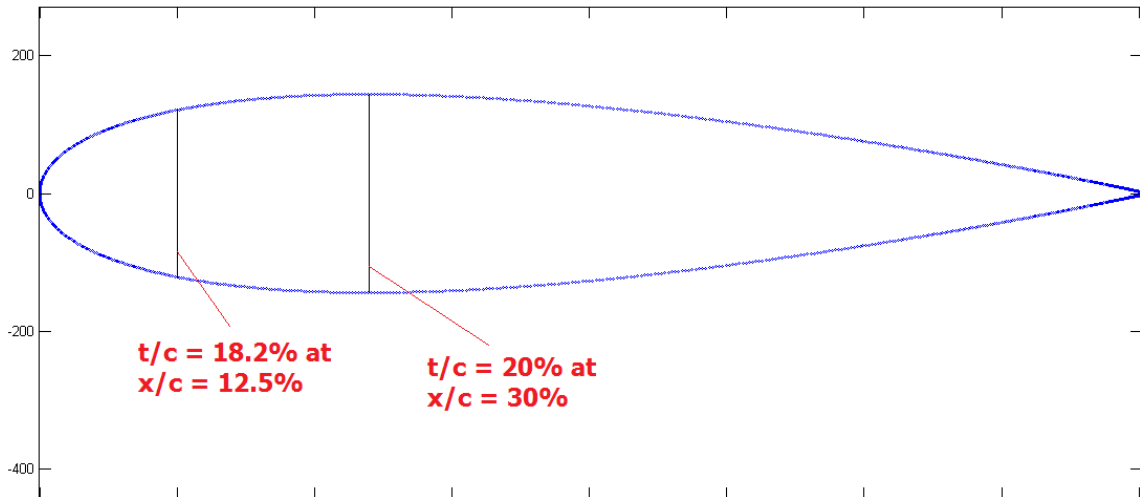


Figure 6.3: Simple airfoil representation of wingsuit

Camber of the airfoil

To keep the model simple, the reference airfoil has no camber.

Span of the wing and chord of the airfoil

The reference wing will have a rectangular shape. To get the wingspan of this rectangle, first the average wing area of the Vampire 5 is determined. The suits are custom made, so exact dimensions will differ per person. The area is determined using Figure 6.4. The sizes are determined by measurements and estimations.

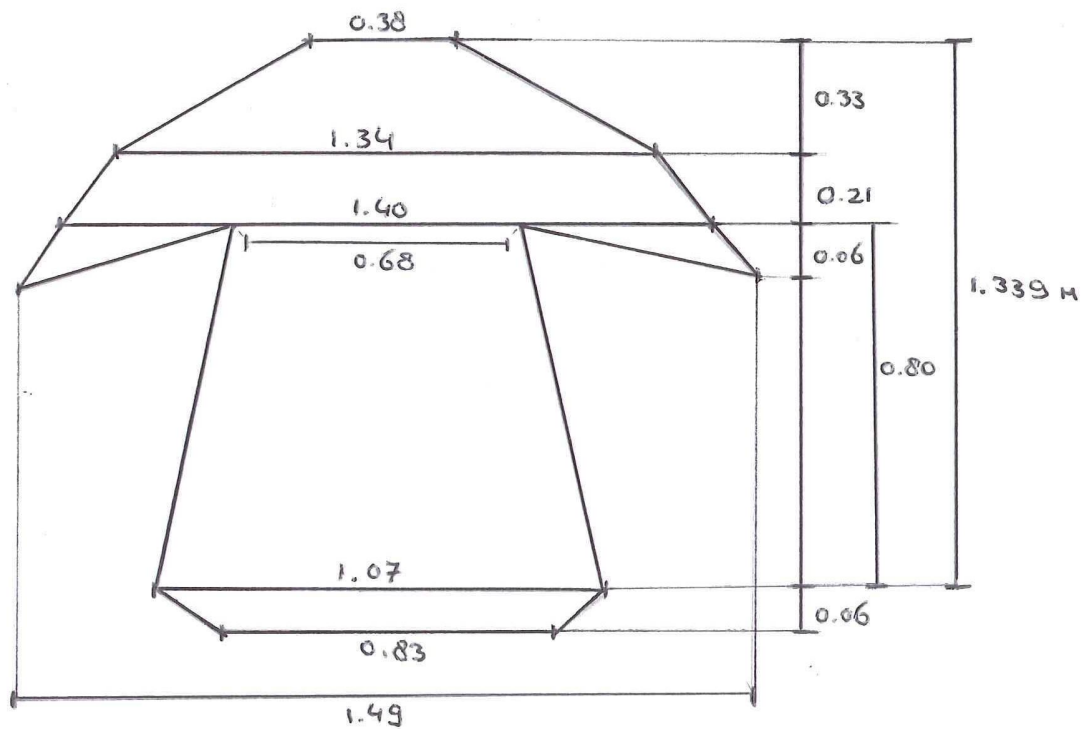


Figure 6.4: Simplified Vampire 5 sizes

Simplifying the suit, such that it consists of only squares and triangles, the total wing area is found to be approximately $1.73m^2$. Since the simplified rectangle has the same height as real wingsuits, this results in a wingspan of 1.28m.

6.2 Construct simple geometrical models of the wingsuit

Four geometrical wingsuit models have been created for the start of the analysis. This section will explain the reasoning behind these models and Section 6.3 will present the results of these models and the steps which have been taken after obtaining the first results. For the reference wing, as described in Section 6.1, it was chosen to use only one airfoil. In order to have more freedom in the adjustment of the model, but still keep it reasonably simple, the choice was made to use two airfoils for the four models.

With or without parachute rig

In current wingsuit designs, the parachute is not integrated into the wingsuit. The bag introduces an increase in thickness which might heavily influence the flow. However, the dimensions of the bag seem small in comparison to the total wing area of the wingsuit (Figure 5.8). Two design options have therefore been chosen to model this influence, which are presented together with their arguments:

- **No parachute rig:** The parachute rig only has a local influence which is negligible in comparison to the rest of the wingsuit. Furthermore the increase in thickness is only present in the middle. Representing this with a spanwise thickness increase would lead to wrong results. Since the airfoil has a moderate thickness, a symmetrical airfoil can be used.
- **Included parachute rig:** Although its thickness increase is only locally, it is substantial due to the low aspect ratio of the wingsuit. This thickness increase should therefore be taken into account. Camber is introduced to better match the flat front side of the wingsuiter.

Tail wing or leg wing

Another important parameter for the wingsuit models is the position of the second airfoil. Two design options were created, which have a different focus on the impact of the second airfoil. Both design options use joined airfoils without a gap in between. The reason for this is the enormous effect of a small position change with respect to the gap [16]. This instability would make the comparison between the two configurations more difficult. The two design options with their arguments:

- **Tail wing:** The Vampire 5, which is used as the main reference suit, has a tail wing with a separate inlet halfway between the knees and the pelvis. Since nearly undisturbed air enters this second wing, this is the most logical place for the second airfoil.
- **Leg wing:** Although the Vampire 5 has a separate inlet for its tail wing, the re-energizing effect might be limited. During the wind tunnel test it was observed that reversed flow was present on the first part of the tail wing, which is not what you would expect if the re-energizing flow would work properly. Apart from the tail wing, the thickness of the human body might be more important. Therefore, the second airfoil should start on the buttocks, where a significant thickness increase is present.

6.2.1 The five wingsuit models

As described in the previous part of this section, two choices have to be made: including the parachute rig and placement of the second airfoil. From these choices, the following four wingsuit models were created, which can be viewed in Table 6.1. For verification purposes, a reference model was created as stated in 6.1.1. To summarize the five models:

1. Wingsuit model 1: No parachute rig, tail wing
2. Wingsuit model 2: No parachute rig, leg wing

3. Wingsuit model 3: Included parachute rig, tail wing
4. Wingsuit model 4: Included parachute rig, leg wing
5. Reference model: a NACA 0020 airfoil, matching the thickness of a wingsuiters chest.

6.3 Compute 2D aerodynamic properties of the geometrical models

For the 2D analytical aerodynamic calculations, there are two computer programs used, JavaFoil and XFLR5. These programs are used since they are free and easy to use. In this section the calculations methods of the programs are explained, the results are discussed. The results themselves can be seen in Appendix R and S.

6.3.1 JavaFoil for 2D simulations

JavaFoil is a Java based applet which uses higher order panel methods to perform potential flow analysis [17]. With an integral method it calculates the boundary layer, separation is calculated using empirical correction methods from Eppler [18],[19],[20]. The main disadvantages of this program are incorrect stall modelling and the infinite wingspan / 2D airfoil limitations. These disadvantages should be considered when the data are analyzed.

JavaFoil settings

First the airfoils should be created in the program. This can be done by importing all the points of the airfoil. When the airfoil is created, the 2D polars can be created. In Figure 6.5 the settings to create the polars can be seen. First the Reynolds numbers are set at the previously calculated limits (Section 6.1). Next, a transition strip can be simulated by changing the T.U. (Transition Upper) and T.L. (Transition Lower) settings. These values will set a specific transition location over the airfoil. Since it is not preferable to have a specific transition location for the first calculations the values are set to 100% which means that the program will calculate the transition point. In order to be sure that every stall angle can be seen in the graph, the range of angles of attack is set to be from 0 up to 50°. The surface of the airfoil is assumed to be smooth. Finally the stall model has to be changed to the Eppler method (settings not visible in the figure), since this method is more accurate than the CalcFoil method [21].

Airfoil Polars								
first Reynolds Number:	<input type="text" value="1630000"/>	[-]	T.U.:	<input type="text" value="100"/>	[%]	first Angle of Attack:	<input type="text" value="0"/>	[°]
last Reynolds Number:	<input type="text" value="5440000"/>	[-]	T.L.:	<input type="text" value="100"/>	[%]	last Angle of Attack:	<input type="text" value="50"/>	[°]
Reynolds number step:	<input type="text" value="3810000"/>	[-]				Angle of Attack step:	<input type="text" value="1"/>	[°]
Surface Finish:	<input type="text" value="smooth finish"/>							

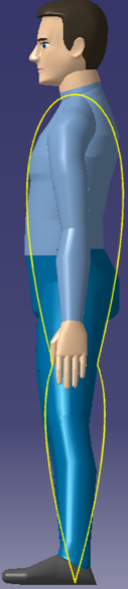
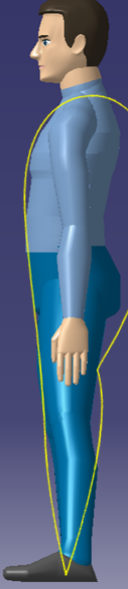
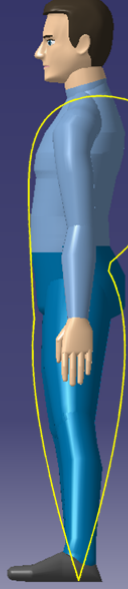
Figure 6.5: JavaFoil polar settings

JavaFoil Results

In Appendix R.1, the results of the 2D JavaFoil simulations can be seen. From the results of the $C_l - \alpha$, $C_D - \alpha$, $\frac{C_l}{C_D} - \alpha$ graphs, multiple conclusions can be drawn.

For instance it can be seen that increasing the camber increases the $C_{l_{max}}$, but also the drag coefficient. Furthermore looking at the $C_l - \alpha$ plot, it can be seen that there are three different $C_{l\alpha}$ values. These values depend on the existence of a second airfoil in the profile and its location: leg or tail wing. Next to the general properties, a few specific conclusions can be drawn. In the $C_l - \alpha$ plot, it can be seen that all the airfoils, except for the reference wing, have a peak in C_l at an angle of attack of 1° or 2°. An

Table 6.1: The four wingsuit models with their geometrical characteristics

Wingsuit model	Specifics	Wingsuit model	Specifics
	<p>Wingsuitmodel 1</p> <ul style="list-style-type: none"> • Upper airfoil: <ul style="list-style-type: none"> – Shape = NACA0028 – Chord = 947mm • Lower airfoil: <ul style="list-style-type: none"> – Shape = NACA0028 – Location = 72.3% – Chord = 654mm 		<p>Wingsuitmodel 2</p> <ul style="list-style-type: none"> • Upper airfoil: <ul style="list-style-type: none"> – Shape = NACA0040 – Chord = 605mm • Lower airfoil: <ul style="list-style-type: none"> – Shape = NACA0020 – Location = 72.9% – Chord = 898mm
	<p>Wingsuitmodel 3</p> <ul style="list-style-type: none"> • Upper airfoil: <ul style="list-style-type: none"> – Shape = NACA25040 – Chord = 947mm • Lower airfoil: <ul style="list-style-type: none"> – Shape = NACA0025 – Location = 72.3% – Chord = 654mm 		<p>Wingsuitmodel 4</p> <ul style="list-style-type: none"> • Upper airfoil: <ul style="list-style-type: none"> – Shape = NACA19063 – Chord = 605mm item Lower airfoil: <ul style="list-style-type: none"> – Shape = NACA0028 – Location = 72.9% – Chord = 898mm

explanation for this behavior might be that the flow over the airfoil for an angle of attack lower than 1° or 2° is laminar. When the angle of attack is increased even further, transition will occur from laminar to turbulent which creates a drop in C_l . Next to the phenomena which occur at every airfoil, airfoil specific phenomena can be seen in the plots. Looking at model 2, it can be seen that there is a large shift in C_l at an angle of attack of 40° . To get a better understanding of this shift, the pressure field around this airfoil is plotted. In Figure 6.6, it can be seen that there is not a large difference in pressure between an angle of attack lower than 40° and higher than 40° . Furthermore, comparative analyses with slightly thicker and thinner airfoils and also configurations with a more aft of more front positioned second airfoil, produced the same discontinuity. Therefore, the conclusion has been drawn that the shift in C_l is probably due to a bug in the program or a wrong setting. The C_d also has a shift in the $C_d - \alpha$ curve which indicates that the values of C_d are probably based on the values of C_l . Since the shift/bug only occurs after the stall point, the bug will not be a problem for this project and can be neglected.

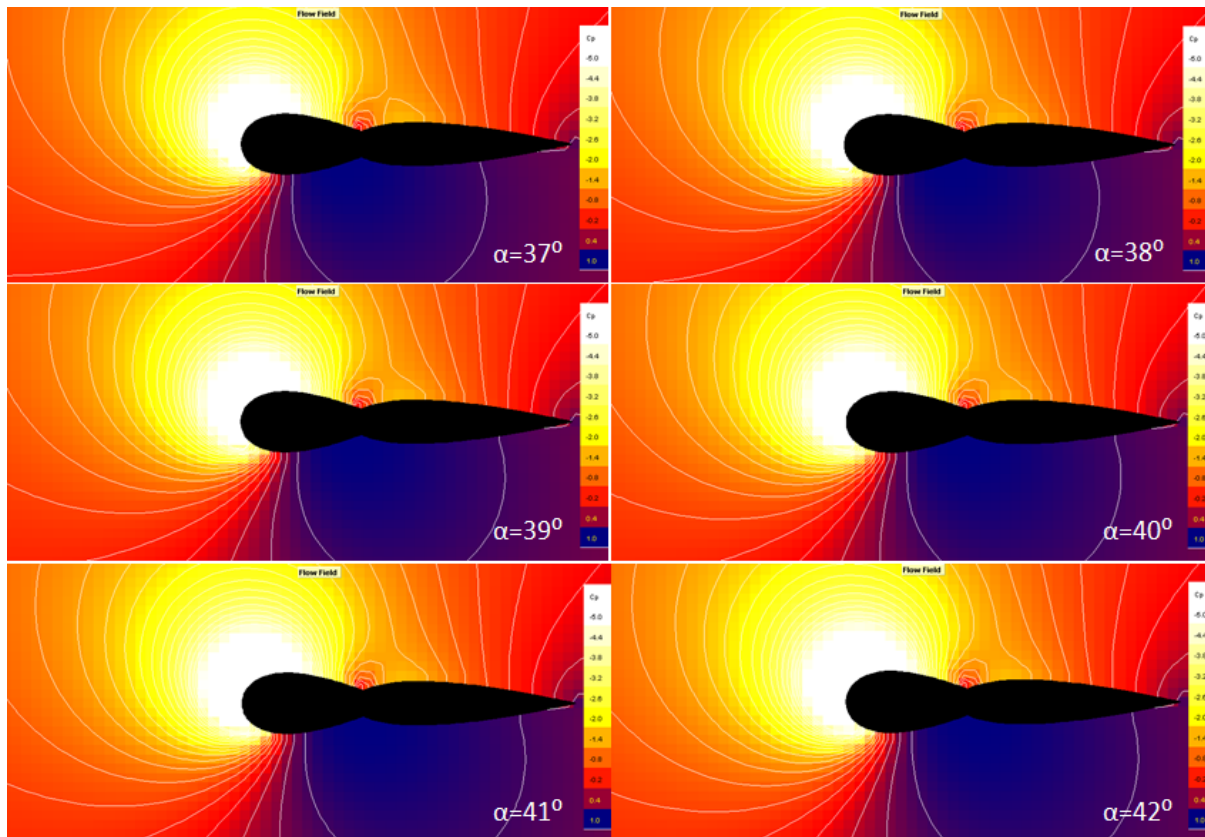


Figure 6.6: Pressure over airfoil (model 2)

6.3.2 XFLR5 for 2D simulations

XFLR5 is a successor to XFOIL, written in $C++$. It is an analysis tool for airfoils, wings and planes operating at low Reynolds numbers [22]. It uses 2D and 3D potential flow panel methods for the analysis of the airfoil, wing or airplane. It has the capability to use (non-linear) Lifting-line Theory (LLT), Vortex Lattice Methods (VLM) and 3D panel methods. Each of these methods has its own limitations. LLT, should not be expected to give accurate results for wings of low aspect ratio and large amounts of sweep and dihedral. With VLM, lifting surfaces are represented by an infinitely thin sheet of discrete vortices placed on the camber line of the airfoil. The calculation of the lift distribution, the induced angles and the induced drag are inviscid and linear, thus independent of the wing's speed and of the viscous characteristics of the air [23]. The viscosity variables are interpolated from 2D polars, generated by the XFOIL part of the program. It is important to note that the VLM method does not show stall. To get an idea of when the 3D wingsuit will stall, one should look at the 2D plots. Apart from values close to the stall angle, VLM should produce reasonable results for a wing with any usual wing geometry, thus sweep, low aspect ratio, dihedral and winglets.

In the 3D panel method, the wing is modelled as a thick surface, with the perturbation generated by the wing modelled by a sum of doublets and sources distributed over the wing's top and bottom surfaces. The strength of the doublets and sources is calculated to meet the appropriate boundary conditions, either Dirichlet or Neumann [23]. The programmer of XFLR5 recommends Dirichlet, since it is less sensitive to geometric changes and creates more reasonable results. XFLR5 recommends to use the 3D panel method when finding pressure distributions is the main focus.

Summarized to perform the calculations for a wing with a low aspect ratio and a main interest in lift and drag polars, VLM is selected as the 3D method. However, for pressure calculations the 3D panel method would be a more suitable choice.

XFLR5 settings

XFLR5 consists of four modules, in each of these modules a different step in the analysis of the wingsuit is done. First the airfoil is imported in the module "Direct Foil Design". The airfoils were imported and normalized. The next step is the module "XFOIL Direct Analysis". In this module the airfoils were analyzed with the batch analysis, namely analysis "Type 1". With this analysis, a polar is created for a range of Reynolds numbers and angles of attack. The transition data were left unchanged and the programs standard settings were used. For each new polar, boundary layers were initialized and the OpPoints, Operation points, were stored.

The foils were analyzed for two sets of Reynolds numbers and an α between 0° and 30° with a stepsize of 0.5° . Reynolds numbers between 1627000 - 1629800, with a Mach number of 0.09, and 5441000 - 5443500 with a Mach number of 0.17, were used, with a stepsize of 1000. These ranges of Reynolds numbers contain the minimum and the maximum Reynolds number which were stated in Section 6.3.2. The foils were plotted for these ranges of Reynolds numbers, to be able to interpolate the data for the 3D plots later in Section 6.4. The Reynolds numbers were again analyzed with XDirect, for an α of 0° and 30° , with the "viscous", "Init BL" and "Store Opp" checked. The polars of the four foils were exported and plotted in MATLAB.

Results

For the four different airfoil models, simulations were done at the maximum and minimum Reynolds numbers. With these results three different graphs were created: a $C_L - \alpha$, $C_D - \alpha$ and a $\frac{C_L}{C_D} - \alpha$ graph. These graphs can be found in Appendix R.2.

Looking at the graphs, a couple of observations and conclusions can be made. For the lift polars, model 1, 2 and the reference have quite similar lift coefficients and stall angles. These models stall between 16° and 18.5° at lift coefficients between 1.5 and 1.6 at a Reynolds number of $1.63 \cdot 10^6$. These models stall between 17° and 19° at lift coefficients between 1.7 - 1.9 for a Reynolds number of $5.44 \cdot 10^6$. In general one can say that for high Reynolds numbers, the lift coefficient and the stall angle is higher. Model 2 has the highest $C_{l_{max}}$, while model 1 has the highest stall angle at respectively 17° and 19° for the low and high Reynolds number. For model 3 stall occurs earlier, around 10° and 12° . Model 4 is even more extreme as stall already occurs at 0.4° with a C_l of 0.02 and 4° with $C_l = 0.31$. All data generated after the stall angle is not usable or relevant for this project.

Looking at the drag polar, the influence of the stall angle is clearly visible. Around the stall angles the graphs show a drastic increase in drag coefficient. Leaving model 4 out, the drag coefficients are approximately the same for small angles of attack. In the graphs it is also visible that for a higher Reynolds number, the airfoils have less drag. The drag coefficient is a function of the Reynolds number [24].

The glide ratio follows from the previous graphs. Because the airfoils are modelled as an infinite wing, the glide ratios obtained are way higher, varying with peaks from 50 - 100, than current wingsuits that have glide ratios of 2.5-3. Model 1 has the most optimal glide ratio of all models and reaches this at about 14° . Model 2 follows with peaks of respectively 55 and 80 for lowest and highest Reynolds numbers around 12° . Finally model 3 has an optimal glide ratio at about 8° .

6.3.3 Comparison between JavaFoil and XFLR5 2D results

JavaFoil versus XFLR5

At first the results of JavaFoil and XFLR5 deviated a lot, with even a difference of factor two at some points. However it turned out that JavaFoil, unless multiple airfoils are selected, only reads the data points up to $x/c=1$. In order to get usable data, the created airfoils should be normalized. In XFLR5 the airfoils were already normalized to be able to analyze them. When the results of the two programs were compared, the deviation in the results was noticed. With the normalized airfoils JavaFoil did lead to acceptable results.

Reference wing

The lift coefficient graph for the reference wing seems to give similar results for JavaFoil and XFLR5: a maximum lift coefficient of 1.76 at an angle of attack of 23° for JavaFoil and a maximum lift coefficient of 1.67 at an angle of attack of 20° for XFLR5. The behavior of the lift coefficient near and after stall differs significantly. JavaFoil, using Eppler methods for viscosity modeling, shows a moderate stall and pretty good lift characteristics after maximum C_l , while XFLR5 shows more abrupt stall behavior. This difference in stall modeling also becomes apparent in the drag coefficient graph which shows an overall increased drag for JavaFoil and a rapid increase in drag near the stall point for XFLR5. These differences in lift- and drag coefficient have their influences in the glide ratio graph, which shows an increased performance for XFLR5 which can be attributed to the low drag for the small angles of attack. The optimal angle of attack is comparable for both calculation methods: 11° for JavaFoil and 10° for XFLR5.

Airfoil model 1

First the difference in stall simulation becomes apparent: JavaFoil has a stall angle which is significantly higher than the obtained angle from XFLR5 (10° and 18° respectively) although the maximum lift coefficient is similar (1.84 for JavaFoil, 1.73 for XFLR5). Also the drag coefficient amplitude seems to be quite comparable: both 0.06 for an α of 20° , but XFLR5 shows a more rapid increase near the stall angle. Because XFLR5 has a lower drag coefficient at small angles of attack and a steeper $C_l - \alpha$ curve, the resulting glide ratio is very high compared to the results from JavaFoil: 106 for XFLR5 and 38 for JavaFoil. The optimal performance angle is comparable: 12° for XFLR5, 10° for JavaFoil.

Airfoil model 2

For airfoil model 2 JavaFoil and XFLR5 have very different simulation outcomes for the lift coefficient: JavaFoil predicts a maximum lift coefficient of 1.83 at an angle of 33° while XFLR5 predicts a maximum C_l of 1.75 at 17.5° . Concerning the drag coefficient, XFLR5 follows a smoother path than airfoil model 1, thereby showing closer resemblance to the drag coefficient graph of JavaFoil. The maximum drag coefficient for XFLR5 is 0.05 and JavaFoil shows a maximum of 0.07 in the same range, so the values of XFLR5 clearly are a lot lower than the predictions of JavaFoil. The resulting glide ratio polar shows a comparable shape, with a maximum glide angle of 11° for XFLR5 and 12° for JavaFoil, but with a huge difference in the glide ratio amplitude: 23 for JavaFoil and 77 for XFLR5.

Airfoil model 3

With the introduction of camber and a relative thick first airfoil it is interesting to see how both calculation methods cope with the airfoil. JavaFoil predicts a very late stall at 40° while XFLR5 predicts an early stall at 12° . As a consequence, the maximum value for C_l is much larger for JavaFoil than for XFLR5. This difference in interpretation is also visible in the drag coefficient graphs for which JavaFoil predicts a smaller drag coefficient than the other airfoil, while XFLR5 calculated a larger drag coefficient and a sharp increase near stall, comparable to the shape of airfoil model 1. XFLR5 also shows that the thicker airfoil has a larger initial drag coefficient (at $\alpha=0^\circ$). The glide ratio graphs show a large difference, both in magnitude and in shape.

Airfoil model 4

Airfoil model 4 has probably the most exotic shape, with significant camber and a very thick first airfoil. As with airfoil model 3, JavaFoil predicts very late stall (even later than airfoil 3, now at 49°) while XFLR5 shows stall already at 5° . The corresponding maximum values of the lift coefficient logically show a very wide spread. As with airfoil shape 3, the initial drag coefficient is relatively high in XFLR5 and JavaFoil also simulates this behavior. XFLR5 shows no data after 7° because no convergence is reached after stall. Both calculation methods predict the glide ratio of Airfoil model 4 to be the lowest of all 5 airfoils. XFLR5 primarily because of the early stall and JavaFoil because of the high drag.

Summary

Although the results from both calculation methods show a very large spread, some patterns have been identified. First the stall characteristics of both methods show a very different interpretation of the airfoil. They seem to be able to model the reference wing correctly, but the more exotic the airfoil becomes, the larger the spread between the results. JavaFoil predicts a maximum stall as large as 50° and XFLR5 shows a maximum stall angle of 20° . This difference also has a big influence on the drag calculations where XFLR5 shows an abrupt increase near the stall angle while JavaFoil models a more smooth transition.

6.4 Compute 3D aerodynamic properties of the geometrical models

The aerodynamic properties shown in the previous section are the 2D aerodynamic properties. This means that these properties are only dependent on the airfoil used. To take the wing area, sweep and aspect ratio of a wing into account, the 3D properties should be determined. Since JavaFoil cannot perform 3D simulations, the 3D properties are calculated manually. XFLR5 can perform 3D simulation, so the 3D aerodynamic properties are calculated directly in this program. In this section, the method and results are shown for both procedures.

6.4.1 JavaFoil for 3D simulations

Since it is rather hard to calculate the exact 3D properties of the simplified wingsuit, the 3D properties will be calculated using a correction factor based on the results of the 2D calculations and the geometrical characteristics of the wing [25]. First the C_L and C_D values will be calculated after which they are combined into a glide ratio polar. Figure 6.7 shows the general idea behind this process:

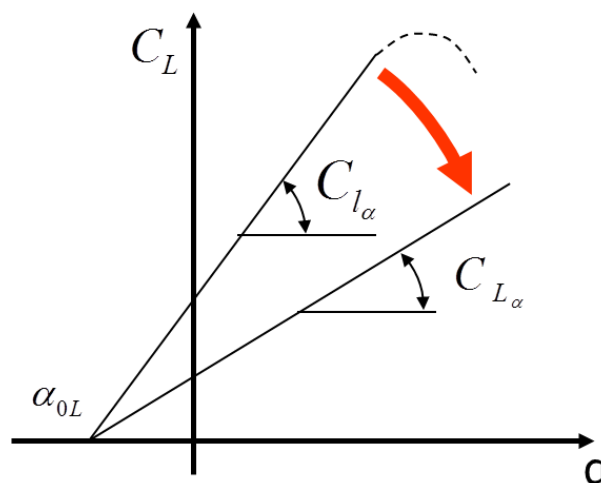


Figure 6.7: Correction of the 2D $C_{l_{\alpha}}$

Calculating C_L

The first step consists of determining the slope of the 3D $C_L - \alpha$ plot, C_{L_α} , with the use of formula 6.3.

$$C_{L_\alpha} = \frac{2 \cdot \pi \cdot AR}{2 + \sqrt{4 + \left(\frac{AR \cdot \beta}{\eta}\right)^2 \left(\frac{1 + (\tan(\Lambda))^2}{\beta^2}\right)}} \quad (6.3)$$

The following inputs were used to determine the 3D C_{L_α} :

- Aspect Ratio, $AR = 0.95$.
This value is determined using XFLR5 when all the inputs were filled in.
- Compressibility factor, $\beta = 1$
Since the wingsuit operates at velocities under $M=0.3$ the compressibility effects can be neglected and the compressibility factor is set to 1.
- Airfoil efficiency, $\eta = 0.95$
Since there is no empirical data known for these airfoils, the airfoil efficiency is set to 0.95, following [25].
- Sweep angle, $\Lambda = 0^\circ$
The sweep of the wingsuit is assumed to be zero in order to simplify the model. This makes it easier to compare JavaFoil and XFLR5 since XFLR5 models the sweep in a different way than equation 6.3.

The calculated C_{L_α} is equal to 1.40 rad^{-1} or 0.0246 deg^{-1} . This new slope is then compared to the corresponding 2D C_{l_α} , which is calculated using a linear regression through the data points from $\alpha = 3^\circ$ till $\alpha = 9^\circ$. The ratio between the 2D C_{l_α} and the 3D C_{L_α} is used to scale the remainder of the $C_L - \alpha$ curves. The influence on this transformation can be seen in Figure 6.8 where both the 2D $C_l - \alpha$ and 3D $C_L - \alpha$ plots are shown for wingsuitmodel 1.

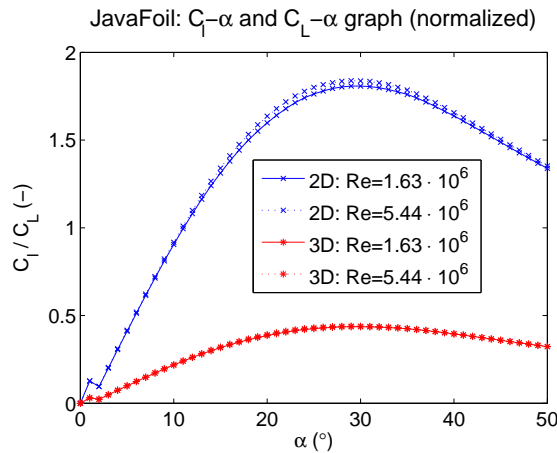


Figure 6.8: The 2D $C_l - \alpha$ graph and 3D $C_L - \alpha$ graph

Calculating C_D

After the lift coefficient of a wing (C_L) is calculated, the value can be used to determine the drag coefficient, C_D . The drag coefficient of a finite wing consists of two different parts, the profile drag, $C_{D,0}$ and the induced drag, $C_{D,i}$. The profile drag depends on the airfoil, this is equal to the drag coefficient, C_d of the 2D calculations. Since this value is known, only the induced drag has to be calculated using an equation based on C_L . As also the lift coefficient of the finite wing is known, the total drag coefficient of a finite wing can be determined by formula 6.4.

$$C_D = C_d + \frac{C_L^2}{e \cdot AR \cdot \pi} \quad (6.4)$$

In this equation an Oswald factor of 0.95 was used, this value was found using Figure 6.9[26]. In this figure the Oswald factor can be found using the aspect ratio which is known for the wingsuit.

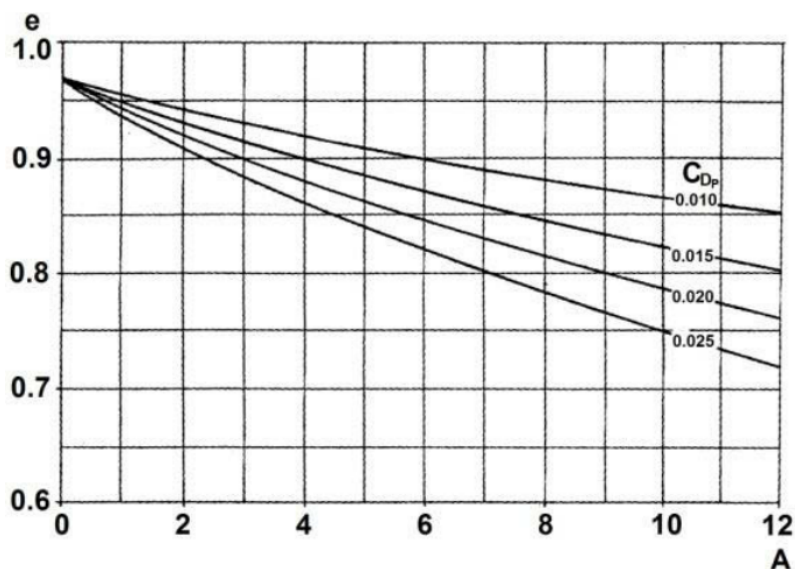


Figure 6.9: Schaufele's diagram for calculating the Oswald factor

Finally the lift and drag coefficients are known for all the different angles of attack. $C_L - \alpha$, $C_D - \alpha$, $\frac{C_L}{C_D} - \alpha$ graphs are made and can be found in Appendix R and S.

Results

Although the 3D aerodynamic properties are scaled from the 2D aerodynamic properties, some conclusions can be drawn. It can be seen that the phenomena happening in the 2D plots also happen in the 3D plot but with a different magnitude. When looking at the magnitude of the glide ratio it can be seen that this magnitude gets closer to the magnitude wingsuits have nowadays. The glide ratio of the single airfoil profile is higher than the glide ratio of a current wingsuit, which is as expected since this airfoil is perfectly shaped. Furthermore, the other wingsuit profiles have a lower glide ratio than the current wingsuits. Another interesting phenomenon is the angle of attack where the highest glide ratio is reached. This angle of attack is in a range of 10° and 15° , while wingsuiters normally fly at an angle of attack higher than 20° [13]. Some hypotheses can be set up to explain this difference. First, the backpack may have an influence on the lift over the wings. Due to cross flow from the top of the backpack to the wings, the flow over the wing may be more energetic which results in a delayed stall. A second option is the fact that most of the flights are under an angle of attack higher than 20° [13], but that the highest performance of a wingsuit is achieved at 10° angle of attack instead. Reliable performance data has not yet been acquired, which could be resolved by means of a test flight. A third option for the low angle of attack might be the slit between the first airfoil and the second. The re-energizing flow adds energy and, if positioned correctly, delays the stall.

6.4.2 XFLR5 for 3D simulations

In this section the settings used in XFLR5 will be explained.

XFLR5 settings

The 3D plots are made in the module "Wing and Plane Design". A new wing was modelled with the dimensions as stated in 6.1.1. Since the Reynolds numbers calculated in are calculated for different lengths than the one used in this model. In order to make a fair comparison, the velocity was adjusted to maintain the same Reynolds numbers. With [11], the density and the kinematic viscosity were found.

These values were filled in, and the airspeed was adjusted to obtain the same Reynolds number as used in 6.1.1

Minimum Reynolds number: $1.628 \cdot 10^6$ ($v=23.67 \text{ m} \cdot \text{s}^{-1}$, $\rho 0.820 \text{ kg/m}^3$, $\nu 1.9627 \cdot 10^{-5} \text{ m}^2 \cdot \text{s}^{-1}$)
 Maximum Reynolds number: $5.442 \cdot 10^6$ ($v=61.725 \text{ m} \cdot \text{s}^{-1}$, $\rho 1.112 \text{ kg/m}^3$, $\nu 1.5312 \cdot 10^{-5} \text{ m}^2 \cdot \text{s}^{-1}$)

To create the 3D polars in analysis definition, the following options were chosen: the VLM method (Viscous), the chosen polar type is "Fixed Speed", and the "Reference Area and Span for Aero coefficients" uses the "Wing Planform".

The wing was modelled in the "Wing Edition". The wing is modelled by 1 panel, mirrored in the x-axis. These panels are defined by their spanwise length, chord length, offset, dihedral, foil, amount of mesh panels in x and y direction and their distributions. For the wing created in this model these values can be found in Table 6.2.

Table 6.2: The panel definitions

Span, y [mm]	chord [mm]	offset [mm]	dihedral	twist [°]	foil	X-panels	X-dist	Y-panels	Y-dist
0.00	1339	0.00	0.0	0.0	Model #	11	Cosine	22	Uniform
640.00	1339	0.00	0.0	0.0	Model #	11	Cosine	22	Uniform

For the mesh distribution along the X-axis, a cosine distribution was chosen. This distribution increases the mesh density at the leading and trailing edge. These points of the airfoil are the most interesting. The break in the middle of the airfoil, will not necessarily be seen with the VLM, since it places vortices on the camber line, as was discussed in [22].

Results

With the previous mentioned settings the four different wing models were analyzed and lift and drag polars created. The corresponding graphs can be found in Appendix S.2. Looking at the $C_L - \alpha$, $C_D - \alpha$ and $\frac{C_L}{C_D} - \alpha$ graph a couple of conclusions could be made.

XFLR5 uses the 2D results to interpolate the 3D polars. It should be noted that the results of XFLR5 are questionable near the stall angle and invalid afterwards. Although it is not shown in the graphs S.2, the wings do stall. This is not modelled by XFLR5. Therefore, it is assumed that the wings stall at about the same angles as the 2D polars R.2.

First of all XFLR5 was not able to calculate the polars for wingmodel 4 for low ($1.63 \cdot 10^6$ Reynolds numbers). The low Reynolds number calculation failed because the lift coefficient in 2D was significantly lower than the lift coefficient calculated in 3D with VLM ($C_l = 0.008$ in 2D versus $C_L = 0.06$ in 3D at $\alpha = 0$). The results of wingmodel 4 for high Reynolds numbers are questionable, since the wing stalls at a low angle of attack, $\alpha = 4^\circ$.

Taking this into account the polars are analyzed. Looking at the lift polar, the manner in which the program calculates the 3D polars is clearly demonstrated. The VLM method focusses for the calculation of the lift polar only on the camber line. Since the length and camber of the wings are the same, the lift polars of model 1 and 2 and the reference wing, all symmetric airfoils, are exactly the same. These graphs also cross, because they are symmetric, the origin. Model 3 is slightly asymmetric, therefore its C_L lies slightly above the other graphs. Because model 4 has significantly more camber, its graph also differs more. Thus the models with a higher camber have higher lift coefficients at the same angles of attack. A last remarkable point of the lift polar in 3D is the fact that, contrary to the 2D plots, it does not show stall.

From the drag polar it can be seen that the models with more camber experience more drag. Investigating the models at the low Reynolds number, they show as expected more drag as the drag coefficient is a function of the Reynolds number. Because the 3D calculation for the drag coefficient consists of both pressure and induced drag, the total drag of the symmetric wings differs, though their induced drag is the same. The reference wing has the lowest drag coefficient as the drag coefficient increases with the

thickness of the airfoil.

The results of the glide ratios, or $\frac{C_L}{C_D} - \alpha$ graphs, can be traced back to the previous discussed results. Because the drag coefficients of all models are relatively lower for low angles of attack, the glide ratios peak around 5° - 7° and have peak values between $\frac{C_L}{C_D}$ 7.5 and 10. These values are more realistic than the results obtained for the 2D simulations, but still quite off compared to current wingsuits with glide ratios around 2.5 - 3. This is probably due to the fact that in real life the wingsuits experience more drag than simulated in XFLR5. Because of its high drag that model 4 experiences, it has a significantly lower glide ratio than the other models. Model 1 has the highest glide ratio, followed by model 3, for low angles of attack. However, after 7° , model 2 is more profitable than 3 concerning the glide ratio. Finally, following from the fact that for higher Reynolds numbers the models have less drag, the glide ratio at higher Reynolds number is also higher.

6.4.3 Comparison between JavaFoil and XFLR5 3D results

The results of the 3D simulations of both JavaFoil and XFLR5 are compared to get a better idea of the reliability of the obtained lift and drag polars.

Reference wing

Looking at the C_L values of the reference wing NACA0020, around 23° it turns out that JavaFoil has a maximum lift coefficient of 0.36. Whereas XFLR5 has a value around 0.48 and continues without stall to 0.55 at 30° . This has to do with the way XFLR5 calculates the 3D values with the VLM. The drag polars look more similar, although the values obtained with XFLR5 are lower. As a result, the glide ratios calculated with XFLR5 are higher with values of 11.1 and 10.94 at angles of attack of 5.5° and 6° , for high and low Reynolds numbers respectively. JavaFoil has lower results for the glide ratios. Furthermore, while XFLR5 has a smooth glide ratio curve, JavaFoil suddenly has a peak at 8° of 7.56. Disregarding this peak, JavaFoil has a higher glide ratio of 7.11 and 7.50 at 6° for low and high Reynolds numbers, respectively. Then, the maximum glide ratios of both JavaFoil and XFLR5 lie at quite low angles of attack, at about 6° .

Wingsuit model 1

The graphs obtained with XFLR5 for model 1 and the reference wing have the same lift coefficients. This can be traced back to the way VLM models these coefficients. Therefore there is no difference visible between these both symmetric airfoils. JavaFoil on the other hand shows higher C_L values of model 1 than that of the reference. JavaFoil also has a $C_{L_{max}}$ of 0.44 at 29° , where XFLR5 has no stall and thus continues till 0.55 for 30° . The drag polar again shows lower values for XFLR5. Hence, lower drag coefficients and higher lift coefficients give higher glide ratios for XFLR5. Maximum $\frac{C_L}{C_D}$ for XFLR5 is around 9.94/8.86 at $6/6.5^\circ$ for respectively high and low Reynolds number. JavaFoil creates values of 5.74/5.39 at 7° . This is quite a huge difference. However the angle at which the maximum glide ratios occur, is approximately the same. Furthermore JavaFoil causes a strange deviation in the beginning of the glide ratio. The same deviation is visible at the lift polar at very low angles of attack.

Wingsuit model 2

JavaFoil gives a strange deviation at 40° . However this has no influence for the comparison with XFLR5 as XFLR5 does not have data points at 40° . Thus continued with the comparison of the lift polar. In the beginning the slope looks similar and JavaFoil has a $C_{L_{max}}$ of 0.49 at 33° . XFLR5 does not show stall and continues to 0.55 at 30° . Moreover XFLR5 has again the same lift coefficients with the other symmetric airfoils; model 1 and the reference, in line with the way the VLM models the lift polar. JavaFoil gives lift coefficients for the first 20° that are approximately the same as model 1. However for model 2 stall occurs later and the $C_{L_{max}}$ is also higher. For the drag coefficients JavaFoil gives a bit higher values for model 2 compared to model 1 and the reference. XFLR5 has the same drag coefficients for these models, but compared to JavaFoil its drag coefficients are lower. For the glide ratios JavaFoil has maxima of 4.23/3.93 at 8° for respectively high and low Reynolds numbers. XFLR5 on the other

hand gives peak values at $6.5/7.5^\circ$ of 8.86 and 7.96. The differences for high and low Reynolds numbers are thus more remarkable for XFLR5 than for JavaFoil.

Wingsuit model 3

First looking at the C_L values; JavaFoil calculated a $C_{L_{max}}$ of 0.57 at 39° , whereas XFLR5 was not able to calculate stall and thus came up with a maximum value of 0.58 at 30° . For the lower angles of attack up to 15° they both have higher C_L values than the reference wing. Afterwards they start to differ, the XFLR5 values stay the same, whereas JavaFoil gets lower values. Concerning the drag coefficients, both have higher results than the reference. Though, compared to each other XFLR5 generated lower values than JavaFoil. As a result, again JavaFoil has lower glide ratios: 4.54/4.22 at $8/9^\circ$ compared to 8.87/7.99 around $6.5/7^\circ$ for XFLR5, for respectively high and low Reynolds numbers. Furthermore, there is again a discontinuity visible in the beginning of the graphs of JavaFoil. Moreover, now the angle of attack for maximum glide ratio clearly differs as JavaFoil obtains the maximum glide ratio at higher angle of attack.

Wingsuit model 4

At the 2D results of XFLR5 it was visible that model 4 obtains very early stall, already at 5° . Therefore, the results after this angle are questionable and should be handled carefully. The C_L values obtained with XFLR5 for model 4 are higher than the values obtained for all other models, with a $C_{L_{max}}$ of 0.58 at 22.5° . JavaFoil has the same $C_{L_{max}}$ value, but obtains this only at 49° . Both results are questionable though, while as said before, the airfoil at 2D encountered very early stall. Both with JavaFoil as XFLR5 the highest drag coefficients of all models are obtained. The lowest Reynolds number of the XFLR5 simulation even gets a drag coefficient of 0.4 at 22.5° , almost four times as high as the other models. The high Reynolds number has less extreme values, but is still remarkably higher than the other models. As can also be seen, XFLR5 has some trouble calculating the values for higher angles of attack, probably due to the early stall at 2D and thus 'messed up' 2D results, where it bases its calculations on. Looking at the glide ratio, model 4 has a huge peak in the beginning. The same can be noticed for the lift coefficients. This is considered as a discontinuity, because it would imply that the highest glide ratio would be obtained at 0° angle of attack. Disregarding it, JavaFoil has maximum glide ratios of 2.84/2.66 around 12° and 13° angle of attack for respectively high and low Reynolds numbers. XFLR5 has a huge difference between the glide ratios of low and high Reynolds numbers, which is not that surprising as this could already be seen at the drag polar. For low Reynolds numbers it does not have an outstanding maximum, but the optimum is 1.48 around $18/19^\circ$. For higher Reynolds numbers it is 4.23 around 5° .

Summary

Summarized, because XFLR5 is not able to model stall with the VLM, the C_L values are higher for higher angles of attack. Furthermore, it also generates lower drag coefficients. And as a result XFLR5 has higher glide ratios than JavaFoil. Also XFLR5 has more difference between the higher and lower Reynolds numbers. However, in general the optimal angle of attack where the maximum glide ratio is obtained is approximately the same for JavaFoil and XFLR5. Finally, JavaFoil encounters at some places discontinuities, whereas XFLR5 does not have this problem.

6.5 Discussion of results

Since the analytical results are calculated by two different computer programs using two different calculation methods, the programs should be validated to get an idea if the results are correct representations of reality

6.5.1 Validation of calculation methods

To get an idea if the results of the computer programs can represent a real life situation, the computer results are validated. This is done by comparing the computer results with real life test results. The

NACA0021 was used since this empirical data was available [27]. The test was performed in a Variable Density Wind Tunnel of the National Advisory Committee for Aeronautics, using a 3D wing with the NACA0021 airfoil having an aspect ratio of 6 and a Reynolds number equal to $3.3 \cdot 10^6$. To be able to make a good comparison between the computer results and the real life test results, the inputs of the tests must be the same. Therefore the inputs of JavaFoil and XFLR5 had to be matched in order to get comparable results. Since the test results of the wind tunnel are the 3D aerodynamic properties of the NACA0021, this validation is a good check to make sure that the calculations from the 2D results from JavaFoil to the 3D results are done correctly.

By evaluating the $C_L - \alpha$, $C_D - \alpha$ and $L/D - \alpha$ plots, which can be seen in Appendix T.1, the programs were validated. In the plots it can be seen that the results of JavaFoil and XFLR5 are in the same order of magnitude and have the a curve shape which look like the empirical data. It can be seen that the results of XFLR5 matches the $C_L - \alpha$, $C_D - \alpha$ good while the results from JavaFoil matches the $L/D - \alpha$ better. This can be explained by looking to the margin of error in the $C_L - \alpha$ and $C_D - \alpha$ from JavaFoil and XFLR5 compared to the empirical data. When looking to the $C_L - \alpha$ and $C_D - \alpha$ results of JavaFoil it can be seen that they are always higher than the empirical data. This error is deleted in the results of the glide ratio because it is the ratio between lift over drag. When looking to the results of XFLR5, it is seen that the $C_L - \alpha$ and $C_D - \alpha$ do match the curve of the empirical data better, but fail when calculating the glide ratio. This error can be explained by the fact that the calculated lift is higher than the real life lift and the drag is lower than the real life drag. When calculating the lift over drag, this error is strengthened which results in a larger error. Furthermore, it can be seen that XFLR5 has the same stall angle as the empirical data since XFLR5 stops calculating when he has reached the stall angle.

To conclude, it can be said that both the programs do match the empirical data good, but XFLR5 matches the results better. Hereby it can be concluded that XFLR5 will be used to verify the numerical simulation.

6.5.2 Conclusion and recommendations

To be able to find a correct simplified model which can be used to represent a wingsuit, multiple calculations were performed. First the Reynolds number had to be determined since this is a driving factor in the air flowing over the wingsuit. After some calculations it was found that the Reynolds numbers were within a range of $1.63 \cdot 10^6$ and $5.44 \cdot 10^6$. Next five wingsuit models were determined, these models differ on different aspects to find a model which represents the wingsuit the best. Finally plots were made of the lift, drag and glide ratio against angle of attack to determine the best wingsuit model, these results can be found in Appendix R and S. After the results were analyzed it could be seen that wingsuit model 4 did not represent a real wingsuit very well. This because of the fact that the airfoil stalls at an angle of attack of 4° in the 2D simulation of XFLR5 which can be seen in Figure R.2. Next it can be seen in the same figure that wingsuit model 3 stalls at an angle of attack 13° , since this is rather low since a wingsuiter normally flies at an angle of attack around 20° this wingsuit is also eliminated in this process. As was stated in the beginning of this chapter the reference wing was an ideal wing to state the boundaries of a wingsuit. Therefore it was stated that this wing will not be the simplified model of the wingsuit since it is not representable for the current wingsuits. Finally two wingsuit model were left which had to be evaluated. Since these wingsuit models do not differ very much, it was concluded that the final wingsuit model would be decided after the numerical simulation is done. Therefore the mistake of choosing the wrong model, since there is no clear evidence why one wingsuit is much better, will not be made.

After the analytical simulations were done, a decision had to be made which simulation program would be used to verify the numerical program. After JavaFoil and XFLR5 were validated using experimental data from a NACA0021 airfoil, the decision was made that XFLR5 would be the program to verify the numerical simulations. This decision was based on the fact that the results from XFLR5 match the experimental data the best. The data were a little bit too positive which gave good lift and drag results but gave a larger error in the glide ratio since this is the ratio between the lift and the drag. Since this is known, it has to be taken into account when verifying the numerical results.

7

Numerical Analysis

The numerical analysis of wingsuits is conducted to get a very detailed quantitative image of the wingsuit's aerodynamics. To achieve this, a CFD program is used, which can provide us with quantitative and qualitative data of:

- Separation point
- Reversed flow
- Stall
- Lift and Drag coefficients
- Pressure gradients

Due to agreement conditions, this report will not publish the results of this Computational Fluid Dynamics software. The conclusions however, may and will be used in this report.

7.1 Overview

Computational fluid dynamics is a difficult and lengthy process. The DSE time is limited to only a few weeks. In order to achieve the best possible results, good organization is required to get as much computational time as possible. The numerical analysis is organized as follows:

- 1. Obtain 2D and 3D models of the wingsuit**
 - Obtain analytical simulation 2D airfoils
 - Create 3D wingsuit models
- 2. Compute 2D aerodynamic properties of the 2D models**
 - Determine lift and drag coefficients of the 2D models
 - Calculate glide ratios of the 2D models
- 3. Compute 3D aerodynamic properties of the 3D models**
 - Determine separation point
 - Determine stall characteristics
 - Determine lift and drag coefficients
 - Calculate glide ratios
- 4. Verify the model**
 - Verify the 2D results
 - Verify the 3D results

The computation of all the 2D and 3D models was a lot of work. More than ten simulations of the 2D models and more than ten simulations of 3D model were run, but none of the results were satisfactory. The group suspected errors in the computation. The flow remained attached far past an angle of attack where usually stall should occur. Therefore, more simulations were run on high angles of attack of 25° and 30°. Even these simulations showed no sign of separation or stall.

After thorough searching, the wrong settings in the program were finally found, these settings are described in Section 7.5.1. By quickly running a 2D simulation, it could be seen that the separation and

stall characteristics were far more accurate to the real life stall characteristics. Although the error was fixed, this did mean that all of the already computed simulations were inaccurate and therefore obsolete.

Unfortunately, this setback had cost so much time, no more time was available to run all of the 3D simulations. Only the 2D simulations run fast enough to start some simulations over again. These 2D model simulations are described in Section 7.3.

The simulations for the 3D models were not an accurate representation of the real air flow, but some conclusions may be drawn from the data plots. This will be done in Section 7.2.2. Last but not least, all the numerical data needs to be verified and validated, especially when it involves some fairly inaccurate data. The verification and validation will be done in Section 7.5.

7.2 Obtain 2D and 3D models of the wingsuit

For the numerical analysis, both 2D and 3D models of wingsuits are modelled and analyzed.

7.2.1 2D Models

The 2D models are copied directly from the airfoil profiles generated by the analytical analysis group. The airfoils are extruded in CATIA to generate solid airfoils. The specific dimensions of these airfoils can be found in Section 6.2.1. The solid airfoils are loaded into the CFD program, into a very thin wind tunnel. The solid airfoil protrudes on both sides of the wind tunnel, so that the wind tunnel walls cut off the airfoil, and no wing tip exists within the wind tunnel. This is essential for 2D analysis of the airfoils.

7.2.2 3D Models

The 3D models are created in CATIA. One model is created as a very generic model of a wingsuit shape. This model has smooth surfaces, smooth edges and thick profiles all throughout the wingsuit and thus does not closely represent the wingsuits of this moment. This model is mostly used to get a general feel for the CFD program. For the real CFD analysis, a model of the Vampire 4 wingsuit is created in CATIA, see Figure 7.1. This model has more rough edges and a thinner profile and is therefore a much closer resemblance of the real life wingsuits. This model undergoes thorough testing.

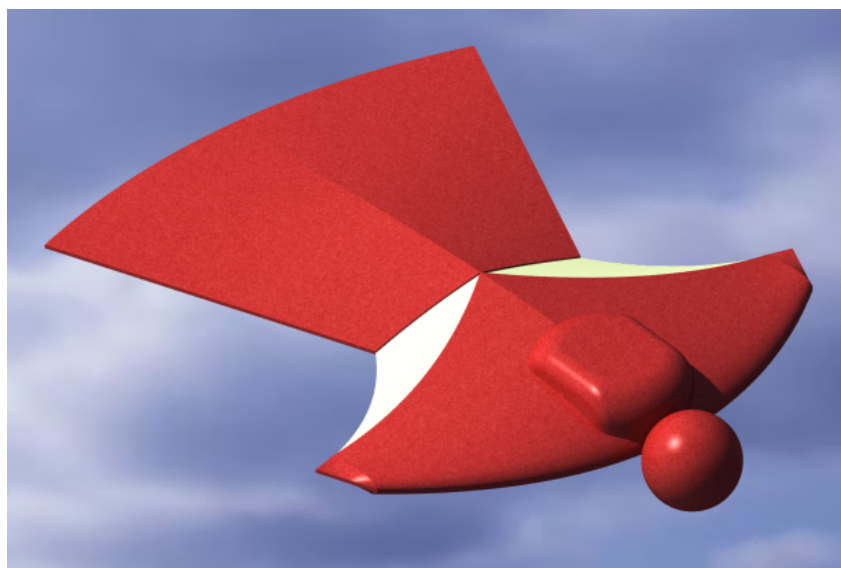


Figure 7.1: CATIA model of Vampire wingsuit

7.3 Compute aerodynamic properties of the 2D models

The CFD program is set to a 2D kernel and a very thin virtual wind tunnel. The Reynolds number during these simulations is calculated using equation 6.2, in which $\rho = 1.225 \frac{kg}{m^3}$, $V = 40[m \cdot s^{-1}]$, $L_{char} = 1.339m$ and $\mu = 1.7894 \cdot 10^{-5} Pa \cdot s$, to be equal to $3.667 \cdot 10^6$.

Since the 2D case requires significantly less computational power than the 3D simulation, the resolution can be refined to 1mm close to the airfoil and 5mm in the wake. Unfortunately, this was still not enough refined for a qualitative analysis of the boundary layer and separation. If refined enough, this qualitative analysis could be used to determine the dimensions of some future concepts.

The program calculates the forces on the model by integrating the pressure distribution along the surface. The coefficients are then calculated using equation 7.1. Since the freestream flow direction is always horizontal the C_y represents C_l . In the same manner C_x represents C_d . In order to get correct values for C_l and C_d the values for v_{ref} and S_{ref} can be user defined.

$$C_y = \frac{2 \cdot F_y}{\rho \cdot V_{ref}^2 \cdot S_{ref}} \quad (7.1)$$

Besides the qualitative analysis, quantitative results are gained for the 2D cases. From these results, values for C_l and C_d are calculated. In U.1 the results of the 2D CFD simulations can be seen. From these results a couple of conclusions can be drawn.

The plotted $C_l - \alpha$ curve is very similar to a plot for a conventional airfoil. It shows a linear progression until 20° where it shows characteristic stall and the curve starts to dip. However, after this short dip the curve resumes its steady progression, which is not representable for a normal stall. This is probably due to the fact that after stall the values for F_y and F_x vary quite a lot (sometimes with differences of more than 1000N) due to shedding of vorticity from the airfoil and an average has been taken in the analysis of these values.

The subplot of the $C_l - C_d$ drag polar shows close resemblance to the shape of the average $C_l - C_d$ drag polar. However, the last point is an outlier due to the before mentioned fluctuations in C_l values.

Also the $C_l/C_d - \alpha$ shape of the curve is quite representative of the conventional L/D plots. The highest L/D ratio is 9.5, which is quite reasonable for a 2D case.

Concluding, the 2D model outputs aerodynamic characteristics which are very similar to the characteristics of a general airfoil. Only the last few data points are less accurate, because they are affected by the simulated shedding. So of this data only the points up to an angle of attack of 25° could be representative for a basic wingsuit model.

7.4 Compute aerodynamic properties of the 3D models

The CFD program is set to a 3D kernel and a relatively big wind tunnel, where the wingsuit is at least one meter away from the wind tunnel walls. The Reynolds number during these simulations roughly equals the 2D wind tunnel Reynolds number. The viscosity is equal, the airspeed is equal ($40m \cdot s^{-1}$), and the chord length is almost equal, which resulted in a Reynolds number of $3.667 \cdot 10^6$. Keep in mind that the data gained from this is not a good representation of the real flow dynamics.

7.4.1 3D Models

Due to the size of the simulated wind tunnel and the relatively high Reynolds number, quite a lot of computational power is required. In order to keep a reasonable run time for one simulation, the resolution can be less refined than the 2D cases. For all simulations, a resolution of 12.5mm near the wingsuit shape and the wake is taken. A smaller number would definitely be beneficial, but time is not sufficient for that.

The 3D model is simulated for angles of attack of 0 to 35° , in steps of 5° . The result of these simulations

was data about C_L and C_D for different angles of attack, indications of the separation point, and reverse flow.

Again note that especially the separation point and reverse flow are way off, so these results are not even considered in this section due to inaccuracy. Some plots of the C_L and C_D values can be shown. In Appendix U.2, a subplot of the $C_L - \alpha$ curve is shown. It can be seen that there is an indication of stall occurring in this simulation. However, after a short dip in C_L , the curve starts to rise again.

Next, the $C_L / C_D - \alpha$ subplot will be looked into. From this plot, the maximum C_L / C_D value (glide ratio) and the corresponding angle of attack can be determined. For the Vampire wingsuit, the maximum C_L / C_D value was 6.1, at an angle of attack of 10° . These are obviously non-feasible results, since the highest C_L / C_D value of current wingsuits approaches only 3.5.

In short, the 3D numerical data was not satisfying. The data was not trustworthy. It is unfortunate that due to lack of time, no proper simulations could be run. However, a basis has been set on which new research can be conducted in the future.

7.5 Verify and validate the model

To assess the quality of the simulations, the results need to be verified and validated. With verification, one checks if the program follows the right calculation procedures. Validation is the comparison between the simulation outcomes and reality to see whether this simulation provides the right tool for a real situation. The numerical simulations are verified and validated with respectively the analytical simulations and empirical data. In this section the results of both procedures are shown.

7.5.1 Verification

To know whether the numerical calculations are correct, the program should be verified with the analytical program, XFLR5. This is done by running 2D simulations of airfoil shape 1 and airfoil shape 2 with the same inputs in both programs. By comparing the results of both simulations, it can be established whether the calculation methods are correct. If the results from both programs are very different from each other, one of the simulations is wrong or the difference should be explained by the assumptions of the program.

First run

After the lift and drag coefficients and the glide ratio were calculated using XFLR5 and the CFD program, it was clear that the results did not match (this could be seen in the CFD program). When looking to the plots in more detail, it could be seen that the lift gradient of XFLR5 was 80% larger than the lift gradient of the CFD program. Besides the lift gradient, the airfoil of XFLR5 stalls at an angle of attack of 18° while the results of the CFD program do not show a stall until 35° angle of attack. Finally the glide ratio of XFLR5 is four to five times higher than the glide ratio of the CFD program. This behaviour might be due to differences in the flow attachment. It was concluded that one of the two programs, XFLR5 or the CFD program, did not perform the correct calculations. Since this was known, multiple things had to be checked. First it was checked if the difference could be the effect of assumptions made by one of the programs which makes such a difference in the results. Since there was not a clear explanation for the difference between the results, the settings of both programs were checked. After a while, it was clear that a mistake was made in the input which calculates the boundary layer wall conditions of the model in the CFD program. In the boundary condition settings, the wrong function was selected, which means that the calculations under-predict the stall characteristics and produce a maximum angle of attack which is a lot higher than reality. This setting was changed. The new setting simulated a much better interaction between the wall of the model and the airflow.

Second run

After the change in settings, the results changed considerably. At first the results for the lift coefficient (which could be seen in the CFD program) still seemed wrong: the lift coefficients from the CFD pro-

gram increased even at angles of attack greater than 30 degrees and no apparent stall position emerged. The velocity vector figure at an angle of attack of 20° gives a good explanation (to be seen in the CFD program). The flow is already completely separated, but the calculation method from the CFD program (integrating the pressure distribution on the x- and y- projected planes) seems to overpredict the lift due to the enormous pressure surplus on the lower side of the airfoil. Therefore the simulation points after $\alpha = 20^\circ$ can be omitted.

What remains is the under predicted lift coefficients until 20°. Another look at the velocity vector in the CFD program, provided an explanation. Flow separation already starts at 10° angle of attack and increases to 20° at which complete stall is achieved. This flow separation starts at the indent of the airfoils.

This flow separation, and associated loss of energy and lift, might explain the difference in slope between the two lift coefficient graphs. Furthermore the separation creates a large increase in drag, which in turn might explain the big difference in the drag coefficient graph (which could be seen in the CFD program). These two effects (decrease in lift and an increase in drag) combine into the enormous difference in glide ratio values.

A comparison can also be made between airfoil shape 1 and airfoil shape 2. The lift coefficients for airfoil 1 are higher than airfoil 2, which can be attributed to the fact that the indent in the airfoil (the junction between the first and second airfoil which combine into the total airfoil shape) is larger for airfoil shape 2, thereby introducing more separation and a loss of lift.

Conclusion and chosen airfoil shape

From the verification results, no final conclusion can be drawn about whether the CFD program is performing the calculations as intended. It seems to underpredict the lift coefficient, but XFLR5, being a vortice lattice method, might be further away from reality which would make the difference less of a problem. More research should be performed to understand the fundamental differences between the two programs in order to fully explain the difference. The influence of the contraction, the location at which the two airfoil shapes meet, does show quite clearly on the the CFD program results. This matches the influence from the parachute rig as found during the wind tunnel tests. Therefore airfoil shape 2, with a more rapid transition between the two airfoils, seems to be a better representation and will be used to test the application of the design options.

7.5.2 Validation

To obtain confidence in the calculations, the results from the calculation method should be compared to experimental data, that is: validating the computational model. The CFD manual provided a few cases which have been investigated. The case of the 2D NACA0012 airfoil seems most appropriate since the reference airfoil is also a symmetrical NACA airfoil. After a quick review of the validation, it has however become clear that this validation is not applicable to our project. First, the Reynolds number at which the experiment has been run is not comparable to our situation. The experimental data has been obtained at $Re=500$ instead of $Re=5000000$, which is the order of magnitude of wingsuit operation. Furthermore, the the CFD program data has been compared to the results from another CFD program, CFL3D , due to a lack of experimental data on low Reynolds numbers.

Since the CFD manual does not provide the desired validation, a new validation has been set up. The reference airfoil (NACA0020) would be a logical choice, but no wind tunnel data was found on the 2D airfoil. Therefore the choice was made to first use the NACA0012 experimental wind tunnel data from [28]. This airfoil is much thinner than the reference wing, but is symmetrical. Figure T.2 shows the validation of the numerical results. The results from XFLR5 and XFOIL are also incorporated. XFLR5 is the successor of XFOIL and the addition of XFOIL to the validation should make sure that no significant changes have been made to the XFOIL code which are not known.

The $C_l - \alpha$ plot can be seen in Figure T.2. When looking to the $C_l - \alpha$ results, it is clear that until an angle of attack of 11° the lift gradient is in the same order as the empirical and analytical data. From this angle of attack a drop in lift can be seen. This is the moment where the flow over the airfoil starts to separate near the trailing edge of the airfoil. This is not in accordance with the experimental data, which shows stall at a much larger angle of 16.5°. Three temporary hypotheses have been set up:

- Too thin airfoil
Which leads to other stalls characteristics.
- Too sharp trailing
This could lead to a shear of flow at the trailing edge which results into a larger vortex going from below to the top of the airfoil
- Too low simulation resolution
If the resolution is too low. The program might calculate different flow characteristics over the airflow.

Due to a lack of time only one hypothesis could be investigated. Since running a simulation with a higher resolution takes more time compared to the other two options, this hypothesis is not investigated. Since the effect of the other two is not known, the choice was made to run the simulation with a thicker airfoil. To run this validation, the NACA2421 was chosen since empirical data was found for this airfoil [29]. This empirical data has a Reynolds number of $6 \cdot 10^6$, which means that the Reynolds number of the simulation should be the same. Therefore the length of the airfoil is set to be equal to 1.5[m] and the flow velocity at $58m \cdot s^{-1}$. Finally the results of the simulations can be seen in Appendix T.3, in the $C_l - \alpha$ plot it can be seen that the lift drop at an angle of attack of 11° is gone. Nevertheless, the lift coefficient of the numerical data, does not match the lift coefficient of the empirical data at any angle of attack. Furthermore, it can not be seen on the plot where the airfoil is stalling. Therefore, due to time, one is not able to validate the CFD program for this project.

8

Performance

From the previous chapter a basic understanding of the aerodynamic properties of a wingsuit is obtained. In this chapter the performance of a wingsuit will be analyzed. First the flight performance is discussed [30], during which the glide ratio and free fall time will be analyzed. Next, the flight envelop will be analyzed in which its stall angle will be discussed.

8.1 Flight characteristics

In order to calculate the flight characteristics, first the equations of motions for straight symmetric flight with thrust are given in Equation 8.1. The variables used are thrust(T), drag(D), weight(W), path angle(γ), gravitational acceleration($g = 9.81 \frac{m}{s^2}$), speed(V), lift(L), time(t) and angle of attack(α). Also $\sin(\alpha_t)$, $\cos(\alpha_t)$ and $\cos(\gamma)$ are assumed to be zero.

$$\begin{aligned} T - D - W \sin(\gamma) &= \frac{W}{g} \frac{dV}{dt} \\ L &= W \end{aligned} \quad (8.1)$$

The first equation of Equation 8.1 can be transformed into the equation in Equation 8.2. P_a and P_r represent the power available and power received. The first and second term of the right part of this equation represent the potential and kinetic energy of the wingsuit flier.

$$\frac{(P_a - P_r)}{W} = V \sin(\gamma) + \frac{1}{2g} \frac{dV^2}{dt} \quad (8.2)$$

As this project uses no engine, $T = 0$ and P_a (power available) is also equal to zero. The wingsuiter is assumed to glide at constant speed, causing the term representing the kinetic energy to drop out. This results in the equation as seen in Equation 8.3.

$$P_r = VW \sin(\gamma) \quad (8.3)$$

8.1.1 Maximum range

Now the performance for maximum range is calculated. Flying at maximum range means flying at minimum drag. From Equation 8.3 and the definition of power required, $P_r = DV$, one can conclude that to fly at maximum range, one has to fly at γ_{min} . As $\gamma = \arcsin(-C_D/C_L)$, this in turn means flying at $(\frac{C_L}{C_D})_{max}$. In Chapter 6.4 and Appendix S, it was seen that $(\frac{C_L}{C_D})_{max}$ is about 4.2, in respect with a hang glider this is 3 times smaller, since a hang glider has a glide ratio of 12:1. If the wingsuiter would jump from a typical altitude of 3500m, subtracting 250m for safe canopy opening, he would be able to fly a horizontal distance of 13650m. Now to calculate at which speed the wingsuiter would have to fly, the resulting C_L from equations 8.4 are entered in Equation 8.5. This last equation was derived from the second equation in Equation 8.1. In this equations A = aspect ratio, e = Oswald efficiency number, C_L = lift coefficient, C_D = drag coefficient and C_{D_0} = zero lift drag coefficient. As an example, a wingsuiter weighing 80kg and flying at 1000m in a standard atmosphere ($\rho = 1.11164 \frac{kg}{m^3}$) with a calculated $C_L = 0.1679$, the wingsuiter would have to fly around $22.2m \cdot s^{-1}$. This is obviously too slow and this shows that there are problems with the analytical results.

$$\left\{ \begin{array}{l} (\frac{C_L}{C_D})_{max} \Rightarrow \frac{d(\frac{C_L}{C_D})}{dC_L} = 0 \\ C_D = C_{D_0} + \frac{C_L^2}{\pi A e} \end{array} \right\} \Rightarrow C_L = \sqrt{C_{D_0} \pi A e} \quad (8.4)$$

$$V = \sqrt{\frac{W}{S} \frac{2}{\rho} \frac{1}{C_L}} \quad (8.5)$$

If this value would be correct, by using simple trigonometry his falling time is then calculated to be 685.58s. Which is quite high as the speed is too low. As most wingsuits do not have any speed measuring equipment which they can check in flight, their attitude angle (θ) was calculated. This was done using the angle of attack (α) and flight path angle (γ) at $(\frac{C_L}{C_D})_{max}$ (-8° & -14° , respectively). Using the relation $\theta = \gamma - \alpha$, it was found that the maximum range is obtained by flying at an attitude angle of -4° , this means the wingsuiter is flying almost horizontal.

8.1.2 Maximum falling time

To glide for the longest time, one must glide at the minimum power required (P_r). This means flying at $(\frac{C_L^3}{C_D^2})_{max}$ as can be seen in Equation 8.6.

$$\left\{ \begin{array}{l} P_r = DV \\ D = \frac{C_D W}{C_L} \\ V = \sqrt{\frac{W}{S} \frac{2}{\rho} \frac{1}{C_L}} \end{array} \right\} \Rightarrow P_r = W \sqrt{\frac{W}{S} \frac{2}{\rho} \frac{C_D^2}{C_L^3}} \Rightarrow P_{r(min)} = (\frac{C_L^3}{C_D^2})_{max} \quad (8.6)$$

The C_L for maximum falling time can then be calculated using Equation 8.7 and the specifications from the analytical Chapter 6, $C_L = 0.21$. Using Equation 8.5 from the previous section, the speed at which the wingsuit will have to fly is found to be $19.9 \text{ m} \cdot \text{s}^{-1}$, which is again to quite low.

$$\left\{ \begin{array}{l} (\frac{C_L^3}{C_D^2})_{max} \Rightarrow \frac{d(\frac{C_L^3}{C_D^2})}{dC_L} = 0 \\ C_D = C_{D_0} + \frac{C_L^2}{\Pi A e} \end{array} \right\} \Rightarrow C_L = \sqrt{3C_{D_0} \Pi A e} \quad (8.7)$$

The maximum falling time can be found at an angle of attack of 10° . Analogue to the previous section, the pitch angle is then found to be 4° . Assuming the wingsuiter jumps from 3500m , the free fall time for maximum falling time is equal to 744.1s . Since these values seem too good to be true, it is concluded that the values are wrong due to too optimistic values for C_L . While the calculated values are incorrect, the equations and relations remain valid, and the difference between flying for maximum range and maximum falling time (endurance) can be observed.

8.2 Flight envelope

As no good 3D simulations with a good enough accuracy were run, it is impossible to say something about the minimum flight speed and stall point. However, the stall point is estimated to be somewhere around 33° , as can be seen in the plots in Chapter 6.

Part III

Conclusions

9

Conclusions

In this chapter the conclusions are presented. The survey and the analyses are the sources for the conclusions. Section 9.1 deals with the conclusions regarding the basics of current wingsuit operation. The lack of substantial research and scientific data and the results from the analyses during the DSE will be covered in section 9.2. Section 9.3 closes this chapter with the conclusions concerning the main topic of this report: the dangerous situations and safety aspects.

9.1 Current wingsuit operation

The interaction between the wingsuit and the person flying the wingsuit is very important. A different body posture can give a significant change in performance. Current wingsuits have a maximum glide ratio of approximately 2.5, but this is decreased to values around 1.5 by partially folding back the wings during proximity flights. These low glide ratios have corresponding high angles of attack, but the exact values have not yet been determined. During these flights, speeds between 150 - 250 km/h are reached, but a pull up maneuver to temporarily gain altitude is probably not possible. The pilot loads during high performance flights form a restriction of the flight time since the arm and shoulders are otherwise too exhausted.

9.2 Current wingsuit knowledge

At the moment very few wingsuits are designed with a scientific approach. Suit designs are based on previous versions. The process iterates by means of trial and error. But these trials are not always structured. For example, multiple modifications or concepts are tested in the same flight. This makes it hard to determine what modification affects the flight in what manner. The wingsuits are bench-marked in a few flight tracks. The flight is filmed, or the wingsuit test flyer tells the manufacturer of the performance of the wingsuit. For example, in this flight, “even though I flew with the same posture, this time I barely made it past the cliff, or I had several meters left”. This test method seems quite subjective and it does not always show the qualities of the modifications. When the performance of the modification is only visible at certain angles of attack, at certain flight speeds or only over a long track, they might be overlooked. It is also questionable if all wingsuit manufactures understand the physics involved with flying and falling. And, maybe because the market is quite small, the suit designs are neither tested in wind tunnels nor with numerical analysis. The angles of attack and L/D, stated earlier in this report, at which the wingsuit operates, are based on estimates. The wingsuit characteristics are determined by means of video analysis and GPS, but there is no real data available.

During this DSE, two wingsuits were tested in the OJF. The wingsuits were covered with tufts to indicate reversed flow and smoke was used to visualize the flow. The largest wingsuit, the Vampire 5, was tested at angles between 20° and 24°, with and without rig. The Phantom 3, was tested with rig at an angle of 27°. From the tufts it was learned that reversed flow occurs between the seams of the different wing compartments, the rig, near the leg wing and the wingtips. The Phantom 3 showed significantly more reversed flow than the Vampire 5. The second leading edge, created by the dented performance foam on the leading edge, influenced the flow negatively. The second leading edge leads to a less optimal leading edge and overall wingsuit shape. In films of wingsuiters on YouTube, these dents are also visible. From the analytical and numerical analysis it can be concluded that wingsuits fly at angles of attack of about 20°.

9.3 Dangerous aspects and situations in wingsuiting

It already has become clear from the movies that wingsuit proximity flying is dangerous. This presumption is confirmed by the accident rates: fatal accidents have increased from 6 fatal accidents in 2008 to 13 casualties in 2012. The wingsuit community consists of approximately 4000 people, with only a fraction performing BASE jumps. Furthermore a staggering 70% of the wingsuiters who filled in the survey have already witnessed a serious accident.

From the survey the two most critical phases are identified as the exit phase and parachute deployment.

As the wingsuiter leaves the mountain, the risk exists that he or she slips. A few fatal accidents happened after a wingsuiter lost his grip. The first seconds hereafter are crucial since the wingsuit is not yet completely inflated and the wingsuit has to reach its aerodynamic shape in order to become fully controllable in flight. Asymmetric inflation-speed or an inflation failure in one of the wings may lead to a spin with a fatal result. It is also crucial to get a perfect body position, otherwise an impact with the mountain might be inevitable.

A few dangerous aspects have been identified with a negative influence on the safety during flight. First of all, wingsuiters fly at very high angles of attack, which brings the angle of stall very close to the normal operating angle of attack. The survey also revealed that there is a very bad situational awareness amongst the wingsuiters. This combines into the unfavorable situation that the wingsuiter stalls easily and does not realise he or she is stalling. This is one example of an emergency situation which could end badly. Another situation could be the necessity to temporarily increase the glide ratio to clear a ledge. In current operation, wingsuiters decrease their performance by partially folding back their wings in order to have a performance margin when necessary. From the GPS logs which are presented at competition websites it is estimated that it is still not possible to produce a climbing flight. The fatigue of the pilot is identified as another potential safety threat during flight. The forces on the arms and shoulder might prevent the pilot from reaching the necessary performance position.

After the exit, the second most critical phase of wingsuit flight is the parachute opening. Because of the low heights at which BASE jumps are performed, only one parachute is present. The first step in the deployment in current wingsuits forms a significant safety risk. The pilot chute is grabbed by the pilot and brought into the free stream. To reach for the pilot chute, the wings have to be folded back and the suit will lose a lot of lift. Furthermore, the excessive fabric can cover the pilot chute. The pilot chute has to be brought far away from the burble to ensure proper functionality. After the pilot chute has been pulled out the main parachute, the wingsuiter needs to reach for his toggles for steering by unzipping his arms. This unzipping can take up to 4 seconds, which is precious time in an emergency situation. Several fatal accidents consist of the impact with a mountain wall because of a lack of steering capability by the toggles. Through the interview with Jarno Cordia it was discovered that the GoPro on the helmet of a wingsuiter can pose serious problems, the GoPro can get easily caught in the wiring.

Part IV

Recommendations

10

Physics of Concepts

This is the first chapter of the recommendations part of this report and covers the development of the detailed design. Here, the concepts chosen in the midterm review are analyzed and it will be discussed how these concepts solve the problems encountered in Part III. Depending on their use and complexity, they are further developed in aerodynamic characteristics (Chapter 11) or structural characteristics (Chapter 12). After this, the stability and control of the wingsuit are discussed (Chapter 14). Then, the final wingsuit design with all the concepts combined will be shown (Chapter 15) after which the sensitivity analysis will be dealt with (Chapter 16). The requirements compliance matrix and feasibility analysis is treated (Chapter 17) after which Part III is concluded with recommendations concerning our own proceedings and ideas about future research (Chapter 18).

The order at which the concepts in this chapter will be discussed is the following: anti-slip, quick-release, shoulder reinforcement, turbulators, vortex generators, passive flap, stall warning, droop, air tunnels, wing connection, Swiss pouch and integrated GoPro.

10.1 Anti-slip

In order to have the suit well attached to the body and prevent it from sliding up the legs, the edges of the wingsuit are pulled over the wingsuiter his toes. To prevent the suit from being damaged and to prevent the wingsuiter from slipping, these edges need to be reinforced. For this, rubber will be used because of its great anti-slip properties compared to for example Polyvinyl chloride (PVC) [31]. These outer soles made from rubber will have to be cemented to an inner sole, which will be stitched to the suit [32]. Anti-slip soles are already used in today's wingsuits. An example can be found in Figure 10.1.



Figure 10.1: Anti-slip

10.2 Swiss pouch

The Swiss pouch is a system currently being developed for releasing the pilot chute, PC, while flying, in a simple thumb/wrist movement unlocking the wingtip pouch. An example is shown in Figure 10.2. This is done without modifying the arm wings position and therefore makes this an ideal feature for large surface wingsuits. The ideal situation for releasing the PC is a laminar flow to avoid deployment hesitation, clean bridle deployment and no nearby snag points.



Figure 10.2: Swiss pouch pull by wrist twist

It is not the case that the Swiss pouch has been developed because the existing systems work perfectly, there are known issues with both the bottom of container, BOC, where the PC is stored in the bottom of the backpack, and wingsuit leg pouch, where the PC is stored in a leg pouch [33]. When using a BOC you have to grab the PC and throw it to the side, hence you have to close and open your wing, which will influence your flight path. Also, during the closing of your arms, some arm wing fabric can go between your hand and the stowed PC. At last, a loose PC throw can result in a deployment delay. In case of a wingsuit leg pouch, the pilot also needs to close and reopen his arms, just as with a BOC. Most of the wingsuit leg pouches do not use spandex or expandable material, but are done in ripstop with just a rubber webbing on the pouch opening. This construction has proven to induce hard pulls if your PC is not stowed properly. Next to some suboptimal design features, a miss pull is a serious problem for experienced jumpers when critical situations occur and the pilot refers to what he is used to.

For the wingtip pouch the under skin of the last arm wing's cell is replaced by a spandex or expandable material. This material is covered by a flap of normal wingsuit material. An example is given in Figure 10.3. The PC is stowed in the empty cell and is pushed inside when you close the flap. Due to the flexible material, the PC gives this last cell the same shape as if it was inflated. The pilot controls the PC with a thin and soft release handle that is placed around the wingtip gripper. The pilot holds the handle between his hand and gripper and can still operate the gripper without accidentally deploying the PC. The PC deployment can be done by rotating his wrist, thereby opening the pouch. After pulling the PC, the bridle from the last cell to the rig needs to be released. This is done by standard wingsuit shrivel flaps. The trailing edge of the arm wing is closed by Velcro and an inner sheath is added. When the release handle is pulled by the wrist, the PC is deployed which in turn pulls the bridle and the shrivel flaps are forced to open.

Just like any other design, the Swiss pouch also has downsides. It is more complex than the BOC and it takes a little more time to pack the PC and route the bridle.



Figure 10.3: Swiss pouch

10.3 Quick-release

When a wingsuit flight approaches its end, the pilot pulls his parachute and needs to free his arms in order to be able to grab the toggles. At the moment, zippers are used to release the arms for canopy flight. Although this is a relatively quick and safe procedure, zippers can fail and sometimes it takes a couple of seconds too long and a collision with a cliff might be the horrible result. Wingsuiters also acknowledged this danger in the survey [9]. As a safety feature, the quick-release system has been implemented to overrule the failed zipper. This feature consists of a plastic cable, which is directed through alternating loops of tough fabric. As this cable is pulled out of the loops, the arm wing will be released from the arm of the pilot. How this system is integrated in the wingsuit can be seen in Figure 10.4.



Figure 10.4: Current lay out of the quick-release system in a Phantom 3 wingsuit, an overview (left) and a close-up (right)

As an alternative design, a quick-release system can be incorporated as the primary method to release your arms. In the new design the parachute will pull the quick-release cables when deploying, hence no pilot effort is needed to release his arms. This design is primarily for BASE wingsuiting since deployment timing is more important for BASE than for skydiving. The downside of the existing system is the amount of effort needed to reattach the arm with the corresponding wing. In order to make this system widely accepted, the reattachment should be simplified. A way to solve this is to incorporate magnets at the outside of the loops, this simplifies the lining up and the reattachment of the safety cable through the loops tremendously. The loops will have alternating North and South magnets, which will attract each other such that the loops line up for the insertion safety cable. This can be seen in Figure 10.5. The magnets will have a 'U' shape such that the loops are also held open. The magnetic force will not be very large such that it holds the arm wing on its place. The weight of the small magnets can be considered negligible when also the rig is taken in account. Also, the positioning of the quick-release cable will change, since it must be attached to the canopy. This way, the canopy pulls out the quick-release on opening. A sketch of the location of this system is shown in Figure 10.5.

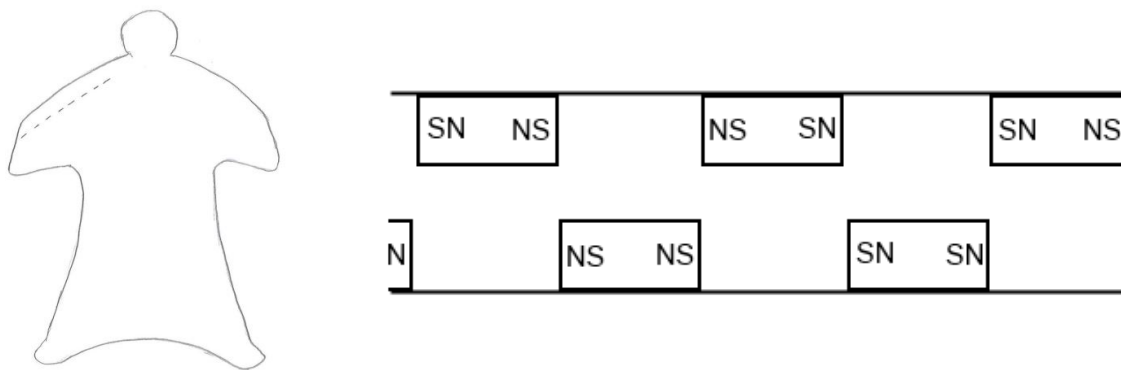


Figure 10.5: Sketch of the quick-release system, an overview (left) and a close-up of the magnets (right)

10.4 Shoulder reinforcement

This section will describe the shoulder reinforcement which was included in the wingsuit in order to reduce the loads on the wingsuiter. This is designed to make the flight more controllable but also to rule out some of the forces on the shoulder. Doing so the athletic performance of the pilot would no longer play a major role on the flight performance. This would mean the wingsuiter performance would become more standardized, hence more predictable and safe. CATIA renders of the shoulder reinforcement can be found in Figure 10.6.

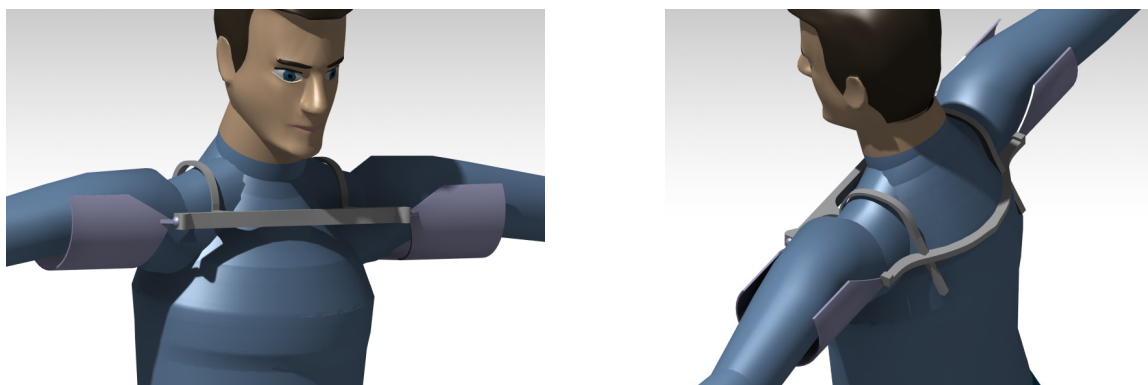


Figure 10.6: Shoulder reinforcement CATIA renders: front and back view

The shoulder reinforcements restrict the downward and backward movement, thereby reducing the loads

on the wingsuiter's arms. A downside of these restrictions is that the pilot is no longer able to pull his pilot chute. Designs have been made using joints, where the pilot could still pull his chute, however these were not very safe. Thus for all designs a Swiss pouch was mandatory. Since all designs required a Swiss pouch, the simplest and most straightforward design was chosen, this was the design that limited the backward and downward movement up to a certain point. A few sketches showing the mobility of the shoulder reinforcements are given in Figure 10.7. The structural aspects of the shoulder reinforcement is discussed in more detail in Section 12.2. Here also the weight is calculated. The material characteristics are further explained in chapter 13

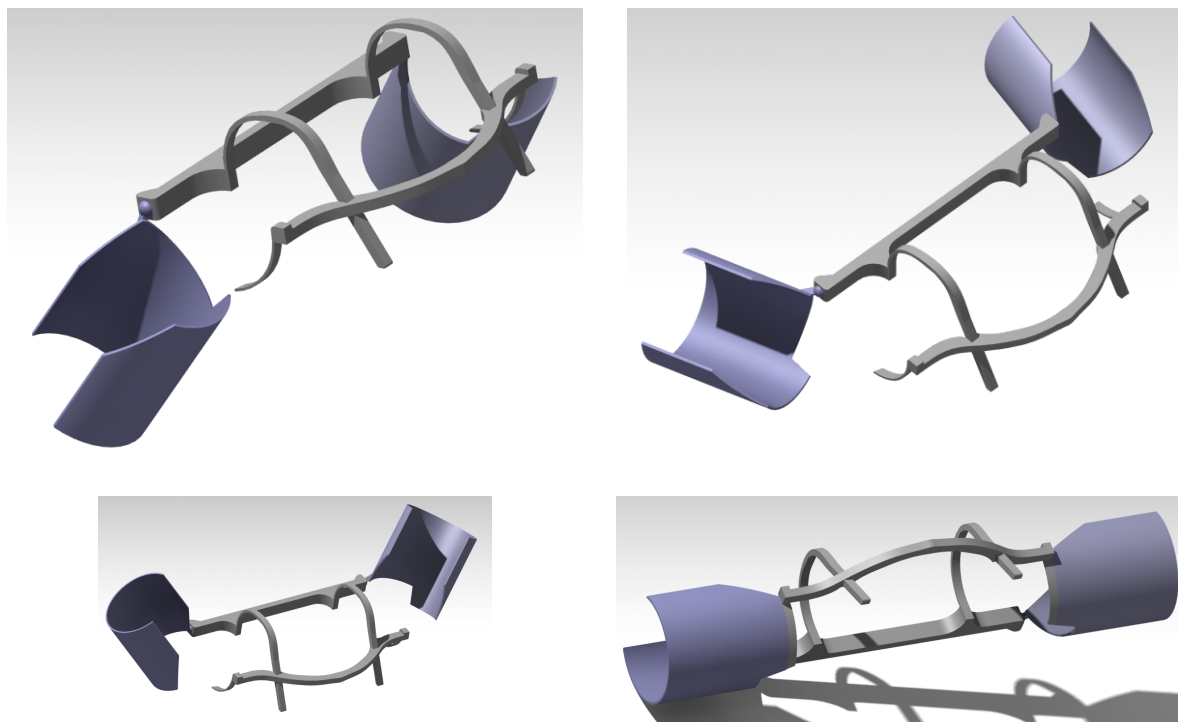


Figure 10.7: Shoulder reinforcement CATIA renders: mobility

10.5 Turbulator and vortex generator

In this section the possibility of adding turbulator strips and vortex generators to the wingsuit are studied. Turbulator strips and vortex generators can increase the overall maximum angle of attack, $C_{L_{max}}$, and reduce small separation bubbles. These can arise from an uneven upper surface since tubes are used for inflation but also from incorrect body positions. First turbulators will be discussed.

10.5.1 Turbulator strips

Turbulators work by creating small perturbations in the boundary layer which turns the boundary layer turbulent and more energetic. Hence they are more effective at low Reynolds number, where laminar flow is the most dominant. Because the turbulators work inside the boundary layer, turbulators should be smaller than the boundary layer thickness at that specific location [34]. Obviously, the exact shape and size of a turbulator strip depends on the application, and more specifically the Reynolds number[35]. The important question is whether the turbulator trips are indeed useful at the Reynolds numbers encountered in wingsuit flying. These are calculated to be between $1.63 \cdot 10^6$ and $5.44 \cdot 10^6$ in Section 6.1. A study was considered where it was concluded that at a turbulence intensity of 5% and a Reynolds number of 365,000 no real changes could be observed anymore in the $C_l - \alpha$ curve[36]. Moreover, another study concluded that turbulators should not be used at Reynolds numbers above 100,000 because turbulators may decrease $(\frac{C_l}{C_d})_{max}$. This because the turbulator itself may cause the flow to separate

hence increasing the pressure drag [37]. Since wingsuits are flown at Reynolds numbers far above 100,000 and with turbulence levels of at least 5%, turbulator strips were not included in our design.

10.5.2 Vortex generators

Vortex generators (VGs), applied on a wing, generate vortices over the upper surface. The vortices bring highly energized flow from the freestream inside the boundary layer. So in contrast to turbulators they also influence the flow outside the boundary layer. This means they energize the boundary layer making it more resistant to flow separation [38]. However, VGs impose an increase in drag caused by the increase in pressure, derived from flow blockage by the device itself, and additional parasite drag due to additional skin friction [39]. That is why normally it is more favorable to change the airfoil thickness or length rather than using VGs. This is however not possible as the wingsuit is limited by the size of the human body. Additionally, even though they will have higher values for Cl_{max} , they will often stall at lower angles of attack [35] and more abruptly [40]. Finally it was found they have a positive effect on hysteresis [41], which is quite advantageous in wingsuit flying. Summarizing this paragraph, VGs would be a good addition on wingsuits even though they would give a small increase in drag. However, the main problem with VGs is that they induce more sudden stall characteristics. So, even though some VGs increase the stall angle, they might still make the wingsuit less controllable. There is however a solution to this problem by having VGs in front of the passive flaps only. These are located on the leg wing; more information on their exact location is given in Chapter 11.3. Finally it is noted that the height of the turbulator strip should be at least the height of the boundary layer (almost equal to, to have the optimum performance).

Not all vortex generators work outside the boundary layer. More recent studies (Lin et al. 2002; Yao et al. 2002) looked into sub-boundary layer VGs. These type of vortex generators only mix the mean-flow momentum within the boundary layer. They have been showed to be much more efficient to standard type of VGs. Giving better results for to their drag penalty. At this point it is clear that VGs in combination with the passive flap would greatly improve our design. However which type of VGs would improve or design the most is hard to say. There is no data available of the flow around wingsuits. So to see which type of vortex generator would produce to most favorable results testing should be done. A first estimate of their shape, as to give a idea of what type of VGs would be test, is given next.

Now that the decision is made to use VGs, the detailed design can start. The more efficient sub-boundary layer will be used for the preliminary sizing, if they proved to be not working, standard VGs could still be used. Some amount of research is already put into the position for passive flow controls using this type of VGs. Recently, Betterton [42] did a detailed study on the wake of VGs. These studies were inspired on those conducted by J.C. Lin et al. The main conclusion was that the spaced counter rotating vane-type VGs, also used by J.C. Lin et al., are the most effective devices. Another recent study [43] showed the influence of the form of these type of vane-type VGs, the triangular ones were most effective. These were test on a 2D airfoil. For swept 3D wing, co-rotating VGs produce better results. So triangular co-rotating VGs will be used. They are triangular plates mounted normal to the airfoil surface. An example can be found in Figure 10.8. Here the parameters that define a vortex generator can be seen, an overview is given:

h Height of the triangular spaced counter rotating vane-type vortex generator

l Length

f_{pd} Skew angle

X_d The leading edge of the triangles is aligned transversely at this abscissa

XCf_{min} Position of the minimum skin friction coefficient

ΔX_{vg} The distance between the trailing edges of the devices and XCf_{min}

\sim Transverse spacing of the devices

L The distance between the trailing edges of two plates

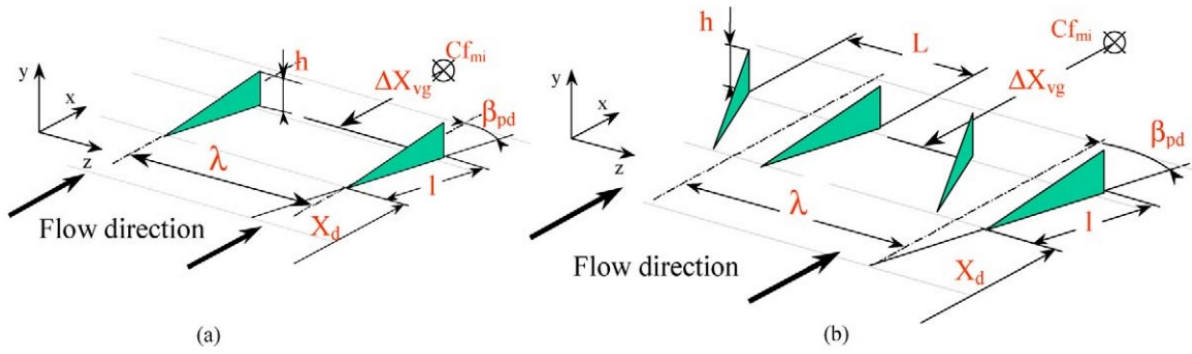


Figure 10.8: Geometry of (a) co-rotating passive devices, (b) counter-rotating passive devices.(reprinted from [42])

Determining the actual optimum shape and location of the sub-boundary layer VGs for the conditions encountered in wingsuit flying can only be done with a CFD analysis combined with wind tunnel tests, which were both found not feasible within this DSE limitations. The CFD tests in the numerical part of this report were done with a resolution accuracy of only 1.25[cm] (due to a lack of time) which is too low to modulate the boundary layer and the VGs. Nevertheless, an estimation is given, which might be useful for the future for more research on integrating of VGs on a wingsuit. This estimate is based on the studies executed by Godard & Stanislas [43]. Their studies were based on those of Betterton [42]. The most effective parameter relations for triangular plates as found by Godard & Stanislas can be found in Table 10.1. Using a boundary layer thickness of 1[cm], which is only a rough estimate, and assuming XCf_{min} to be located at the start of the passive flap, these formulas can be solved. It is important to keep in mind that these relations were obtained using different conditions. For example, a bump model instead of an actual wingsuit was used, the 3D effects were ignored, Reynolds numbers were different (max speed of 10[m/s] in test by c), their surface was of steel instead of Para-pak, etc. Nevertheless, these results, given in Table 10.2, are a good starting point for future research and give a good indication in this preliminary detail design of what the VGs will look like. A sketch of the VGs integrated with the wingsuit is given in Section 11.6.1.

Table 10.1: Effective parameters as found by Godard & Stanislas

Model used	Type	Geometry	$\frac{h}{\delta}$	$\frac{\Delta X_{vg}}{h}$	$\frac{l}{h}$	$\frac{L}{h}$	$\frac{\lambda}{h}$	β_{pd}
Bump	Counter rotating	Triangular	0.37	57	2	-	6	18°

Table 10.2: Estimates vortex generator design parameters (in meter)

h	ΔX_{vg}	l	L	λ	β_{pd}
0.0037	0.211	0.007	-	0.06	18°

10.6 Passive flap & stall warning

In nature, birds have found a simple way to prevent their wings from stalling near the trailing edge. They have additional feathers that can pop up to prevent further proliferation of flow separation. The main working principle depends on the blockage of the reversed flow from the trailing edge region to the suction peak, resulting in a delayed flow separation. The passive flap would split the separation region into two, and cause a recirculation flow that is more capable of pulling the freestream flow down, thereby creating more lift. It can be seen that the flap finds its own equilibrium position and that this position is stable [44].

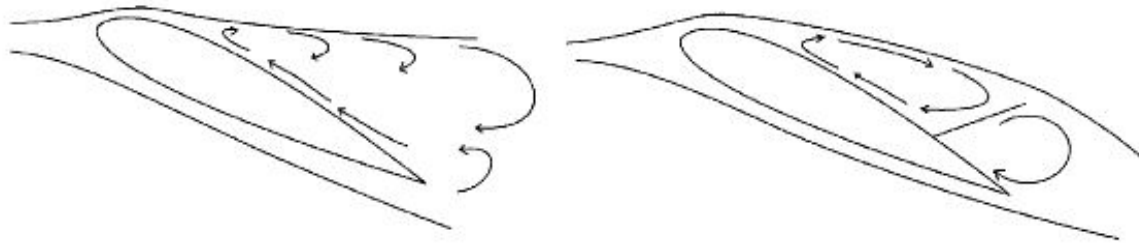


Figure 10.9: Sketch of the principle of a passive flap on an airfoil [45].

The advanced wingsuit design would also include a stall warning for the wingsuiter. This is linked to the passive flap. Thus, when the passive flap reaches a certain angle, the pilot needs to be aware of that. This way, the pilot would know that he/she is near a stall and should take care that the angle of attack does not increase more.

10.6.1 Design of the passive flap

According to [45], the chord of the passive flap and its chordwise placement follows from a 2D airfoil analysis. The spanwise placement of the flap is done with the knowledge of the 3D airflow behavior on the wingsuit. Passive flaps work best if they are located away from the wing tips since wing tip vortices reduce the local angle of attack and therefore delay stall significantly at the tips. What the stall characteristics along the wingsuit are, depends greatly on the geometry of the suit, e.g. sweep. During the wind tunnel experiment, the wing tips were very prone to stall because of the movements by the wingsuiter and because of the sweep angle of the arms. It must also be noted that the effectiveness of a passive flap is not yet tested in the unsteady flow field of a wingsuit.

The principle of the passive flap is tested for low Reynolds numbers[45]. It is said that higher Reynolds numbers, and hence higher freestream velocities, could result in larger flap displacements due to a more powerful recirculation. Higher Reynolds numbers caused a slightly delayed post-stall recovery and a slightly less relative increase in lift. However, the post-stall lift coefficient was higher. The effect of a passive flap can be seen in Figure 10.10.

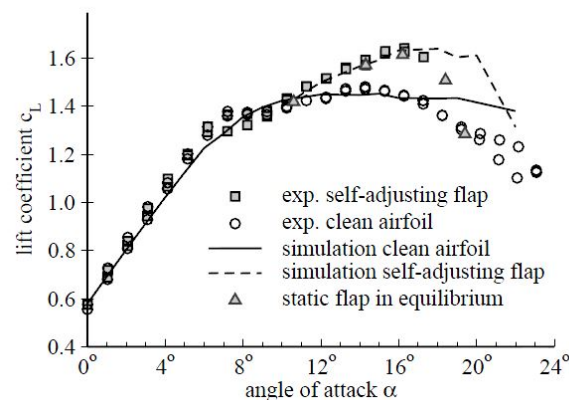


Figure 10.10: Effects of a passive flap on the lift coefficient [44].

Attention needs to be paid to the material and construction of the passive flap. The weight of the flap needs to be such that the flap starts moving upward when there is reversed flow. The flap also needs a certain stiffness to avoid phenomena like flutter or other vibrations. The passive flap will consist of a frame in the shape of the letter 'N'. Two vertical beams to counteract the bending forces and a diagonal beam to keep the construction from bending sideways. Fabric is spanned over the construction and

attached to the two outer beams. A clarification of this construction and more details about the design of the passive flap can be found in Chapter 11(aerodynamics) and Chapter 12(structure).

10.6.2 Design of the stall warning

The stall warning system needs to be as simple, but effective, as possible. The system needs a trigger to start working and a method to give a signal to the wingsuiter. The trigger will be linked to the angle limiter of the passive flap. If a tension force is applied to the trigger by the passive flap, this trigger will send a sound signal to the headset of the wingsuiter. This can be seen in Figure 10.11.



Figure 10.11: Sketch of the principle of the stall warning.

The thick black line is the passive flap at its maximum angle where it is held in position by thin wires. These thin wires apply a tension force to the measurement unit just under the surface of the suit. This unit then sends a signal to the FlySight¹[46] device of the wingsuiter, who hears a sound signal making him/her aware of the near stall situation. The wire will be like the wires used in the fishing sport, these wires can sustain a lot of tension and are very thin. The measurement unit is going to be a stationary tension meter like the ODT seen in Figure 10.12. This sensor can measure forces from 2 gram to 1 kilogram.



Figure 10.12: Picture of a stationary tension meter

The wire will be stretched around the three circular points. The more the wire is tensioned, the more the circles will align. This way the meter could measure the tension force in the wire. The meter has a maximum tension detector that provides a low voltage signal when tensions exceed the user set limit [47]. This meter should however be adapted to make sure it can be attached to the wingsuit and such that the wire does not get loose from between the circles. To make sure that the measurement unit sends the right signal at the right tension, the tension meter will need to be calibrated before use.

¹FlySight is an audio device attached to a GPS receiver. This device can provide information on the glide ratio performance or fall rate.

10.7 Droop

Another concept is the variable droop leading edge. The principle is that the wingsuiter can apply a droop of the leading edge by (endo)rotating the arms and move it back by (exo)rotating the arms or with pronation/supination of the forearms. A droop is a leading edge high lift device. An example is given in Figure 10.13. It moves the nose of the wing towards the flow (hence bringing up the stagnation point). This way it delays stall and shifts the $C_L - \alpha$ curve to the right. Research has shown that droop reduces the tendency of the airfoil to enter the dynamic stall state. Even when it does, the strength of the dynamic stall vortex is significantly reduced [48]. The research that already has been done applies to droop leading edges that rotate at about $0.2c$. Since the shoulders of the wingsuiter (which serve as the natural hinge points of the droop) are located at the leading edge, the chord length of the applied droop will be much shorter and thus less effect is expected. The droop also has to be made of a stiff material in order to move the leading edge further upstream, away from the shoulder. It was also found that outboard leading edge cuffs were enhancing stall behavior while leading edge cuffs over the entire span resulted in poor spinning characteristics [49].

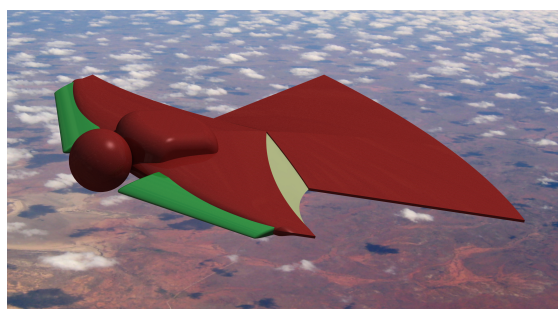


Figure 10.13: Detailed CATIA render of droop

When considering the droop of the wingsuit, a distinction can be made between a static and dynamic situation. The purpose of the droop is to increase the stall angle and decrease the drag at high angles of attack. For a dynamic situation, the lift slightly decreases at high angles of attack while the drag greatly decreases [48], which means an increase of the L/D ratio. Research has also been done into static situations, here the drag and lift coefficients did not vary a lot, but the loss of lift due to stall was less [49]. This can be seen in Figures 10.14-10.15.

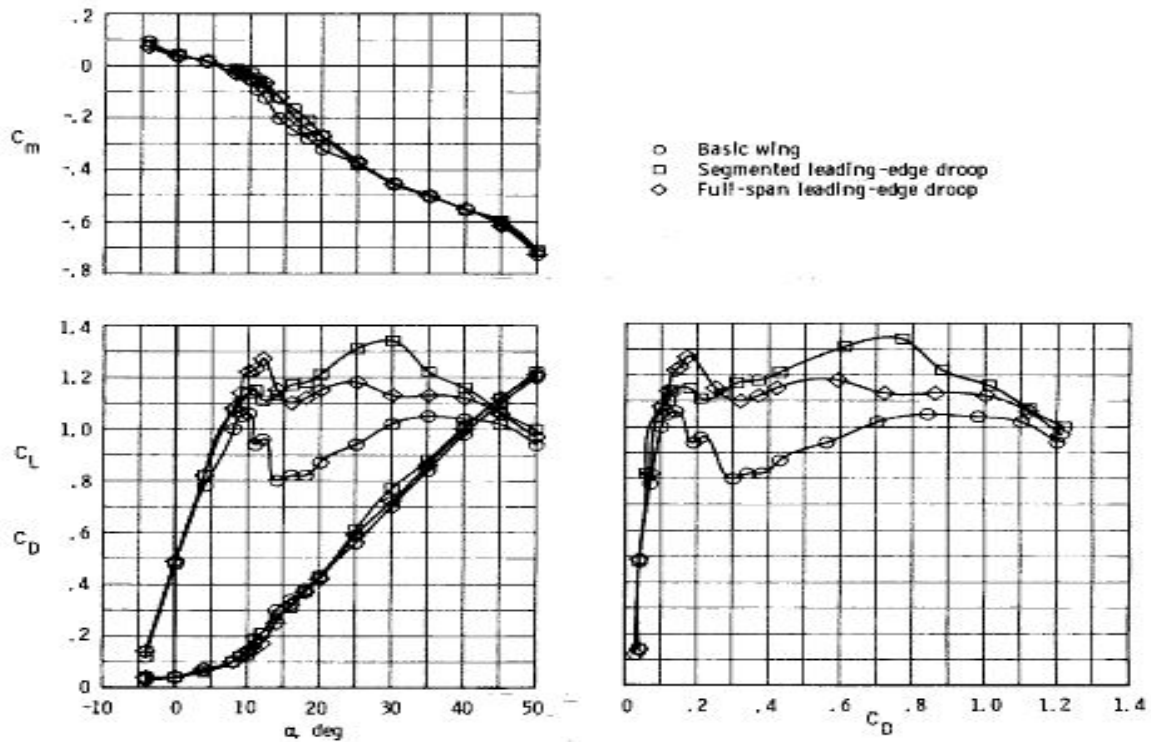


Figure 10.14: Effects of droop on the static performance [49].

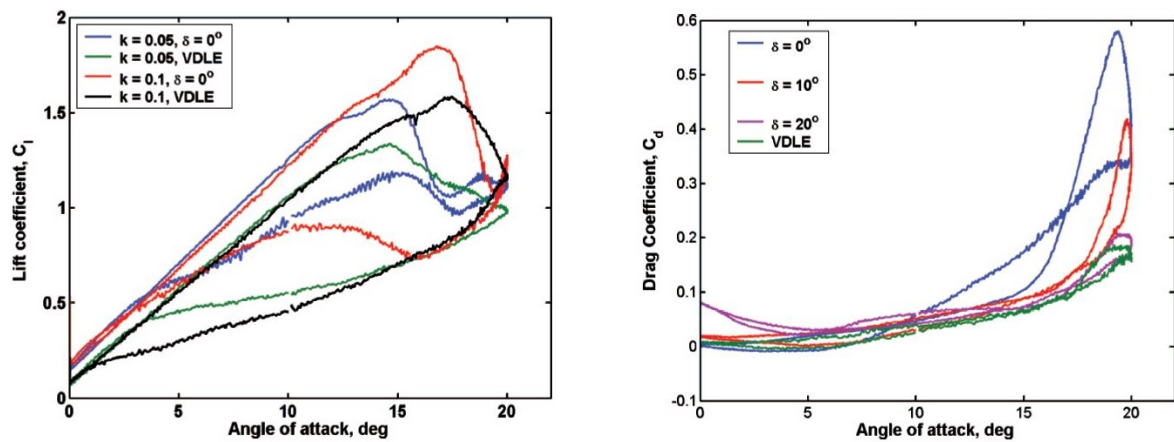


Figure 10.15: Effects of droop on the dynamic performance [48].

Figure 10.14 shows the results of research done by NASA. It shows the C_L , C_D and C_m with different leading-edge droop configurations. This is data from a static force test. Figure 10.15 shows the results of a test where the angle of attack was varied dynamically in order to simulate an unsteady simulation. The highest drag coefficient corresponds with no droop angle. The higher the droop angle, the lower the drag coefficient becomes at high angles of attack. More about the design of the droop can be found in Chapter 11 and Chapter 12.

10.8 Air tunnels & wing connection

A way to improve the performance of a flow field around a body is to move the transition point aft and hence delay separation. If an airflow separates from a smooth body it means the momentum in the

flow is not sufficient to overcome the adverse pressure gradient. Therefore, a way of dealing with this problem is to re-energize the flow in order to cope with the pressure gradient. Blowing a boundary layer can be done, among others, by steady blowing or periodic perturbations. Research showed that periodic perturbations have a larger improvement, whereas combining this method with a small steady flow has a less positive effect. [38] Steady blowing is the least complex method, but it might be possible to develop a system to incorporate the more effective periodic perturbations in a wingsuit, but for our time frame it is considered too complex.

On the present wingsuits the airflow behind the rig is disrupted, which asks for (aerodynamic) improvement. On the Phoenix-Fly Vampire V4 a slot is made between the legs just under the crotch. This slot redirects energetic air onto the leg wing just above the knee. This is already an improvement, however, the fabric between the rig and the extra inflow is still far from optimized. The aim of the concept described in this part is to improve the aerodynamics in that very area. Next to determining the method of putting this extra energy in a flow, it is also important to decide where the air input is coming from and how the tubing is positioned. Since the aim is non-powered flight, ram-air inlets will be used and can be placed on the belly of the suit around the height of the sternum. In order to limit the amount of energy lost in the air tunnel tubing, the number and size of turns should be kept to a minimum. Another option is the branching of the pressurized tubes of the arm wings. This saves the additional two inlets on the suit.

As a part of the flow optimization behind the rig, a smooth transition from the rig to the suit fabric is an important feature. Performance foam can be used to incorporate both this transition and house the exit of the air tunnels for re-energizing. Attention should be paid to the canopy, since the performance foam should not interfere with the deployment of the canopy. More details about this foam can be found in Chapter 13. Another feature that was investigated is the use of vortex lift, which is common on fighter aircraft with delta wings to increase flight envelope by allowing larger angles of attack. Fighters use wing-body strakes along the nose to generate vortices over the wing surface which increases lift, but also increase drag. This is useful for supersonic fighters for landing and extreme maneuvers because the vortex lift increases the airfoil camber. However, since the wingsuit is non-powered, the drag is a big issue and therefore vortex lift will not be implemented.

The ram-air inlet should not interfere with the rig harness. A ram-air intake uses the static air pressure to direct air into the cells. The air is decelerated inside the wingsuit, increasing the static air pressure inside, thus allowing a greater mass flux to enter and give the cells the desired airfoil shape. Just as used in present day wingsuits, inlets should be reinforced with plastic rings such that the inlet cannot close in flight. The air tunnel connecting the ram air inlet and outlet can be made of normal wingsuit fabric, possibly reinforced with plastics to obtain and maintain the optimal pliancy and rigidity and ensure maximum mass flow. The width should be such that it does not interfere with the arm wings but allows for an optimal mass flow. Whether the tunnel should converge or diverge towards the exit depends on the chosen outlet size and shape and the momentum deficit in the boundary layer. This is treated in detail in Chapter 11. The optimum exit point is close to the point of minimum pressure around the bottom of the rig. This should be done as after the minimum pressure point, the adverse pressure gradient has to be dealt with and re-energizing the flow does have a significant beneficial effect from that point on.

The outlet should be combined with the performance foam. Attention should be paid to the wing connection, which should also be integrated in the same piece of performance foam. The wing connection concept consists of the left and right wing being connected. This will be done on the back of the suit just behind the rig. In combination with performance foam, this results not only in a better aerodynamic shape of the back, but also preventing the danger of getting into a spin caused by deflation of one wing. However, since both wings also inflate each other, there is the risk that if you suddenly close one wing, the other might get inflated too much. Fortunately, when each wing has its own inlet, this overpressure can exit the wing by this inlet. Another option might be an overpressure valve in each wing that prevents one wing being affected too much when the other wing is suddenly closed during, for example, a maneuver. The concept can be seen in Figure 10.16.

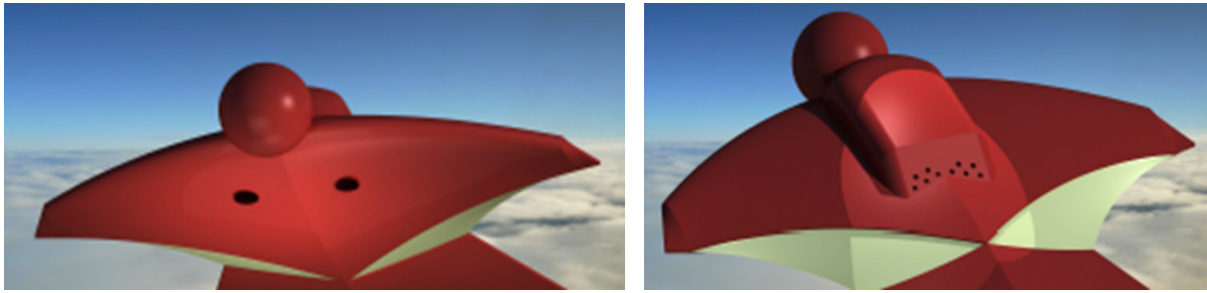


Figure 10.16: Air tunnels concept.

10.9 Integrated GoPro

Since the development of small high definition cameras, a lot of wingsuiters jump with cameras mounted on their helmets to film their jump. These cameras often disturb the airflow around the helmet and thus affect the performance of the wingsuit. Especially when wingsuiters mount more than one camera on their helmet, the effects could become very unfavorable. An extreme situation of cameras mounted on a helmet can be seen in Figure 10.17.



Figure 10.17: Cameras mounted on the helmet of a wingsuiter.

A number of wingsuiters mount two cameras on their helmet, one to film the wingsuiter's view as he is flying and another one to film the back of the suit and other wingsuiters flying behind. Therefore, the helmet could be adapted such that there are two places to insert a camera in the helmet, both at the front and the back. These holes can of course be sealed if no camera is inserted. Due to limited time in this preliminary design, this concept is not worked out furthermore. A sketch of where the cameras could be integrated in the helmet is shown in Figure 10.18.

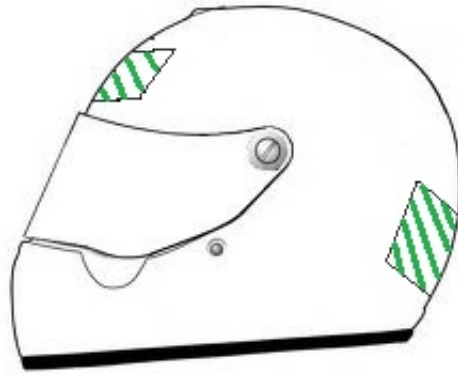


Figure 10.18: Cameras inserted in the helmet of a wingsuiter

11

Aerodynamic Characteristics

In this chapter, the aerodynamic characteristics of the basic wingsuit, the passive flap, leading edge droop, air tunnels and wing connection are further developed. These are compared to the results of the numerical simulations.

11.1 Basic wingsuit

To get a better understanding of the increase of aerodynamic performance of the concepts, first the aerodynamic properties of a wingsuit has to be known. These aerodynamic characteristics are determined in Chapters 6 and 7 where the results and conclusion of aerodynamic calculations are shown.

11.2 Vortex generators

Since no simulations about the effect of vortex generators could be performed, there are no estimates of the performance increase due to the vortex generators.

11.3 Passive flap

In order to be able to design the passive flap, flow visualization is needed. With flow visualization one can learn of the thickness of the shear layer, separation and its behavior and design the passive flap such that the trailing edge of the flap the just slightly touches the detached shear layer.

The location of the flap will be on the leg wing, since the wing tip vortices at the arms make the stalling process more complex. Furthermore, separation is likely to start at the trailing edge. Therefore the passive flap is placed on the leg wing to prevent trailing edge stall. The span of the flap will not be as wide as the entire leg wing since the downwash from the tips would counteract on the flap [45].

It was found in the experiments that the trailing edge of the movable flap should be located slightly upstream ($\geq 1\%$ chord) of the trailing edge of the airfoil, otherwise it would not respond properly to flow separation. On the other hand, the farther upstream the flap is located, the farther upstream the flow separation would have to have already spread before the flap starts to respond. The larger the flap is, the more increase in lift is created. However, for large flaps, the behavior of the flap is different for increasing angles compared to decreasing angles. Opening of the flap would occur if flow separation has reached the upstream edge of the flap, while the reattachment only would occur for an angle of attack where the reattachment line of the normal airfoil (without passive flap) has moved downstream of the flaps trailing edge. This hysteresis would make the passive flap and the wingsuit harder to handle [44].

It is found that an optimum angle δ is achieved when the flap just slightly touches the detached shear layer. In the case of lower flap angles, the flap remains inside the reverse flow region which it splits into two parts. When the flap has a larger angle, the passive flap acts as a spoiler and creates only additional drag.

Since the working principle of the passive flap is based on flow separation, the effects of it on the performance can not be simulated correctly using JavaFoil. The sizing of the passive flap will be done according to some flow visualizations in the CFD program that is used for the numerical analysis in Chapter 7. The span of the flap will be 80% of the wing span at the feet of the wingsuiter since this was found to be optimal in literature [45]. No further research is done to the span of the flap because of the computing

time and the high complexity of 3D flow simulations on a wingsuit.

A 2D simulation of the chosen airfoil is performed to visualize the flow separation at the trailing edge. Reversed flow was clearly seen at in the CFD program. Due to this reversed flow, the principle of the passive flap could be working and really enhance the performance of the wingsuit.

As already stated in Chapter 7, the performance increase of the passive flap is very dependent on its dynamic behavior since it needs to put itself into an equilibrium position. This makes it very hard to simulate the passive flap at a realistic opening angle for a particular angle of attack. Xflow is able to simulate the fluid-structures interaction, this could be an aid in the detailed part of the design process. Unfortunately, sufficient time is lacking for the computations. Since the placement of the passive flap is connected to the stall warning, real flight tests should be performed to make sure that the passive flap does not trigger the stall warning too early. Therefore more analysis on the stall angle and the flow field during the early stall needs to be done in order to design the passive flap and the stall warning in more detail.

11.4 Leading edge droop

Because the arm wings are very prone to separation, the droop leading edge would be placed on the arms. This would also come in handy if the mobility of the arms of the wingsuiter is taken into account. It is much easier to only rotate the forearms instead of the whole arms. In Chapter 10, it is also stated that outboard droop is more favorable than inboard droop, for spinning and stalling characteristics. But since there would be a discrete change in the leading edge, the leading edge (and thus the droop) is applied on the whole arm. Although it could give many advantages, dynamic situations will not be taken into account in the design process, since time is limited for this preliminary design.

At first, an estimation of the effect of the droop on the C_l and C_d is made using the 2D airfoil that is chosen in the analytical simulation. This effect is simulated in JavaFoil and the results are compared. Next, the effect of the droop on the whole 3D wingsuit is estimated. The 2D results from JavaFoil are converted to the 3D situation with some correction factors, as is already done in Chapter 6. The results are compared and shown in Figure S.3 in Appendix S. The Reynolds numbers that are used in the simulation were also calculated and used before in Chapter 6.

Of course, in this preliminary design of the droop leading edge there are several assumptions made that need to be noticed. The assumptions are as follows

- At first the thickness of the leading edge in the real situation is as thick as the arm of the wingsuiter. The thickness in the 2D simulation is the assumed thickness of the simplified airfoil.
- A real wingsuiter will apply a varying droop angle along the leading edge because of the rotational constraints of the arm. The simulation used constant droop angles.
- In JavaFoil, the hinge point of the droop in the model is located more to the back of the airfoil than the shoulder is in the real situation.
- JavaFoil uses several assumptions itself, these are all described in Chapter 6.

It must be noted that because of the thickness of the simulated airfoil, the effect of the droop is less noticeable in the airfoil shape. When designing such a droop leading edge, the mobility of the wingsuiter must be taken into account. A human arm has two hinge points; the shoulder and the elbow. In these hinge points the arm can rotate and bend. The leading edge on the forearm can rotate the most since it can rotate about both the shoulder and the elbow. The humerus (from shoulder to elbow) can be rotated less easily.

First, a droop angle of 10° at a hinge point of $0.25c$ is used. Due to this droop, the airfoil shape proves to have a higher stall angle of attack and thus has a higher $C_{L_{max}}$. The drag of this shape turns out to be less than the original shape, especially at high angles of attack. These improved characteristics give a slightly worse glide ratio at low angles of attack but an increase in glide ratio at very high angles

of attack. This shows that the droop should be applied by the wingsuiter at angles of attack near the stall angle (Not in optimal glide flight). The droop angle proves to be more effective for higher Reynolds numbers, however unpredicted spikes occur in the data. The results can be found in Appendix S.3.

To approach the real situation better and to get new results without the spikes, an iteration is made with a new droop configuration. The new droop angle is 20° and the hinge point lies more to the front at $0.15c$. On a wingsuit, the hinge point will lie more to the front of the airfoil but the droop would also be the more noticeable due to the thinner airfoil shape. Because of the lower droop area of this configuration, the effect on the C_L is less favorable. However, the droop still contributes to a higher glide ratio at high angles of attack. The drag at higher angles of attack is less than the original, this however is only a minor effect.

The results obtained from JavaFoil are only used to give a rough estimate of the effect of such a droop leading edge. Therefore, a 2D simulation is run in the CFD program to validate the method used and to visualize the flow field around the airfoil. Only the droop configuration with the 20° droop angle is compared to the original airfoil shape. These results can be found in Appendix U.2.1.

From these results it could be concluded that the droop leading edge is a feasible concept. It can improve the performance of the wingsuit, especially at higher angles of attack. Since the simulations of the higher angles of attack are not validated, it is not possible to come up with an exact quantitative analysis of the performance increase by the droop. At an angle of attack of 20° , the lift of the drooped airfoil is lower as the original shape, which was not expected. But the lower angles of attack do benefit from a droop. At 15° angle of attack, the droop increases the lift with 25%. The drag is decreased with 2%. This gives an L/D increase of about 27%. However more analysis is needed in order to ensure that the effect on the real wingsuit will be in the same order. Probably, when more detailed analysis is done and a more realistic droop model is used, the performance increase will surely be less high. These results are also elaborated on in Section 11.6.2.

11.5 Air tunnels & wing connection

As discussed in section 10.8, air tunnels redirect air from the inlets at the belly side of the suit to the outlets just below the rig. In this section, calculations will be done regarding the cross-sectional area of the inlets and outlets. Since wingsuiting occurs at low subsonic speeds, the flow is assumed to be incompressible. The density is assumed to be constant, and thus for a constant cross-sectional area and a constant velocity, the mass flow rate is assumed to be constant. The formula for the mass flow rate is shown in Equation 11.1.

$$\dot{m} = \rho V A = cst \quad (11.1)$$

Since the air density is assumed to be constant at a certain altitude and at a fixed velocity the cross-sectional area of the inlet and outlet will determine the achievable mass flow rate.

In order to calculate the mass flow rate required through the air tunnels, the boundary layer around the airfoil should be observed. Looking at the belly side of the wingsuit at the position of the inlets, the pressure at that point can be used in the calculation for the required mass flow rate. For the location of the required outlet flow, just below the rig, it is important to know the boundary layer profile to determine how much separation has occurred at that very position. When the amount of separation is known, one can calculate with the momentum thickness how much energy is needed to compensate for the separation at that point. It should also be taken into account that the air flowing through the tubing also results in some energy loss.

For the calculation of the momentum deficiency in the boundary layer, the boundary layer thickness, displacement thickness and momentum thickness should be defined [50]. The boundary layer thickness is defined as the perpendicular distance from the wall to the point where the flow velocity has reached essentially the freestream velocity. The point that is essentially the freestream velocity is customarily defined as $v = 0.99v_0$, where v_0 is the freestream velocity [$m \cdot s^{-1}$]. The displacement thickness can be seen in Figure 11.1 and is the distance a streamline just outside the boundary layer is displaced away from the wall compared to the inviscid solution. The momentum thickness is the distance that, when

multiplied by the square of the freestream velocity, equals the integral of the momentum deficit across the boundary layer. The displacement and momentum thicknesses are used to obtain the shape factor of the boundary layer. The shape factor is used to determine the nature of the flow and is defined as

$$H = \frac{\delta^*}{\theta} \quad (11.2)$$

where δ^* is the displacement thickness and θ is the momentum thickness. Also, the boundary layer thickness is referred to by δ . The higher the H , the stronger the adverse pressure gradient. This can greatly reduce the Reynolds number at which transition into turbulence may occur. The displacement thickness and momentum thickness can be written as

$$\delta^* = \int_0^\delta \left(1 - \frac{v(y)}{v_0}\right) dy \quad (11.3)$$

and

$$\theta = \int_0^\delta \left(1 - \frac{v(y)}{v_0}\right) \frac{v(y)}{v_0} dy \quad (11.4)$$

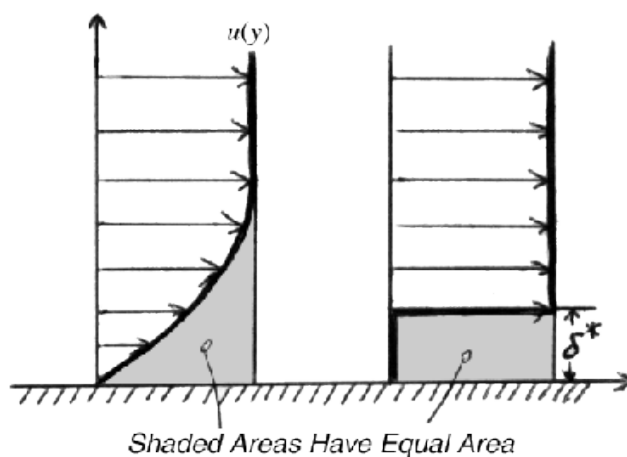


Figure 11.1: Total momentum for displacement thickness of boundary layer. [51]

In order to find the pressure distribution over the boundary layer just aft of the rig, use can be made of a step shape approach [51] since the aft section of the rig has a backward-facing step shape. The article that was just cited to in the previous line did research in determining at subsonic speeds the distribution of surface pressure and that of mean and fluctuating velocities in the flow over a backward-facing step. In Figure 11.2 the step is shown together with the visualized flow. The cavity flow which is indicated in Figure 11.2 is a formation of reverse flows and vortices. Experiments were conducted in both a wind tunnel and in a water tank through which the model was towed. In all cases in the wind tunnel, there is a negative pressure found on the step face, called the base pressure. This is followed initially by a slight drop in pressure downstream of the step, after which a rather rapid rise of pressure occurs. This indicates the reattachment of separated flow on, in our case, the leg wing. “It is seen from these results that the pressure distribution is rather insensitive to the changes in the step height as well as in the thickness of the approaching boundary layer. In particular, the base pressure is essentially the same for different step heights except for very low steps, and the pressure rise by reattachment increases slightly as the height increases.” [51]. Figure 11.3 shows the pressure distribution on the step face and the bottom surface for various heights, h . The maximum step height used in [51] is 4cm , which is smaller than the actual base rig. However, no information could be found on a thicker backward facing step. Another aspect of the base rig is that it is not an exact rectangle, but has smoothed corners. This will definitely affect the flow, but as a first approximations the article [51] will still be used.

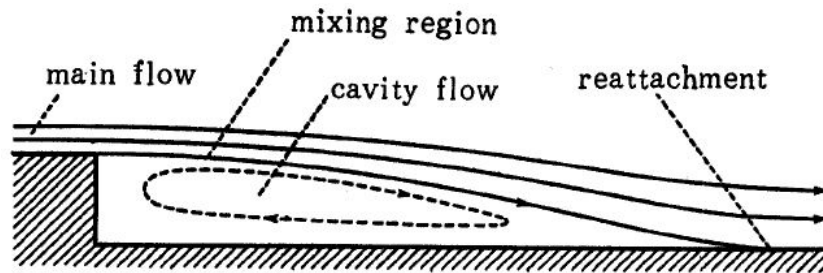


Figure 11.2: Backward facing step with cavity flow. [51]

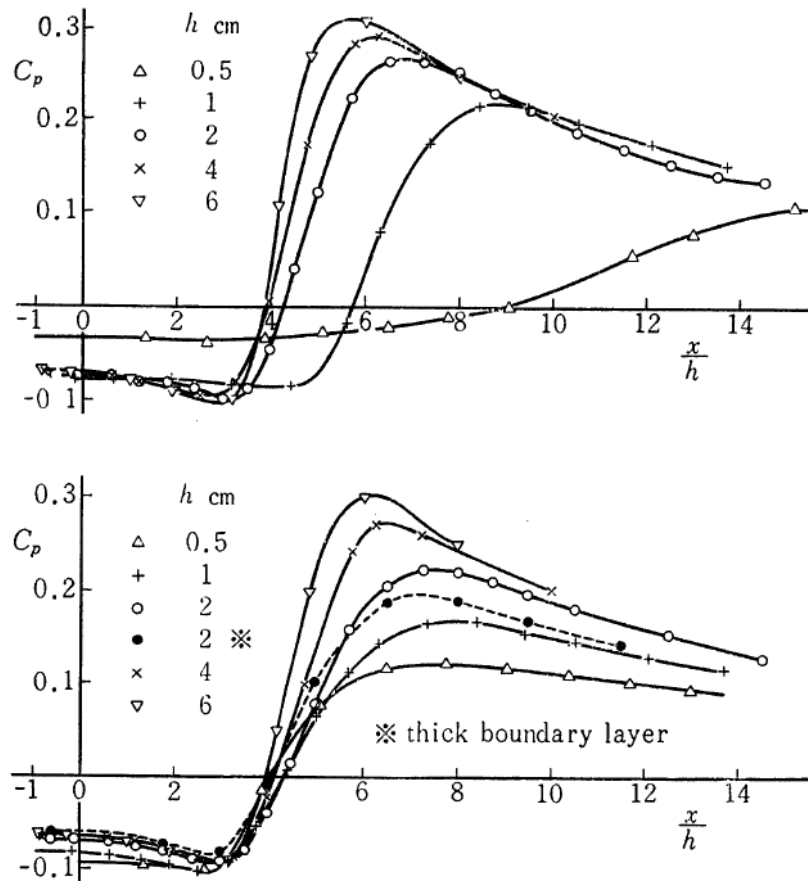


Figure 11.3: Pressure distribution on the step face and the bottom surface for various step heights. For the upper figure $U_0 = 10\text{m} \cdot \text{s}^{-1}$ and for the lower figure $U_0 = 28\text{m} \cdot \text{s}^{-1}$. [51]

In the experiments on flow separation [51] different configurations were used to see the changes in pressure distribution. In Figure 11.4 the results can be seen for different sizes of a triangular fillet, placed against the step. "No appreciable change is observed in the pressure distribution until the fillet height exceeds one half of the step height." [51] The second configuration change is shown in Figure 11.5. In this case a fence of the height of one half the step height is placed at various positions on the bottom surface. "The effect of the fence is most appreciable when it is placed at a distance of twice the step height from the step." [51]

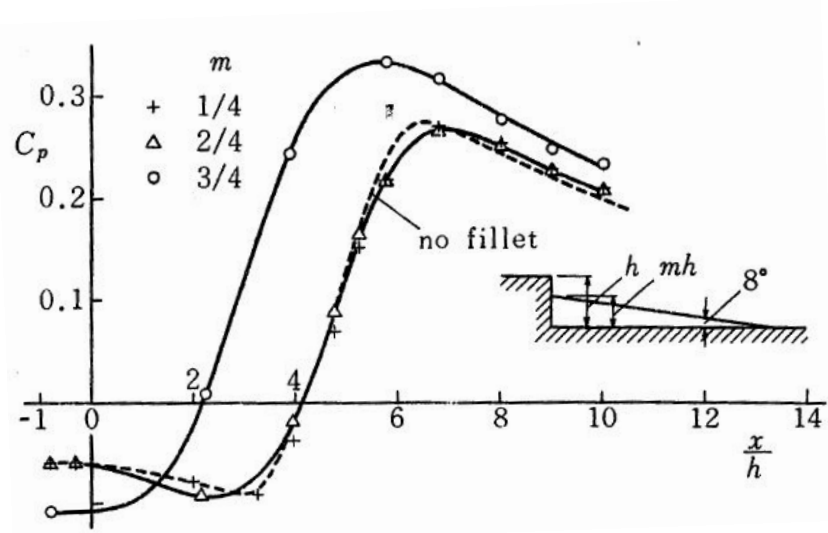


Figure 11.4: Pressure distribution on the step with a triangular fillet. $h = 4\text{cm}$, $U_0 = 28\text{m} \cdot \text{s}^{-1}$. [51]

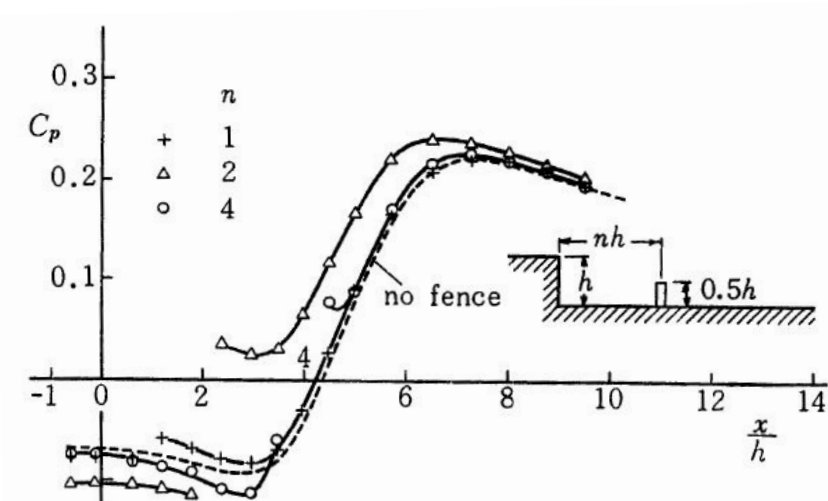


Figure 11.5: Pressure distribution on the step with a fence on the bottom surface. $h = 2\text{cm}$, $U_0 = 28\text{m} \cdot \text{s}^{-1}$. [51]

Also, the longitudinal component of mean velocity U across several transverse sections in the mixing regions were measured [51]. "From the distribution of mean longitudinal velocity, and also by taking into account of the mean flow direction determined by hot-wire measurements, a mean streamline can be drawn that starts from the step shoulder and approaches the bottom surface in the reattachment region. This line can be considered as that dividing the cavity flow region from the main flow. (...) It is seen that both the turbulence and shear stress increase downstream in the mixing region and that the positions of maximum turbulence and maximum shear stress approximately coincide at the outset with the mean dividing streamline, but deviate outward as the reattachment is approached."

Another point to be noticed from Figures 11.6 and 11.7 is that the distributions across the mixing region of mean velocity, turbulence intensity and shear stress are quite insensitive to changes in the step height as well as in the thickness of the approaching boundary layer. Figure 11.8 shows the result of similar measurements extended to the more downstream stations for $h = 4\text{cm}$. The turbulence and shear stress set up by the flow in the mixing region decrease downstream in the boundary layer, initiated by the reattachment of separated flow. On the other hand, a new system of turbulence and shear stress grows up in the reattached layer, until a fully developed turbulent boundary layer having a maximum shear

stress at the surface is established at some distance from the reattachment location. In Figure 11.9 the picture of short exposure reveals the intermingling of distinct eddies in cavity flow region, while that of long exposure indicates something like the mean dividing streamline. (...) As mentioned above, the base pressure is essentially the same for different values of step height and boundary layer thickness. Even the difference in character of the approaching boundary layer flow, laminar or turbulent, makes no essential difference except for the step of very small height. This is conceivable because the laminar boundary layer when separated becomes turbulent over a very short distance. (...) The base pressure, and also the pressure rise by reattachment, are hardly affected even by the insertion of a triangular fillet behind the step. This suggests that the interaction between the cavity flow and the external flow remains unchanged unless the cavity flow region is unduly oppressed. On the other hand, a considerable change in pressure distribution is found when the reverse part of the cavity flow is interrupted by means of a fence." [51]

According to the previous experiment, when adjusting our wingsuit by just placing fill-up performance foam behind the rig might not be enough to delay separation. Although, if the performance foam is shaped such that the flow (almost) does not separate, the pressure increase for reattachment is a lesser problem. Although, the boundary layer still has to cope with the energy loss in the lower boundary layers. As can be seen in Figure 11.7, re-energizing flow can make the difference.

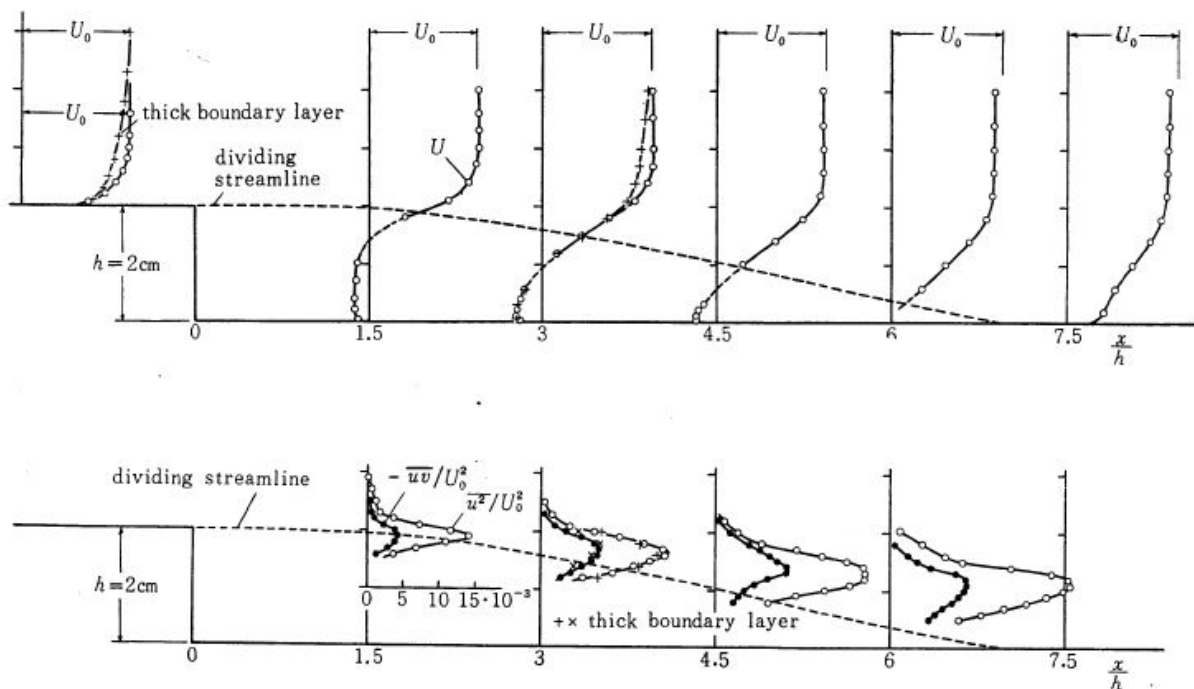


Figure 11.6: Distribution across the mixing region and reattached layer of flow over a step of longitudinal component of mean velocity (upper part), turbulence intensity and turbulent shear stress (lower part). $h = 2\text{ cm}$, $U_0 = 28\text{ m} \cdot \text{s}^{-1}$. [51]

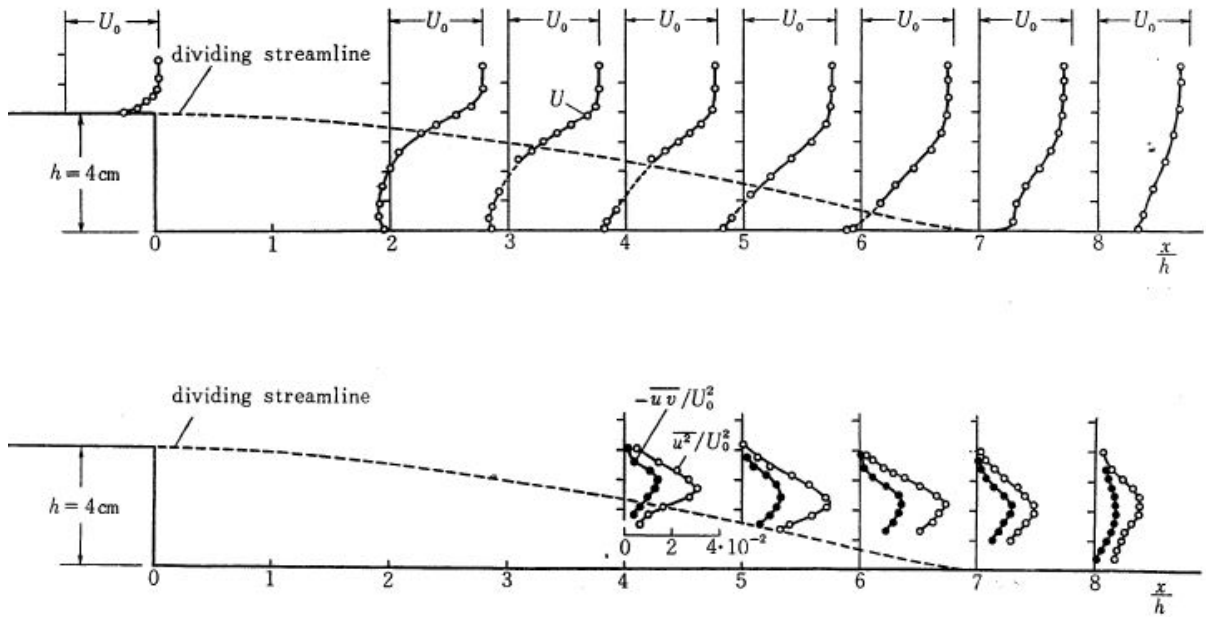


Figure 11.7: Distribution across the mixing region and reattached layer of flow over a step of longitudinal component of mean velocity (upper part), turbulence intensity and turbulent shear stress (lower part). $h = 4\text{cm}$, $U_0 = 28\text{m} \cdot \text{s}^{-1}$. [51]

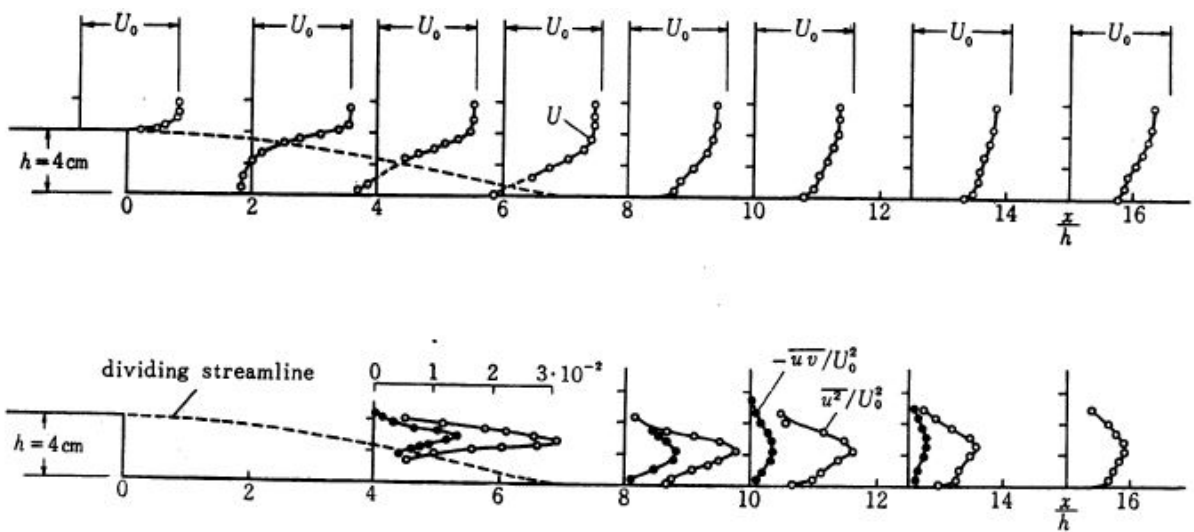


Figure 11.8: Distribution across the mixing region and reattached layer of flow over a step of longitudinal component of mean velocity (upper part), turbulence intensity and turbulent shear stress (lower part). $h = 4\text{cm}$, $U_0 = 28\text{m} \cdot \text{s}^{-1}$. [51]



Figure 11.9: Aluminum-powder pictures of streamlines over a step. Exposure time 0.5(upper) and 5 seconds (lower) [51]

At this moment, the theory about the energy loss over the rig is known and the energy needed for re-energizing can be calculated through momentum thickness. Just as a recap, the displacement thickness and momentum thickness were given by Equations 11.3 and 11.4. The shape of the boundary layer velocity distribution should be integrated and compared to the integrated velocity distribution that is desirable, the reference distributions can be seen in Figure 11.10.

The momentum deficit can be determined and from this the required momentum flux from the air tunnels can be obtained. When this momentum flux is known and a reference outlet diameter is chosen, the inlet diameter can be determined for different flight speeds. At first, calculate the momentum thickness for both velocity distributions, where θ_{pre} and θ_{des} are the present and desired momentum thickness, respectively. As a reference, $v_0 = 50[\frac{m}{s}]$ is used for the cruise flow velocity over the rig and a boundary layer thickness of $\delta = 3[mm] = 0.003[m]$ is assumed. Hence, equations 11.3 and 11.4 become

$$\theta_{pre} = \int_0^{0.003} \left(1 - \frac{v(y)_{pre}}{50}\right) \frac{v(y)_{pre}}{50} dy \quad (11.5)$$

and

$$\theta_{des} = \int_0^{0.003} \left(1 - \frac{v(y)_{des}}{50}\right) \frac{v(y)_{des}}{50} dy \quad (11.6)$$

Since the exact equations for v_{pre} and v_{des} are not known, the polynomials for the velocity distributions need to be determined from Figure 11.10. This can be done by determining the coordinates of the distribution line by hand and putting them in the polyfit function of MATLAB. For ease of the polyfit function, the profile was turned 90 degrees in clockwise direction. It was found in 11.10 that it does not matter much if the flow approaching the backward facing step is laminar or turbulent. The reason for this is that the laminar flow turns turbulent really fast when flowing over the step. For the present and desired velocity distribution respectively, the following two polynomials were found:

$$y_{present} = -1.8814 - 3.1013 \cdot 10^4 x + 7.1374 \cdot 10^7 x^2 - 7.2724 \cdot 10^{10} x^3 + 3.3006 \cdot 10^{13} x^4 - 4.9703 \cdot 10^{15} x^5 \quad (11.7)$$

and

$$y_{desired} = 15.3211 + 2.8060 \cdot 10^4 x - 5.6507 \cdot 10^6 x^2 \quad (11.8)$$

The Momentum Thickness Equation for the present and desired distribution gave $1.7984m$ and $5.9859m$, respectively. Hence, the $\Delta\theta = 4.1875m$. In this calculation a rig width of $0.3m$ is used and hence the

$\Delta\theta = 1.256N$. For the outlet, a cross-sectional area of $A_2 = 8 \cdot 10^{-4}m^2$ is assumed, leaving the outlet shape to be determined. If the outlets are designed too small, the flow could get choked because the tube is filled with nothing but boundary layer. To calculate the required inlet diameter of the air tunnel inlets together, the free stream velocity at the inlet is assumed to be $50[\frac{m}{s}]$ and $\rho = 1.225[\frac{kg}{m^3}]$ is used. In combination with Equation 11.1 and Equation 11.9.

$$\theta = \dot{m}V^2A \tag{11.9}$$

it can be calculated that the required momentum flux can be obtained by an outlet velocity of $V_2 = 35.80m \cdot s^{-1}$. In Figure 11.11 the boundary layer in an air tunnel is shown. Due to the boundary layer viscosity, the velocity at the outlet, v_2 , can be written as $v_2^* = v_2/0.7$ [50]. This results in $v_2 = 51.15m \cdot s^{-1}$. With ρ assumed constant and recalling $v_1 = 50m \cdot s^{-1}$, the required inlet cross-sectional area is $A_1 = 8.18cm^2$. For this inlet, the same shape can be used as on the arms of the pilot.

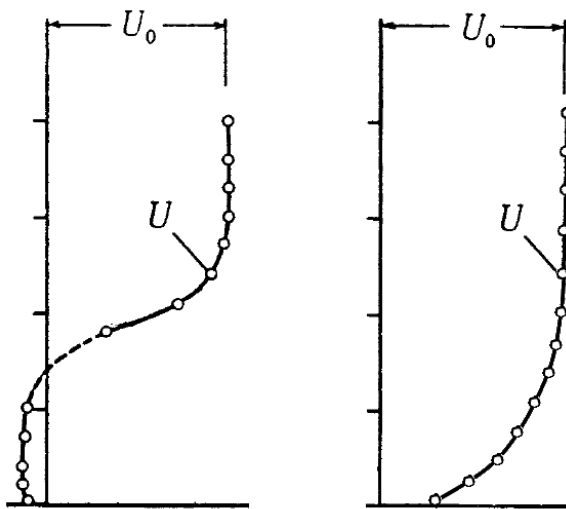


Figure 11.10: Velocity distribution

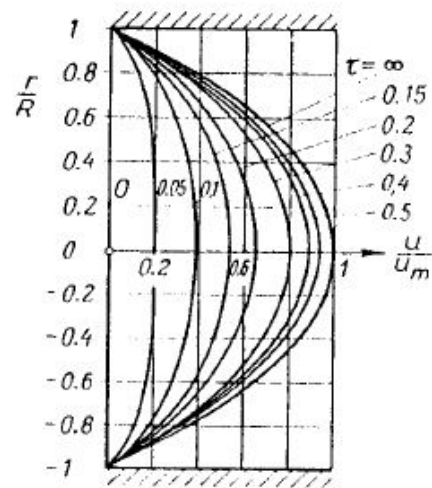


Figure 11.11: Boundary layer in an air tunnel

11.6 Numerical concept analysis

In order to properly assess the aerodynamic contribution of the concepts, it is required to have a numerical analysis of the aerodynamics of the concepts. This analysis was also done using the CFD program of the Numerical Analysis. To conduct the analysis, we used a specific workplan, listed below.

1. **Create models of the safety concepts**
2. **Compute 2D aerodynamic properties of added concepts**
 - Separate concepts on the 2D models
3. **Compute 3D aerodynamic properties of added concepts**
 - Separate concepts on the wingsuit model
 - One fully assembled wingsuit model

11.6.1 Safety concept models

A basic understanding of the wingsuit aerodynamics was gained, and used to develop safety concepts. Now, to check the aerodynamics of the new advanced wingsuit, several concepts are added to the airfoil shapes and the wingsuit. These concepts affect the aerodynamics of the wingsuit and should therefore be simulated in the CFD model. The concepts possibly affecting the aerodynamics are:

1. Passive Flap

2. Droop
3. Vortex Generators
4. Air Tunnels and Wing Connection

Only the droop leading edge is attached on the 2D models. But every concept is first integrated separately onto the Vampire 4 wingsuit. Afterwards, one final wingsuit model is created, which is fully equipped with all the different concepts.

Passive Flap Model

The passive flap, as described in Section 10.6, is used to stop the reversed flow on the wingsuit. This can be qualitatively simulated in the CFD, and afterwards the quantitative data can be gathered. This simulation is done using a wingsuit model with only the passive flaps added, see Figure 11.12. Here, the angle of the passive flap with the wingsuit tail is 30° . The simulation for this concept runs at a wind speed of $40 \text{ m} \cdot \text{s}^{-1}$ under an angle of attack of 30° .

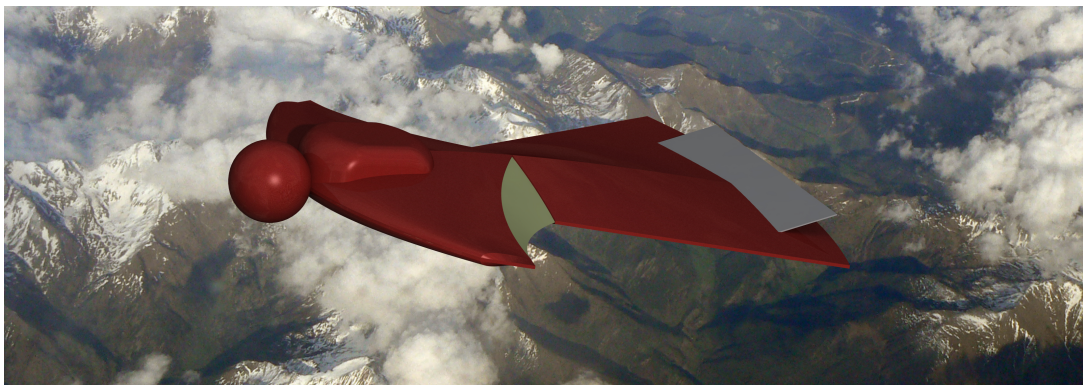


Figure 11.12: CATIA model of Vampire wingsuit with passive flap

Because of the unsatisfactory results, more attention was paid to the method used for the simulation. It occurred that the passive flap in the simulations is fixed on its position, because there was not enough time for dynamic calculations. To simulate this statically, one would need to perform numerous simulations in order to find an equilibrium point of the passive flap at a certain angle of attack. Thus because of the difficulty to simulate the real working of a passive flap, the passive flap is not simulated with the latest 2D analyses.

Droop Model

As described in Section 10.7, the purpose of the droop leading edge is to increase the stall angle and decrease the drag at high angles of attack. Therefore this concept will be simulated for a range of angles of attack in the 2D analyses, to observe whether the L/D ratio increases enough for an emergency situation. Figure 11.13 shows how the droop is integrated into the 3D wingsuit. The 3D simulation for this concept runs at a wind speed of $40 \text{ m} \cdot \text{s}^{-1}$ under an angle of attack of 30° .

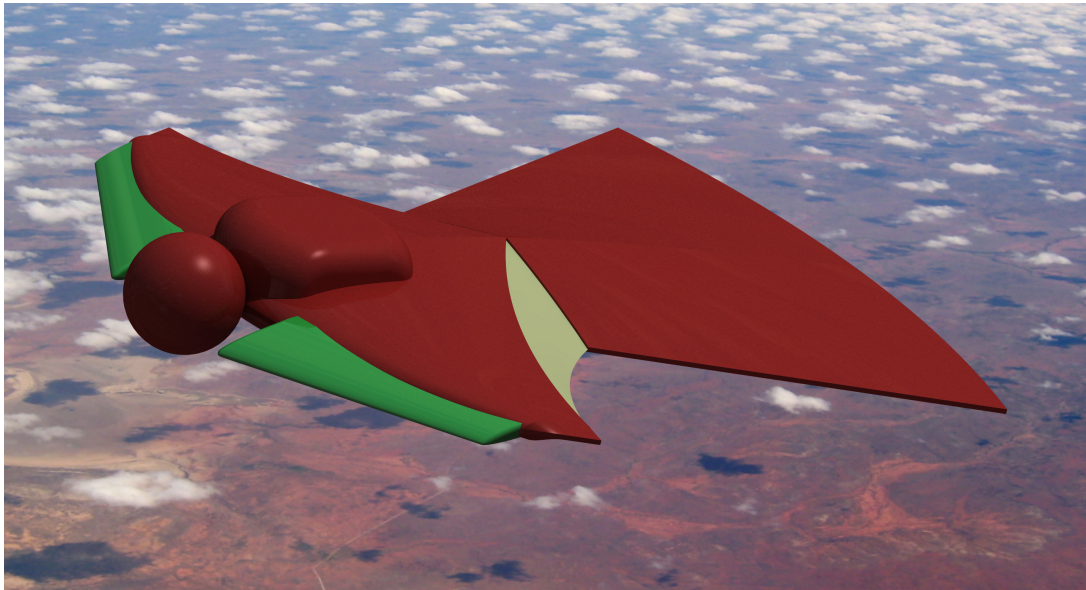


Figure 11.13: CATIA model of Vampire wingsuit with droop

Vortex Generators Model

The vortex generators (see Section 10.5.2) on the wingsuit cause small vortices, which have a positive effect on the air flow. This effect can be measured both quantitatively and qualitatively using the CFD program. The effect depends on the location of the vortex generators. See Figure 11.14 for a clear overview of how and where the vortex generators are placed.



Figure 11.14: CATIA model of Vortex Generators, an overview (left) and a close-up (right)

However, because of the height of the vortex generators, the simulation needs to run with a high resolution in order to be able to simulate the boundary layer and the effect of the vortex generators. If the vortex generators are smaller than the resolution block, no effect on the air flow would be seen in the simulation. With the required resolution, the simulation would take too long. Since this project needs to be finished within ten weeks, the effect of the vortex generators on the wingsuits performance is not simulated.

Air Tunnels and Wing Connection

The air tunnels are described in Section 10.8. They are used to re-energize the airflow and delay the separation by blowing the boundary layer. Obviously this can only be clearly visualized in a 3D simulation of the CFD program, and it can be determined how these air tunnels will affect the performance. For a clear image of the implementation of the air tunnels, see Figure 11.15.



Figure 11.15: CATIA model of Air tunnel concept, front view (left) and rear view (right)

Fully Assembled Wingsuit Model

The final model is the fully assembled wingsuit, which includes the all four of the concepts described in the previous paragraphs. This model is created to determine the effects and interference of several concepts on one wingsuit. Unfortunately, due to the limited DSE time and the long run times of the simulations, this model is not run. For future research on this safety design, it is highly recommended that a number of simulations of this fully assembled model are run.

11.6.2 Compute 2D aerodynamic properties of added concepts

In the end, for the 2D concepts, only the droop concept was simulated with usable results. The results of this simulation can be found in Appendix U.2.1. It is seen that the droop gives an increase in C_l , especially at higher angles of attack. The lift is slightly higher until an angle of attack of 20° . At this point, it could be that the airfoil is stalling, however a clear dip is not seen. Thereafter, the configuration with a droop has again increased lift, while the lift of the normal airfoil almost remains constant. These results however, should be treated with care. Since the lift prediction method of the CFD program is influenced by the shedding as explained before in this chapter.

The C_d curve of the droop configuration strongly resembles the curve from the original airfoil shape. At the highest angles of attack, the drag coefficient of the droop airfoil becomes larger than without droop. This result was not expected.

The L/D ratio of the droop is higher at every point except for angles of attack between 5° and 13° . It was expected that the L/D ratio would be better at high angles of attack for the droop, because the droop is used to increase the L/D at angles of attack higher than the max performance angle. Unfortunately, only a few data points are simulated for that range of angles.

There is not a lot of difference between the flow fields of the drooped airfoil and the original airfoil. The main thing is that the low pressure region at the front top of the airfoil is enlarged by the droop. Also in the velocity plots, the high velocity region is larger for the droop configuration. The flow field does not seem converged because of the 'pressure oscillation structure' (alternating pressure gradients) in the wake.

Concluding, it can be said that the airfoil with the applied droop performs better than the original one. The results should be interpreted with care since the simulated droop is only a rough sketch of the droop applied on the wingsuit. Also more data points should be simulated for the angles of attack between 10° and 25° . On top of that, a higher resolution is also desired to get more accurate results.

11.6.3 Compute 3D aerodynamic properties of added concepts

After the basic computations of the 3D models have been computed, these computations can be used as a reference. When the aerodynamic concepts are added to the 3D models, the new models' aerodynamics can be computed for comparison. The program remains in the 3D kernel and uses exactly the same conditions and settings as the previous 3D model simulations.

Simulated concepts

For the passive flap concept, the focus is put on the angle of attack where separation and the start of the stall are clearly visible. This is where the passive flap will start to have an effect on the aerodynamics. This is at an angle of attack of 30° . Only one simulation of this concept is run at 30° . The impact of the passive flap on the stall behavior was visible in the 3D graphic representation of the model, in the CFD program. As described in Section 11.6.2, the passive flap cannot be dynamically simulated, which decreases the performance of the concept.

This data cannot be used, because the separation point is non-existent, and therefore the impact of the passive flap on the detached flow is not representative.

The droop concept is also more effective within a specific range of angles of attack. The simulations runs on an angle of attack of 30° . The simulation shows that for an angle of attack of 30° with droop under an angle of 20° , the drag coefficient of the wingsuit decreases very slightly (by 0.02), while the lift coefficient only increases marginally (by 0.05). This results in a slightly higher C_L / C_D value of 2.08, see Figure U.3. This indicates that droop does help, but for this simulation it is only a very minor improvement. This could be due to the fact that the wrong settings were used for the simulation or by the fact that the CATIA drawing is only a sketch and not a real detailed drawing with the actual smoothness of transition from the leading edge over the shoulder.

Non-simulated concepts

The vortex generator is a proven concept, which is now added to the wingsuit. Unfortunately, the vortex generators are so small that their initial effect is only visible within the boundary layer of the wingsuit. According to Section 10.5.2 the effect of the vortex generators propagate outside of the boundary layer and will have a significant effect on the airflow. However, the CFD program is not able to simulate this effect at the moment due to a low resolution used. The resolution of the CFD program is bigger than this boundary layer, and therefore, it can not compute the initial effect of the vortex generators within the boundary layer and therefore will not compute the propagation outside of the boundary layer. This concept has not been simulated.

The last concept is the wing connection with the air tunnels. This concept is supposed to improve the flow right behind the parachute rig. This is done by making a smoother transition from the rig to the back, and adding air ducts to re-energize the flow. This concept has not been simulated.

Conclusion

In short, due to lack of time, insufficient 3D numerical data was gathered. The data was not trustworthy. It is unfortunate that due to lack of time, no proper simulations could be run. However, a basis has been set on which new research can be conducted in the future.

12

Structural Characteristics

In this section the structural characteristics of the inflatable cells, shoulder reinforcements, passive flap and leading edge droop are further analyzed. More information on the choice of materials and its characteristics will be given in the next chapter, Chapter 13.

12.1 Inflatable cells

The inflatable cells of the wingsuit determine the shape, strength and bending stiffness of the lifting surfaces of the suit. Only a slight overpressure is required to obtain the optimal shape. However in actual flight the airflow over the suit will interact with the inflatable cells, which makes it harder to maintain that very shape. The ideal position for the inlet is at the stagnation point of the airfoil. Assuming a cruise flight speed of $50m \cdot s^{-1}$, a constant air density of $\rho = 1.225 \frac{kg}{m^3}$ and a static pressure equal to the ambient pressure at sea level, the stagnation pressure is given by the sum of the static and dynamic pressure which are given by Equation 12.1.

$$p_{stagnation} = p_{static} + \frac{1}{2}\rho V^2 = 102856.25Pa. \quad (12.1)$$

The inlets also receives airflow at the cruise velocity and should be designed such that the momentum flux through the inlet is such that wingsuit has the desired buckling condition. In current suits, the shape of the airfoil is maintained with a series of ribs in longitudinal direction. The advantage of this design is that it is relatively easy to manufacture. However, in flight the different cells are easy identifiable since the airfoil is not one smooth piece of fabric. This can be better approached by another technique which uses drop-stitches, which can be seen in Figure 12.1. This design connects the upper and lower airfoil fabric at a large number of points, this results in a smoother airfoil. The disadvantage is the labor intensive manufacturing process of the airfoils, but a compromise can be made between the two designs. Instead of using a huge amount of evenly distributed drop-stitches, use can be made of multiple sets of a couple drop-stitches as can be seen in Figure 12.2.

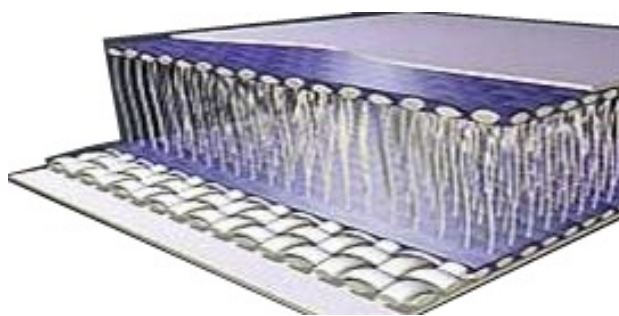


Figure 12.1: Drop-stitches distributed in multiple sets.



Figure 12.2: Evenly distributed drop-stitches.

Since drop-stitches were found to be too labor intensive for both designs, our wingsuit will be manufactured with the well-known ribs.

12.2 Shoulder reinforcement

This section will discuss the shoulder reinforcements in more detail. The shoulder reinforcement will be constructed from Mylar and aluminum. More information on the material will be given in Section 13.5.

For the critical regions a stronger material is desirable, that is where aluminum will be used. Now to check these critical regions, the force encountered at these locations will be studied. The most critical points were identified to be the joint encapsulation and its connection to the arm part. In order to calculate the stresses at that location the force exerted by the arm on the arm part need to be studied. This force is not simply the force exerted by the arm-wings on the arm, since also the ram-air inflation carries parts of these loads. The force was estimated to be never higher than 20N in backward direction for the statics situation. This is quite large if you keep in mind that all wingsuiters are able to carry this load without any proper training. The calculation will be performed with a force of 100N, this force is determined by incorporating a safety factor of 10 to include the dynamic situation. It is assumed that this force works backwards in the middle of the part as can be seen in Figure 12.3.

So examining the first critical region, the connection of the joint to the arm part is checked by checking the reference area as seen in Figure 12.4. Using the force from Figure 12.3 and some basic statics the shear stress in backward direction (τ_{yx}) was estimated to be $2307337 \frac{N}{m^2}$ and the tensile stress (σ_y) was estimated to be $1357257 \frac{N}{m^2}$. As mentioned these critical sections will be made from a stronger material. Aluminum 7075-T6 is chosen. The reason for this material choice will be explained in Section 13.3. Comparing these results to the properties of aluminum 7075-T6 ($\tau_{yx} = 331MPa$, $\sigma_y = 503MPa$ [52]) it is concluded this area will not fail in flight and can still cope with much higher loads. Looking at the situation over time and hence comparing these forces to the fatigue strength at 10^7 cycles ($\sigma_{fatigue} = 152MPa$ [52]), it can be concluded the shoulder reinforcements will not fail over time neither. These calculations were performed in MATLAB, the code can be checked in Appendix W.1.

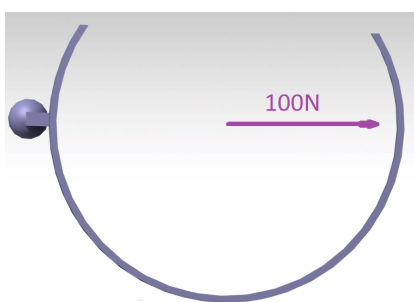


Figure 12.3: Resultant force of arm on arm part

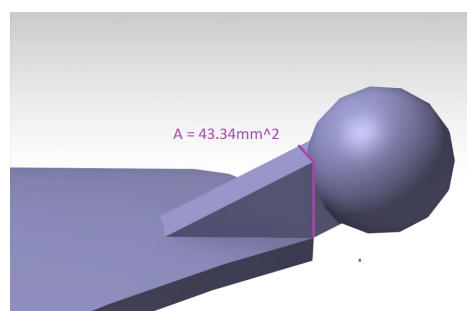


Figure 12.4: Reference area critical section

The second critical area was the encapsulating part of the joint as seen in Figure 12.5. This paragraph checks if the tensile force on the joint does not destroy the encapsulation by shear stress. For this, the point of maximum shear stress has to be determined. Logically this would be somewhere along height h , which is shown in Figure 12.6. Using statics and assuming that the ball exerts a constant force on the encapsulation in the direction of the tensile force, the critical section was found to be at a height of $0.0003m$, also shown in Figure 12.6. The shear stress (τ_{zy}) at that location was calculated to be $659040Pa$. An overview of the shear stress along the height h is shown in Figure 12.7. This stress was also found using the $100N$ backward force of Figure 12.3. These calculations were also done in MATLAB. The code can be checked in Appendix W.1. Again comparing these results to the yield stresses and fatigue strengths of aluminium, it is concluded that both critical sections are well designed, maybe over designed, but will certainly not fail in flight.

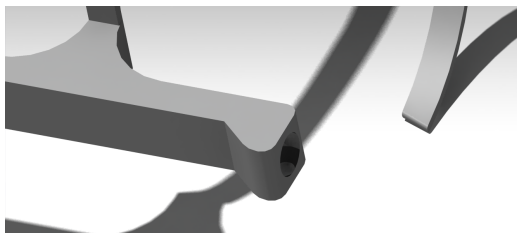


Figure 12.5: Detail render of socket joint on shoulder reinforcement

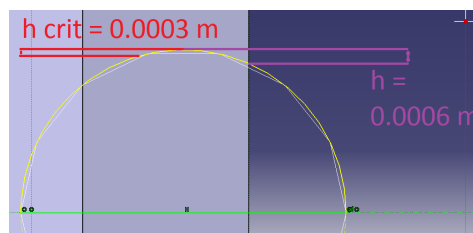


Figure 12.6: Details of the second critical section, the yellow circle represent the sketch of the ball of the socket joint

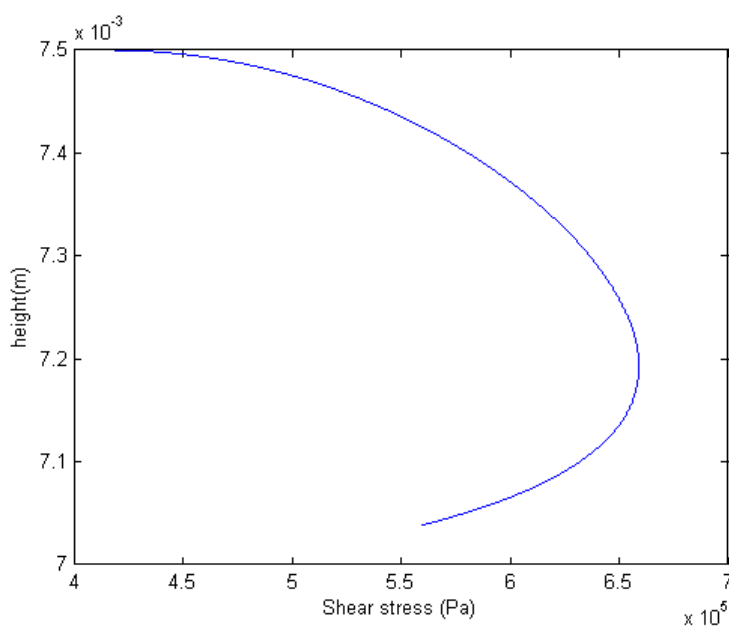


Figure 12.7: MATLAB plot of the variation of shear along the height of the second critical section.

The final step of this section consist of calculating the additional weight of the shoulder reinforcement. The volume was estimated using the CATIA models. The total volume was found to be 278cm^3 from which 45.6% was made from Mylar. Using a density of $1390\text{kg}/\text{m}^3$ for Mylar [53] and $2810\text{kg}/\text{m}^3$ for aluminum 7075 – T6 [52], the total additional weight for the shoulder reinforcements is 0.6kg . So wrapping up this section it can be concluded that the section will not fail and that the pilot will be relieved from all backward forces at the cost of 0.6kg of additional weight.

12.3 Passive flap

The construction of the passive flap needs to be stiff and light at the same time as the passive flap needs to be able to get pushed up by reversed flow. Therefore, fabric is used and a composite frame is incorporated to keep the fabric from bending and fluttering. The thickness of the frame depends on the forces that act on the passive flap at maximum angle and on the maximum permitted mass to still allow the passive flap to rotate.

To determine the force acting on the passive flap, Equation 12.2 is used [44].

$$M_F = \frac{1}{2} c_F \rho c^2 u_0^2 b \quad (12.2)$$

Here ρ is the air density, c is the chord of the passive flap, u_0 is the free stream velocity and b is the span of the passive flap. The flap coefficient c_F is described in [44] and is a function of the angle of attack and the opening angle of the passive flap. This moment is caused by a pressure distribution on the passive flap. The moment can be used to calculate the distributed pressure on the passive flap with Equation 12.3.

$$p = \frac{2 \cdot M_F}{c^2} \quad (12.3)$$

With the distributed pressure force p on the passive flap, the internal forces and stresses can be determined according to the free body diagram (FBD) in Figure 12.8.

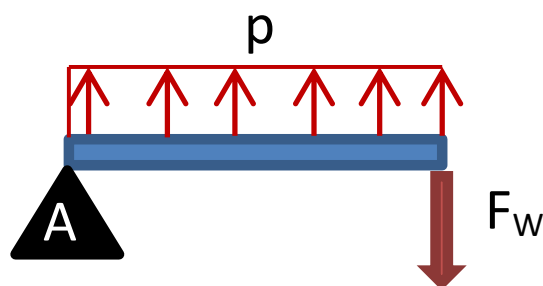


Figure 12.8: Free Body Diagram of the passive flap

In this FBD, it is assumed that the force in the wire F_W is equal to the reaction force in hinge point A and in the same direction. The weight force is neglected since the critical stress would occur if the flap is at the most vertical position and thus the weight would have a minor influence on the hinge moment.

With the knowledge of statics, the maximum internal moment can be found at the middle of the beam. Using this maximum bending force and the material properties, the needed area moment of inertia can be found with Equation 12.4.

$$\sigma = \frac{M \cdot y}{I} \quad (12.4)$$

With M the bending moment, y the vertical position from the neutral line and I the area moment of inertia. σ is the tensile strength of the used material.

Besides the geometry, the mass of the passive flap is also limited by the total hinge moment. In order to get the passive flap moving, the moment caused by the fluids M_F must be larger than the moment caused by the weight of the flap M_G . To scale the weight of the construction, M_F is calculated for different angles of attack and different opening angles, again with Equation 12.2. For each of these situations the maximum M_G is calculated and compared to M_F . If the moment due to the weight is larger, another iteration is used to determine a new geometry or material.

It is found that the needed area moment of inertia is very small and almost any geometry would fulfill this requirement. The chosen geometry consists of two circular pipes with a thickness of $2mm$ and an outer diameter of $2cm$. The material will be high-modulus carbon-fiber epoxy. Properties of this material can be found in Chapter 13. This way, the construction can cope with all the applied forces. The moment induced by the pressure force is also slightly less than the moment induced by the weight of the passive flap. The passive flap would thus be almost in equilibrium.

Afterwards, an additional plate is added to the geometry to attach the fabric once more and to make the construction more stiff and hence prevent it from deforming. The construction of the passive flap is sketched in CATIA and shown in Figure 12.9.

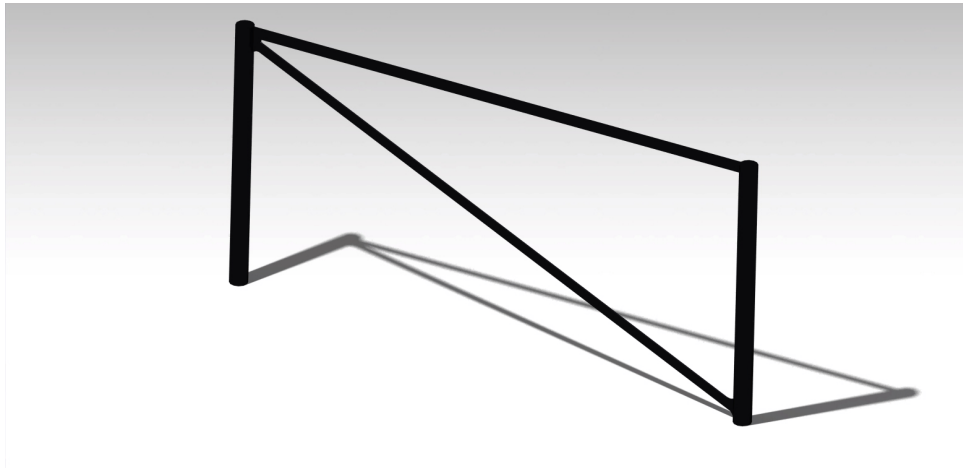


Figure 12.9: CATIA sketch of the passive flap construction.

12.4 Droop leading edge

The droop leading edge is no load bearing construction. It only needs to remain stiff in order to maintain its shape during the flight. This mainly depends on the foam that is used. More on the foam material can be found in Chapter 13. An important part of the leading edge however, is the interaction between the structure and the movement of arms. As said before in this report, the arm has three hinge points. These three hinge point need to remain free, in order to let the wingsuiter reach his toggles and steer the canopy.

To let the wingsuiter keep his mobility, the leading edge at the elbows needs to consist of a softer foam than the one used on the other places. Because it is attached to the harder foam it will remain its shape while allowing the wingsuiter at the same time to alter the position of the arms during flight or reach for the toggles of the canopy.

Another point of attention is the fitting of the suit around the wingsuiter. The wingsuit, especially the arm wing, should fit very tight to the wingsuiter. If the arm wing is fitted tightly to the arm, then the droop will rotate with the movement of the pilots arm.

13

Material Characteristics

13.1 Fabric

Nowadays, three kinds of fabric are primarily used for wingsuits; Para-pak, F-111 and Cameroon Ultra Light Fabric. Para-pak is thicker and heavier than other materials, but extremely durable and abrasion resistant. Next F-111 is a zero-porosity balloon fabric and is normally used for the wings and body. However in case of heavy use, Para-pak can also be used for the wings and body. Finally Cameroon Ultra Light Fabric is the lightest of the three and is a slick fabric which has low drag characteristics. It is also more durable and sturdier than F-111. The latter fabrics are predominantly nylon. The major differences include the weave, weight, and finish [54]. For example, a weave with heavier threads woven into the material inhibits the tearing process and results in stronger fabrics. The material properties of the fabrics can be found in table 13.1 except for Cameroon Ultra Light, since these could not be found. Due to the durability Cameroon Ultra Light is chosen.

Table 13.1: Material properties of Para-pak and F-111 [54]

Type	Specification	Tear strength	Breaking strength	Identification	Comments
Para-pak	PIA-C-7219 class 3, 7.25 oz, 420 denier	20 [lb]	275-325 [lb]	1-1 plain weave	400 denier, inside urethane coating
F-111	PIA-C-44378, 1.12 oz	5 [lb]	45 [lb]	ripstop nylon (zero-porosity)	

13.2 Foam

To form the (droop) leading edge and to house the wing connection and air tunnels, performance foam is used. During the wind tunnel test it was seen that the leading edge of current wingsuits is very soft. This causes the leading edge to deform and disturb the airflow. In the advanced wingsuit, more and stiffer foam will be used in order to prevent these situations.

For the performance foam specifications, the material used, pliancy and compressibility of the material should be looked at. Relatively rigid foam should be used which can be bent for arm movement and folded for packing after flight. Therefore the Young's modulus should be of moderate value to allow the required movement. Also, air pressure should not deform the foam at high flight velocities. Also different types of foam can be used in order to allow movement around hinge points (e.g. the elbow) and to counteract deformation. If deformation does occur, it should be elastic such that it can return to the optimal aerodynamic shape. Hence, next to a high density and a high hardness, the yield strength should be rather high such that the strain is recoverable.

Closed-cell foam is a lightweight cellular material that consists of discrete gas pockets, each completely surrounded by solid material. [55] By adjusting this ratio, the required foam specifications can be obtained. Compared to open-cell foam, which has interconnecting pores, closed-cell foam has a higher compressive strength, is denser, has a higher dimensional stability and has a low moisture absorption coefficient.

13.3 Aluminum

For the shoulder reinforcement, the main material chosen was aluminum 7075-T6. Straightforward advantages of this material are the high resistance to fatigue and high strength. A disadvantage is the

slightly less resistance to corrosion compared to other aluminum (Al) alloys. But the true usefulness of this material presents itself when compared to another popular aluminum alloys, aluminum 6061-T6, and to a really strong material used in the landing gear of the Boeing 787 [56]: Titanium (Ti-10V-2Fe-3Al). An overview of the Yield strength, density and cost is given in Table 13.2. These are transformed to the ratios in Table 13.3 [57]. Here it can be seen that the strength over cost and strength over density ratio of Al 7075-T6 is really good compared to the Al 6061-T6. The Titanium alloy performs better on this second ratio, but its cost is way higher. Furthermore these costs are only for the material itself, not for the manufacturing. This will even worsen the cost of titanium which is difficult to manufacture. That is why Al 7075-T6 is chosen.

Table 13.2: Material properties Al 7075-T6, Al 6061-T6 & Titanium

	Density [$\frac{\text{kg}}{\text{m}^3}$]	cost [$\frac{\text{EUR}}{\text{kg}}$]	Yield tensile strength [MPa]
Al 7075-T6	2.77e3 - 2.83e3	2.20 - 2.42	359 - 530
Al 6061-T6	2.67e3 - 2.73e3	2.13 - 2.35	193 - 290
Titanium (Ti - 10V - 2Fe - 3Al)	4.63e3-4.67e3	21.0-23.3	1000-1110

Table 13.3: Material properties Al 7075-T6, Al 6061-T6 & Titanium

	$\frac{\text{Yieldstrength}}{\text{Density}}$	$\frac{\text{Yieldstrength}}{\text{Cost}}$
Al 7075-T6	129.6	163.2
Al 6061-T6	72.3	90.6
Titanium (Ti-10V-2Fe-3Al)	216.0	47.6

13.4 Carbon fiber-epoxy

The material properties of both high modulus and high strength carbon fiber-epoxy can be found in Table 13.4. This material is chosen because it is extremely stiff and still has a low weight. It is used in the construction of the passive flap. As it will be exposed to the surroundings, an epoxy with UV protection like West System 207, should be used.

Table 13.4: Material properties of carbon fiber-epoxy [58]

Type	Specific gravity	Modulus [GPa]	Tensile strength [MPa]	Modulus to weight ratio	Strength to weight ratio
High strength	1.55	137.8	1550	9.06	101.9
High modulus	1.63	215	1240	13.44	77.5

13.5 Mylar

Mylar is already in use on wingsuits in the reinforcing ribs of the wings. After doing some research and comparing Mylar to other popular polymers like (polyvinyl chloride) PVC and polypropylene, Mylar was decided to be a good choice for the non-critical sections of the shoulder reinforcements. It is one of the strongest, but also a soft and lightweight plastic. Some properties of Mylar are given in Table 13.5 [57].

Table 13.5: Material properties Mylar(50% long glass fibers)

	Density [$\frac{\text{kg}}{\text{m}^3}$]	cost [$\frac{\text{EUR}}{\text{kg}}$]	Yield tensile strength [MPa]	Fatigue strength at 10^7 cycles [MPa]
Mylar	1.83e3-1.87e3	2.39-3.05	123-136	56.8-73.9

14

Stability & Control

This chapter discusses the stability and control of a wingsuit as well as the effects of the different concepts on these characteristics.

14.1 Current wingsuits

Determining the stability and control characteristics of current wingsuits is a tricky business, because the wingsuit and the pilot are no rigid structures.

Stability

There has been no previous research in the field of wingsuit flight tests to determine the flight stability derivatives and valid equations of motion. When asked about longitudinal and lateral stability, the wingsuiters that were contacted responded that a lot of the practice of wingsuit flying was based on feeling and intuition, which are qualities that are impossible to analyze. It is for example hard to determine whether (and if so which) pilot control inputs are applied continuously to the wingsuit in case it is unstable, or that it is inherently stable itself. It is these uncertainties that make wingsuit stability hard to analyze scientifically. More research is needed into the influences of the movement and position of the wingsuiter on the performance of wingsuits.

Control

There are a number of ways wingsuiters can control the way they fly. These are listed below:

- **Feet** Wingsuiters can control their wingsuit by moving their feet up and down. By moving the right foot up and left foot down, the wingsuit will veer to the left by the twisting motion of the leg wing.
- **Arms** By folding the arms closer to the body, a pilot can control the amount of lift he generates. This is especially handy if a pilot wants to maneuver into or out of a dive. The hands can also be used to control the rolling of the wingsuit, by deflecting the grippers upwards or downwards.
- **Head** According to wingsuiters that were spoken to, the direction of yaw is controlled by moving the head from side to side. The direction in which the pilot looks is also the desired flight direction.
- **Spine** From the wind tunnel test was learned that by arching forward or backward, the wingsuit flyer is able to control respectively his pitch up/down movements.

As a great deal of these controls are based on the pilot's senses, the above list is certainly not complete, but illustrative for the different ways in which the airflow may interact with the human body at high speeds.

14.2 Effects of concepts

In this section, an overview of the effects of the concepts of the safety wingsuit on the stability and control will be given.

- **Anti-slip** The anti-slip layer on the bottom side of the wingsuit foot inserts has a positive contribution to a stable and controlled exit.

- **Quick-Release** The control aspect, especially, is positively affected by the implementation of a quick-release system. The canopy will be flyable by the wingsuiter in an earlier stage of parachute deployment than was previously possible. In terms of stability, the quick-release does not affect the behavior much.
- **Shoulder Reinforcements** The shoulder reinforcements help the wingsuiter to keep control of himself and handle any extra forces when the extra added droop provides more lift.
- **Vortex Generators** Vortex generators cause the air flowing around the wingsuit to be attached longer. This has an added benefit of providing the wingsuiter with more control at higher angles of attack. The effects on stability during normal flight are negligible.
- **Passive flap & stall warning** The passive flap and stall warning both contribute to control and stability in their own ways. First, the passive flap will avert stall, which is positive for the stability aspect of flying a wingsuit. Secondly, the passive flap together with the stall warning will make the wingsuit more controllable for the wingsuiter. As an imminent stall will be detected earlier, control measures to counter that stall can be made by the pilot in an earlier stage.
- **Droop** Droop is designed to be able to fly out of dangerous situations. The ability for the pilot to implement the droop will make the wingsuit more controllable.
- **Air tunnels** The air tunnels implemented on the wingsuit design will make the flow behind the wingsuit reattach faster to the leg portion of the wings. This will cause more lift to be generated by the leg wings, thereby decreasing C_{m_α} , which will make the wingsuit more stable. The wingsuit will also become more controllable by the pilot's legs, as airflow will be more attached there.
- **Swiss pouch & Integrated GoPro** These concepts will not affect stability and control directly.

15

Configuration / Layout

This chapter describes the final physical appearance of the wingsuit. The overall lay-out of the design is based on the Vampire 5 wingsuit from Phoenix-Fly. This because on one hand the project focuses on BASE-wingsuit flying, and particularly on the most extreme and advanced wingsuiters, it is chosen to go for an expert suit with a larger plan form area than the beginner suits. But on the other hand the purpose is to make it safer. And the latest wingsuits, that have the largest wing area (also called mattresses), were considered too hard to handle to be really safe. A compromise between the 'mattresses' and the novice suits was found in a suit like the Vampire 5. The locations of the new concepts were explained in their particular sections. As a short and simplified recap, the passive flaps were located at the rear of the leg wing as the wingsuit would be stalling there first (Shown in Figure 11.12). The VGs were only placed in front of the passive flap to overcome their most negative characteristic: more sudden stall (Figure 11.14). The droop was placed all along the leading edge to improve the general airfoil shape (11.13). The air tunnels were used to better integrate the rig, hence they their exits are just behind the rig (Figure 11.15). An overview of the final design can be seen in Figure 15.1.

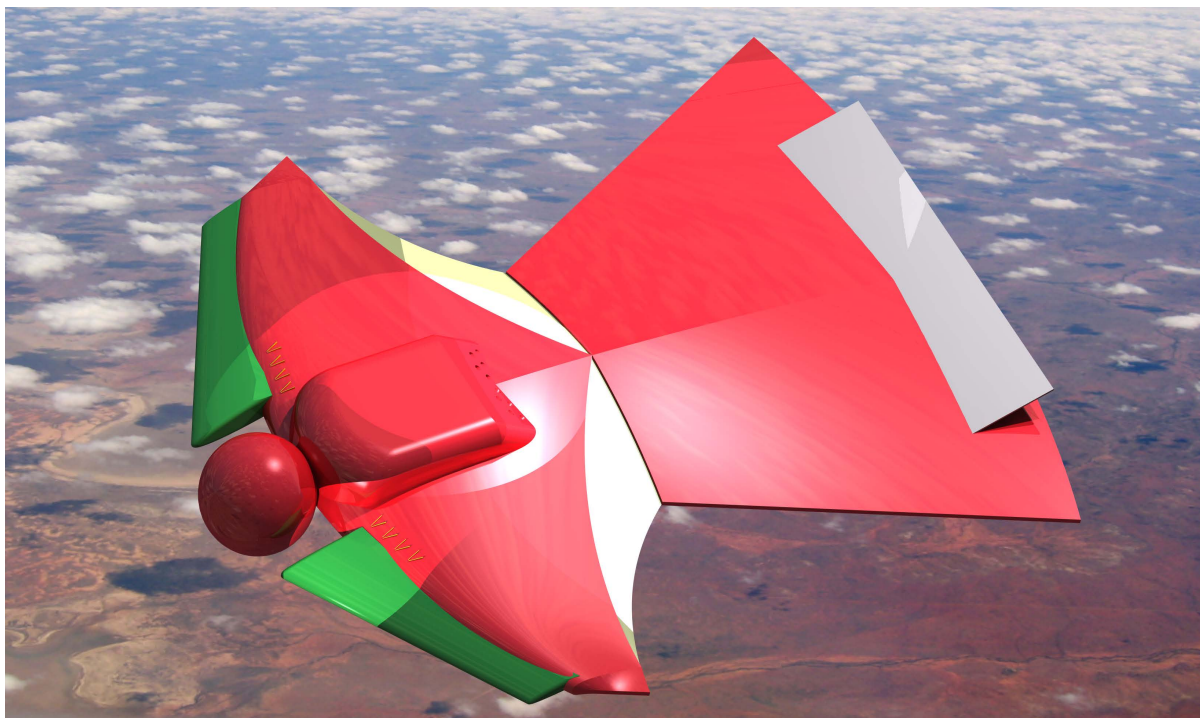


Figure 15.1: CATIA render of the final layout of the advanced wingsuit

16

Sensitivity Analysis

This sensitivity analysis will investigate the robustness of the general improvements to the wingsuit, listed below, in the face of uncertainty in the main parameters of the wingsuit: planform shape, area, wingsuit material, and leading edge characteristics. First, in Section 16.1, the selection of the main parameters will be discussed. Then, the impact and sensitivity of all general improvements will be analyzed in Section 16.2. After that, the impact on the safety concept specifics and the wingsuit characteristics will be discussed in Sections 16.3 and 16.4 respectively.

16.1 Selection of main parameters

The selected main parameters are the parameters that will most likely have the biggest impact on the overall wingsuit structure and the general improvements.

Obviously the planform shape and the corresponding area will have a big impact on the structure and the aerodynamics of the wingsuit. It will change the aerodynamic coefficients and the whole geometry of the wingsuit.

The wingsuit material is a parameter that will have an impact on the structure of the wingsuit and therefore most likely also on the general improvements.

The leading edge characteristics are very important in defining the attached flow over the wingsuit. This parameter will definitely have an effect on aerodynamic characteristics.

16.2 Sensitivity of the general improvements

For a general sensitivity analysis, the main parameters will be varied and the impact on several concept will be calculated. Unfortunately, due to the limited time available, no specific numbers can be tied to the analysis of general improvements, the safety concepts specifics or the wingsuit characteristics. The effects of changes to the main parameters could not be calculated, simply due to lack of time. Therefore this analysis is more of a qualitative sensitivity analysis instead of a quantitative analysis. Following, the impact of the main parameters on general improvements will be discussed in a qualitative manner.

Anti-slip The anti-slip surface solution is not generally influenced by a change in the planform shape, total area, leading edge and wing span parameters. It is however slightly dependent on the material chosen to construct the main wingsuit body of. As the choice of this material changes, the material to be used for anti-slip surface might also change. This is due to the fact that the adhesion method for this anti-slip surface must apply to that specific wingsuit material.

Quick-release The quick-release system freeing the wingsuiter's arms is sensitive to changes in the wingsuit material, leading edge characteristics and wing span. As the wing span (part of the planform shape) increases, so does the chance the quick-release will get snagged on the wingsuit material and hamper the quick-release mechanism. A change in material could also increase the risk of lines snagging. The type of foam or other material used for the leading edge, as well as its shape and size also influences the way the quick-release works, as they lie close together in the entire wingsuit system.

Turbulator strips The placement and size of the turbulator strips is mainly affected by the shape of the leading edge and the planform. If these parameters change, the turbulator strips will have to be redesigned.

Wing connection The wing connection is influenced by the planform and the wing area. These will determine the placement and size of the wing connection.

Summarizing, the general improvements will not change the design drastically. The parameters will influence the design in a positive manner, if these are correctly sized and placed. However, absence or incorrect placement of these parameters will not make the wingsuit unflyable. Nonetheless, the performance of the safety concept without, or incorrectly placed and sized parameters, will not be as good as a wingsuit with these parameters. The parameter quick-release will increase the safety level of this design.

16.3 Sensitivity analysis of safety concept specifics

The main features are the Swiss pouch, the droop leading edge, shoulder reinforcement, air tunnels and the passive flap with attached stall warning.

Swiss pouch The Swiss pouch is, just as the quick-release, sensitive to changes in the wingsuit material, planform and wingspan. If there are changes in the overall design, the design of the Swiss pouch will need to be adjusted.

Droop leading edge The sizing and placement of the droop leading edge has quite some influence on the design. A droop leading edge over the entire wing will result in a design with poor spin characteristics. The droop leading edge will not be majorly influenced by other parameters such as the size of the planform. The (leading edge) material used in the suit however can influence the connection of the droop to the suit.

Shoulder reinforcement Shoulder reinforcements lower the pilot loads. Removing the shoulder reinforcements from the design will not make the design unflyable, if the planform area is not drastically increased. However they might interfere with the quick-release and the air tunnels and as such, the shoulder reinforcement design is sensitive to the other design solutions.

Air tunnels Air tunnels are influenced by the planform and the wing area. These parameters determine the amount, placement and size of the air tunnels. The air tunnel system is also influenced by the shape and material of the leading edge and depending on the placement of the tunnels and the shoulder reinforcement.

Passive flap with attached stall warning Passive flaps with the stall warning have a positive influence on the stall characteristics of the wingsuit. However, removing these will only make the wingsuit less safe than the current safety design. Though the wingsuit will not become less safe in comparison to the current competitors.

16.4 Sensitivity analysis of wingsuit characteristics

Planform The planform and the wing area influence each other, and are limited by the pilot loads and the usability. A planform change will result in a new definition of the area and vice versa.

Area The area is limited by the pilot loads and the usability in general. An area increase enlarges the loads on the pilot. However, this limit can be extended with the use of shoulder reinforcements.

Material The material determines the weight, rigidity and flyability of the design. A change in the material of the suit would call for a check on all these parameters. However, different parts of the wingsuit can use different materials.

Leading edge The shape and rigidity of the leading edge determines the airfoil shape and characteristics. The usability of the suit is also determined by the leading edge. If the leading edge is very rigid, the usability of the suit will be lower. On the other hand, if the leading edge is too soft, the wing will not achieve the right shape.

17

Requirements Compliance Matrix and Feasibility Analysis

The final design has to be analyzed to check whether or not the optimal design was found. This is done in different ways. First of all in Section 17.1 a compliance matrix is created, in which will be investigated if the requirements are met. The exact values and or situation of the requirements will be explained in Section 17.2.

17.1 Compliance matrix

To be able to sufficiently rate the design, a compliance matrix is built, see Table 17.1. In this matrix all predefined requirements for the design are stated and checked whether they are met or not. The killer and driving requirements are also indicated. Killer requirements are extremely important to meet. If they are not met, they will 'kill' the design. Requirements that drive the design more than average are called driving requirements. Further explanation on the level the requirement is met or not is given in Section 17.2.

17.2 Feasibility analysis

One requirement is not met, more details about this requirement are explained in Section 17.2.1. Furthermore for some requirements it is still unknown if the current design meets them or not. This is further elaborated in Section 17.2.2. Finally some more details about the achieved requirements are given in subSection 17.2.3 by referring to the different features of the final design.

17.2.1 T-Sft-03

The requirement 'Pilot should be able to detect a collision course' was not met as the wingsuit will not help the pilot to predict the collision course. Besides for visual detection, no extras are currently on the design to help detect a collision course. The visual detection is improved though by the integration of the GoPro which makes head movements easier. However at the first brainstorm session some ideas were thought of to improve the detection. For example by in-flight visualizations displayed with for example 'Google Glass'. However getting information displayed will reduce your visual detection and might increase the risk of a collision course. Furthermore building the simulations behind the in-flight simulations is outside the scope of this project, but definitely a recommendation for the future. Therefore for this DSE it was decided to focus on making wingsuiting safer by adaptations to prevent collision by other means rather than detecting it. For example the droop is added to be able to get temporary a better lift over drag ratio, to change his course it is noticed this would otherwise lead to collision. Furthermore a quick-release will make sure that the pilot is able to quickly get out of trouble by deploying the parachute and immediately being able to steer.

17.2.2 Unknown requirements

T-Str-03

At the moment it is not known for sure if the design will not fail before 800 jumps or 10 years. Current wingsuits have this life span. The new features of wingsuits are mostly made of material that is already used for the wingsuits or are proven in other ways to probably last for the same amount of time as the

Table 17.1: Compliance Matrix

ID-number	Requirement	Satisfied		
		YES	NO	Unknown
T-Str-01	Material should be strong enough to sustain flight (DRIVING)	✓		
T-Str-02	Wingsuit should not fail before 800 jumps or 10 years			✓
T-Str-03	Pilot should be able to cope with flight- and parachute loads	✓		
T-Str-04	Pilot should be able to deploy parachute (DRIVING)	✓		
T-Str-05	Pilot should be able to control parachute	✓		
T-Str-06	Wingsuit should not lose aerodynamic shape during operation	✓		
T-Str-07	Wingsuit should generate lift (DRIVING)	✓		
T-Fly-01	Wingsuit should be controllable about 3 axes (DRIVING)	✓		
T-Fly-02	Wingsuit should reach aerodynamic shape within 2 seconds (KILLER)	✓		
T-Fly-03	Wingsuit should be pitch stable			✓
T-Fly-04	Wingsuit should be yaw stable			✓
T-Sft-01	Pilot should be able to detect stall	✓		
T-Sft-02	Pilot should be able to detect spin	✓		
T-Sft-03	Pilot should be able to detect a collision course		✗	
T-Sft-04	Pilot should be able to recover from stall (DRIVING)	✓		
T-Sft-05	Pilot should be able to recover from a spin (DRIVING)	✓		
T-Sft-06	Pilot should be able to divert from collision course (DRIVING)	✓		
T-Sft-07	Pilot should be able to release wingsuit within 1 second	✓		
T-Sft-08	Wingsuit should have a reliability as high as possible (KILLER)	✓		
C-Des-01	The weight of the total gear should not exceed 10kg (KILLER)	✓		
C-Des-02	The cost of the wingsuit should not exceed €5000,- (DRIVING)	✓		
C-Des-03	The volume of the wingsuit should not exceed $0.02m^3$ (DRIVING)	✓		
C-Des-04	Wingsuit should have L/D of at least 2.5 (DRIVING)	✓		
C-Des-05	Wingsuit should be able to operate within 50 - 150+ km/h (DRIVING)	✓		
C-Des-06	Minimum exit altitude should not exceed 100m (DRIVING)	✓		
C-Des-07	Wingsuit should operate without a propulsion system	✓		
C-Des-08	Pilot should be able to jump out of a plane	✓		
C-Dev-01	The project must be completed within DSE limitations (KILLER)	✓		
C-Dev-02	The results of the project reduce fatalities with factor 10 (DRIVING)			✓
C-Dev-03	Wingsuit should be produced with minimal waste	✓		
C-Dev-04	Wingsuit should be produced with non-toxic materials	✓		
C-Dev-05	Wingsuit should be able to be produced sustainably	✓		

rest of the wingsuit. Or they can be repaired easily without causing the wingsuit to fail. Therefore it is expected that the wingsuit will meet this requirement, however time will have to prove this.

T-Fly-03 & T-Fly-04

It is currently not known if wingsuits are stable or not. Because interviewed wingsuiters were not able to describe how their made and resulting movements for flying exactly go and the group lacks own experience, the stability of wingsuits can only be guessed. Interpreting the stories of wingsuiters, it seems that the wingsuit is not pitch or yaw stable. With the current improvements as air tunnels the flow around the leg wing is improved, which will result in a better stability. However it is still not sure if this makes the wingsuit less unstable or more stable. Furthermore to prevent fatality of for example pitch instability, the passive flap and stall warning offer a solution.

C-Dev-02

A driving requirement of the project is 'reduce fatalities with a factor 10'. In Table 17.2 an overview is given of the cause of death of current BASE fatalities. [8]

Table 17.2: Cause of BASE fatalities

Cause of death	Percentage [%]
No Pull	38
Strike (Body)	30
Strike (Canopy)	9.5
Off-Heading Opening	8
Line Twist	8
Exit Slip	3
Drowning	3
Electrocution	0.5

The new design will make wingsuiting safer, however it is hard to determine with which factor it is exactly reduced. At the moment fatality is caused a lot by human error and also stupidity plays a part in quite some accidents. For example folding the parachute incorrectly can lead to an off-heading opening of the parachute, which can be fatal. Currently the main cause of death is no pull. No pull implies that the wingsuiter did not have time anymore to be able to pull the parachute. The implementation of the Swiss pouch and quick-release should drastically reduce this number of fatalities. The Swiss pouch makes it easier to pull the pilot chute and the quick-release provides the ability to start steering and controlling the canopy flight straight after the pull. Another big cause of fatal accidents is the impact of the body with an object (strike, body), most of the time the cliff wall. This can happen straight after the exit, but also during the flight and can have different causes such as a spin or stall. To prevent this, several adaptations were made to the wingsuit. For example the wing connection should make sure the wings get inflated quickly and a spin that can lead to collision will be prevented. Furthermore air tunnels, droop and vortex generators should improve the flow over the wingsuit, delay stall, increase the maximum lift coefficient and thus offer a solution to deviate from a collision course.

Impact can also occur after canopy deployment (strike canopy). To prevent this, the combination of the Swiss pouch and quick-release should make sure the pilot can easily and quickly switch from wingsuit flying to canopy flying and it improves steering, as the quick-release makes sure the arms are free immediately.

Another thing that can happen at the canopy deployment is an off-heading opening, line twist or that the canopy gets sucked in the burble. The burble is reduced with vortex generators, air tunnels and the use of the switch pouch which makes it easier to throw the pilot chute outside the burble. An off-heading opening is furthermore mainly due to incorrect packing of the canopy, but human error can never be crossed out completely. Exit slip will be reduced with the anti-slip feature on the wingsuit. Finally drowning and electrocution can only be prevented by making sure that directly after the pull, steering is enabled and this is done with the quick-release.

One important thing to keep in mind is that you cannot fight stupidity. Hence, the number of deaths will never reach zero, especially not in an extreme, adrenalin sport as wingsuiting. The safer the design gets, the more risk some will take. However with the current features of the design wingsuiting gets safer and the fatality rate will be reduced.

17.2.3 Achieved requirements

The requirements that are met, will now be shortly discussed in order. **T-Str-01** The material of the designed wingsuit is the same as current wingsuits and has proven to be strong enough to sustain flight. **T-Str-03** At current wingsuits the pilot loads are bearable, but not always comfortable. With the shoulder reinforcement the pilot loads are reduced. **T-Str-04 & T-Str-05** The pilot also has to be able to deploy and control the parachute. To ensure this can easily be done, the Swiss pouch and quick-release were added to the design. **T-Str-06** The wing connection helps the wingsuit to keep the aerodynamic

shape. Furthermore air tunnels, droop and vortex generators make the flow around the wingsuit more optimal. **T-Str-07** They furthermore increase the maximum lift coefficient and maximum angle of attack. **T-Fly-01** Looking at the controllability of the wingsuit, the wingsuit is controllable about 3 axis. This controllability is improved with the droop and air tunnels. **F-Fly-02** The wing connection helps the wingsuit to reach the aerodynamic shape quickly. **T-Sft-01** For the safety, the stall warning helps the pilot to detect stall. **T-Sft-02** Spin can easily be detected both visually and with other senses as the pilot won't be flying 'straight' anymore. The wingsuit itself is however not able to detect it, however the wing connection will help prevent some cases of spin. **T-Sft-04** To recover from stall, the passive flap will prevent stall to occur. Also the droop and vortex generators will delay the stall. **T-Sft-05** As mentioned before the wing connection solves the case of one wing deflating, resulting in spin. **T-Sft-06** To divert from a collision course, the design offers a couple of new options, first of all the quick-release can make sure that when noticed directly can be adjusted from a collision course as steering is enabled straight after the pull. Furthermore the droop helps increasing the glide ratio and thus can help changing a fatal line. **T-Sft-07** It is also possible to release the wingsuit within one second, with the quick-release the arms are free immediately after the pull to throw out the pilot chute. **T-Sft-08** The final technical requirement is that the reliability should be as high as possible. The new design features are carefully selected on their feasibility and are kept as simple as possible to make the reliability higher.

Besides technical requirements, also the constraints needed to be met. **C-Des-01** The first one was the total weight of the gear. Wingsuits at the moment weigh maximum 2 kg and also a BASE backpack is lightweight. With the new features, not that much extra weight is added as the heaviest one, the shoulder reinforcement is only 0.6 kg. Therefore the weight is definitely below 10kg. **C-Des-02** The total cost of the new wingsuit will be around €500, thus below the requirement of €5000. **C-Des-03** The new adaptations to the wingsuit will not drastically increase the volume and hence, it stays below $0.02m^3$. **C-Des-04** With current wingsuit already glide ratios of at least 2.5 can be reached. The advanced wingsuit will definitely have the same if not better performance, as with the droop the glide ratio can be increased. **C-Des-05** However the speed range was left unchanged compared to current wingsuits. **C-Des-06** Continued with the minimum exit altitude of 100m. The wing connection and other adaptations ensure quicker inflation, so the minimum exit altitude will only be decreased. **C-Des-07** Even though a lot of new features are added to the wingsuit it is made sure that the wingsuit is still without a propulsion system to keep the experience of flying as close to birds as possible. **C-Des-08** Furthermore these new features are not that big that carrying and wearing the suit in a plane and jumping out of it afterwards, would be made impossible. **C-Dev-01** Another very important constraint and killer requirement is that the project should be done within DSE limitations. To achieve this, some simplifications and choices had to be made for the design to be able to succeed within the available time. **C-Dev-03** The advanced wingsuit will be handmade, just as before, and customized to size for each customer. Furthermore production should be as economical as possible to ensure minimal waste to be produced. **C-Dev-04** Wingsuiting is already an extreme sport, so killing the wingsuiter already by making the wingsuit of toxic materials might not be the best idea. Therefore the materials are carefully selected. However the production of carbon fiber, used for the passive flap can be dangerous and thus should be carefully executed and done only by professionals. **C-Dev-05** Finally the wingsuit should be produced sustainably. Because sustainability is always considered of paramount importance, during the design process this is always carefully taking into account. Moreover with an eye on getting the sustainability as high as possible, the production is looked into and thus also this requirement is met.

17.2.4 Conclusion

The main goal of designing a next generation wingsuit was to drastically improve the safety. With this in mind the requirements were set up. All killer requirements are met, thus the project is not a failure. Of the driving requirements, the most important one of 'reducing fatality with a factor 10' is still unknown if it is met in the absolute sense. Safety is increased and fatality will be reduced, but if a factor 10 is reached is not absolutely sure. One of the other requirements was not met as at the moment besides visual sight the pilot is not able to detect a collision course and therefore this is definitely an option for further research. This to ensure the design is even safer and the reduction with a factor 10 is guaranteed for sure.

18

Future research

This project was a learning process, problems were encountered, counter measures were taken, some were solved, but there were some defeats. This chapter will present the recommendations for both the content of the report and the ideas for a new project.

18.1 Future project research

In this project a foundation of the basic wingsuit knowledge is made for the wingsuit community, however there is still a large part which can be determined in order to design a perfect wingsuit. Using a flight test, one would be able to determine the stall angle and glide ratio which will further decrease the gap in basic wingsuit knowledge. Real life flight data can be obtained via an IMU, GPS, altimeter and a self adjusting pitot tube with a potentiometer. In order to also get qualitative flight test data from the same test flight, one could be flying above the test pilot filming the flow over the wingsuit which is visible using tufts.

With more time, simulations can be done using a higher resolution. This resolution will make sure the results of the program are more accurate which results in better calculations of the wingsuit characteristics. If these characteristics are calculated more accurately, different concepts, as a passive flap, droop, ..., can be tested and proven to work using the CFD program. Since the passive flap is a highly dynamic device which reaches an equilibrium position in the flow, a fluid-structure interaction software is needed, in order to be able to draw founded conclusions on the usefulness of this concept. When combining the flight test results with better CFD calculation results, one is able to validate the CFD program better so the results can be used for further calculations.

18.2 New project options

Since the structure of the wingsuit is a human body, it is far from rigid. When the wingsuiter gets tired, his body posture will change and the airflow around the suit changes. With the right body posture, the flight performance can be maximized. During the wind tunnel test this was confirmed, but no further research on this topic has been done during this DSE project. Further research on the influence of different body postures on the performance, their limitations and advantages could be interesting.

This project could be combined, with a research on the optimization of the wingsuit. Can the shape of the wingsuit be improved, and how? Should material be added, the rig integrated, a hoodie implemented to aid in transition from the helmet to the rig? There are more than enough options. Also, the manufacturing process of drop-stitch might be improved such that this can be incorporated to smoothen and strengthen the airfoil.

Since wingsuiters come in all shapes and sizes, a single size suit cannot cover the entire wingsuit population. Also, because a proper fit is essential for optimal performance and safety, a suit has to be custom made for each and every wingsuiter. It might be interesting, for another DSE project, to do more research on the performance and create a program that designs the optimum wingsuit in accordance with body dimensions of the customer and hsi demands on performance.

With the mission statement in mind, "Design a next generation wingsuit to improve the safety of flying while keeping the thrilling aspects of the sport.", this project focused mainly on the base jumping market, since most accidents occur there. To keep the company economically healthy, it might be interesting to focus on the mid-range wingsuits as well, and develop these with the improvements of the advanced wingsuits. This would result in a company that is not dependent on a niche share of customers.

Bibliography

- [1] unknown, *Human Flying Squirrel Zooms Through Air*, Popular Science Monthly, September 1930.
- [2] Kuosma, J., “Birdman Story,” <http://www.bird-man.com/company/story/>, april 2013.
- [3] Thummas Corporation, “Wingsuit Manufacturers,” http://www.texaswingsuitacademy.com/wingsuit_manufacturers-BF.php, april 2013.
- [4] Squirrel, “Squirrel Wingsuits,” <http://www.squirrel.ws/>, april 2013.
- [5] Rugai, N., “Nitro Rigging,” <http://nitrorigging.com/>, april 2013.
- [6] “BIRDMEN, The Original Dream of Flight,” Documentary, march 2012.
- [7] Knutson, M., “Fatality Statistics,” http://www.blincmagazine.com/forum/wiki/Fatality_Statistics.
- [8] BLiNC Magazine, “Fatality Statistics,” http://www.blincmagazine.com/forum/wiki/Fatality_Statistics, May 2013.
- [9] DSE group ‘Advanced Wingsuit’, *Wingsuit survey*.
- [10] Selig, M. S., Deters, R. W., and Williamson, G. A., “Wind Tunnel Testing Airfoils at Low Reynolds Numbers,” *AIAA Aerospace Sciences Meeting*, 2011.
- [11] NASA - Glenn Research center, “Reynolds number,” <http://www.grc.nasa.gov/WWW/k-12/airplane/reynolds.html>, June 2013.
- [12] unknown, “Paralog, GPS based performance racing,” <http://paralog.net/ppc/>, June 2013.
- [13] Robson, G. and D’Andrea, R., “Longitudinal Stability Analysis of a Jet-Powered Wingsuit,” *AIAA Guidance, Navigation, and Control Conference 2 - 5 August 2010, Toronto, Ontario Canada*.
- [14] unknown, “Windtunnel test with wingsuit model,” <http://www.youtube.com/watch?v=uUbfAMfRV9Y>, June 2013.
- [15] Marzocca, P., “The NACA airfoil series,” [http://people.clarkson.edu/\\$\sim\\$pmarzocc/AE429/The\%20NACA\%20airfoil\%20series.pdf](http://people.clarkson.edu/\simpmarzocc/AE429/The\%20NACA\%20airfoil\%20series.pdf), June 2013.
- [16] SQUIRE, L., “Interactions between wakes and boundary-layers,” *Prog. Aerospace Sci.*, Vol. 26, No. pp. 261-288, 1989.
- [17] Hepperle, M., “About JavaFoil,” http://www.mh-aerotoools.de/airfoils/jf_about.htm, June 2013.
- [18] Eppler, R. and Somers, D., “A Computer Program for the Design and Analysis of Low-Speed Airfoils,” *NASA TM-80210*.
- [19] Eppler, R., “Praktische Berechnung laminarer und turbulenter Absauge-Grenzschichten,” *Ingenieur-Archiv*.
- [20] Eppler, R., “Turbulent Airfoils for General Aviation,” *Journal of Aircraft*, Vol. 15, No. 2, 1978.
- [21] unknown, “Aerodynamics of Model Aircraft,” <http://www.mh-aerotoools.de/airfoils/javafafoil.htm>, 2008.
- [22] Deperrois, A., “XFLR5,” <http://www.xflr5.com/xflr5.htm>, June 2013.

- [23] Deperrois, A., “XFLR5 Analysis of foils and wings operating at low Reynolds numbers, Guidelines for XFLR5 v6.03,” 2011.
- [24] J. D. Anderson, JR, *Fundamentals of Aerodynamics*, McGraw-Hill, 2007.
- [25] dr. ir. G. La Rocca, “Wing design - part 3,” *Aerospace Design and Systems Engineering Elements II AE2101 - lecture slides*, 2011.
- [26] Niță, N. and Scholz, D., “Estimating the Oswald factor form basic aircraft geometrical parameters,” *Deutscher Luft- und Raumfahrtkongress 2012*, 2012.
- [27] Jacobs, E. N., “The aerodynamic characteristics of eight very thick airfoils from tests in the variable density wind tunnel,” *National Advisory Committee For Aeronautics*, , No. 391, 1931.
- [28] Jr., L. K. L. and Cohen, K. S., “Aerodynamic characteristics of a number of modified NACA four-digit series airfoil settings,” *National Advisory Committee For Aeronautics*, 1947.
- [29] Ir. A. H. Abbott, *Theory of wing sections, Including a Summary of Airfoil Data*, Dover Publications, Inc. New York, 1959.
- [30] Ruijgrok, G., *Elements of airplane performance*.
- [31] Bata Inc., “Shoe Material,” <http://www.bata.com/learn-shoe-material.php>, June 2013.
- [32] Advameg Inc., “Running Shoe,” <http://www.madehow.com/Volume-1/Running-Shoe.html>, June 2013.
- [33] Lucifer, blincmagazine, “Wingtip Pouch pilot chute system,” http://www.blincmagazine.com/forum/wiki/Wingtip_Pouch_pilot_chute_system_-_SWISS_pouch, March 2013.
- [34] Delnero, J. S., nón Di Leo, J. M., Camocardi, M. E., Mariano, D. G. F., Martinez, A. M., and Colman, J., “Vortex generator effect on low Reynolds number airfoils in turbulent flow,” 2008.
- [35] Delnero, J. S., non Di Leo, J. M., and Camocardi, M. E., “Experimental study of vortex generators effects on low Reynolds number airfoils in turbulent flow,” *Int. J. Aerodynamics*, Vol. 2, No. 1, 2012.
- [36] Delnero, J. S., non Di Leo, J. M., Martinez, M., Bacchi, F., Colman, J., Scarabino, A., and Boldes, U., “Effects of Turbulators on an airfoil at low Reynolds number in turbulent flow,” 2007.
- [37] Lissaman, P. B. S., “LOW-REYNOLDS-NUMBER AIRFOILS,” 1983.
- [38] Tilmann, C. P., John, K. J. L., Betterton, G., and Wilson, M. J., “Characterization of Pulsed Vortex Generator Jets for Active Flow Control,” .
- [39] Prince, S. A., Khodagolian, V., Singh, C., and Kokkalis, T., “Aerodynamic Stall Suppression on Airfoil Sections using Passive Air-Jet Vortex Generators,” *AIAA*, Vol. 47, 2009.
- [40] Reuss, R. L., Hoffmann, M. J., and Gregorek, G. M., “Effects of Surface Roughness and Vortex Generators on the NACA 4415 Airfoil,” 1995.
- [41] Heine, B., Mulleners, K., Joubert, G., and Raffel, M., “Dynamic Stall Control by Passive Disturbance Generators,” *AIAA Applied Aerodynamics Conference*, Vol. 29, 2011.
- [42] J.G. Betterton and K.C. Hackett et al., *Laser Doppler anemometry investigation on subboundary layer vortex generators for flow control*, Appl. of Laser Tech. to Fluid Mech.
- [43] Godard, G. and Stanislas, M., “Control of a decelerating boundary layer. Part 1: Optimization of passive vortex generators,” *Aerospace Science and Technology*, Vol. 10.
- [44] M. Schatz et al., “Separation Control by Self-Activated Movable Flaps,” *AIAA*.
- [45] C.H. John Wang and J. Schlüter, “Stall control with feathers,” *Comptes Rendus Mécanique*, Vol. 340, No. 1 - 2, 2012, pp. 57 – 66, Biomimetic flow control.
- [46] Bionic Avionics Inc., “FlySight GPS,” <http://www.flysight.ca/features.htm>, June 2013.

- [47] ELECTROMATIC Equipment Co. Inc., “ODT, Stationary Tension Meters,” http://checkline.com/stationary_tension_meters/ODT, June 2013.
- [48] Chandrasekhara, M. S., Martin, P. B., and Tung, C., “Compressible Dynamic Stall Control Using a Variable Droop Leading Edge Airfoil,” *Journal of Aircraft*, Vol. 41, No. 4, 2004.
- [49] Staff of Langley Research Center, “Exploratory Study of the Effects of Wing-Leading-Edge Modifications on the Stall/Spin Behavior of a Light General Aviation Airplane,” .
- [50] Schlichting, H. and Gersten, K., *Boundary-layer Theory*.
- [51] Tani, I., Iuchi, M., and Komoda, H., “Experimental investigation of flow separation associated with a step or a groove,” 1961.
- [52] ASM material, “Aluminium 7075-T6,” <http://asm.matweb.com/search/SpecificMaterial.asp?bassnum=MA7075T6>, juni 2013.
- [53] Grafix Plastics, “Mylar film and sheet properties,” http://www.grafixplastics.com/mylar_prop.asp/, june 2013.
- [54] Australian Parachute Federation, “FAA Handbook,” http://www.apf.asn.au/ArticleDocuments/75/FAA-Handbook-8083-17_Chs_2.pdf.aspx, August 2010.
- [55] Roland, I. et al., “Foam,” *International Journal of Pharmaceutics*, Vol. 263.
- [56] TMS, “Attributes, Characteristics, and Applications of Titanium and Its Alloys,” <http://www.tms.org/pubs/journals/JOM/1005/boyer-1005.html>, June 2013.
- [57] Granta Design Limited, “CES EduPack 2013,” .
- [58] Composite Resources, “Composite Properties,” <http://www.composite-resources.com/composites/composite-properties/>, june 2013.
- [59] Thorington, R. W., Darrow, J. K., and Anderson, C. G., “Wing tip anatomy and aerodynamics in flying squirrels,” *Massachusetts Institute of Technology*.
- [60] Kernan, M., “How Squirrels Fly,” *Smithsonian magazine, February 2001*, February 2001.
- [61] Jr, R. W. T. and Ferrell, K. E., *Squirrels: The Animal Answer Guide*, The Johns Hopkins University Press, 2006.
- [62] Pennycuik, C., *Theoretical Ecology Series: Modelling the Flying Bird, Chapter 16: Evolution of Flight*, Elsevier, 2008.
- [63] Desktop Aeronautics, Inc., “Applied Aerodynamics: A Digital Textbook,” <http://www.desktop.aero/appliedaero/potential3d/fsw.html>, January 2007.
- [64] Dropzone Forums, <http://www.dropzone.com/cgi-bin/forum/gforum.cgi>, april 2013.
- [65] Uragallo, T., “TonySuits Wingsuits,” <http://www.tonywingsuits.com/index.html>, april 2013.
- [66] Phoenix-Fly, “Phoenix-Fly,” <http://www.phoenix-fly.com/>, april 2013.
- [67] Phoenix-Fly, “Phoenix-Fly Order FAQ,” http://www.phoenix-fly.com/products/order_faq, april 2013.
- [68] “How to Make a Smoke Bomb,” <http://chemistry.about.com/od/demonstrationexperiments/ss/smokebomb.htm>, april 2013.
- [69] Phoenix-Fly, “Price List,” http://www.phoenix-fly.com/products/price_list_, June 2013.
- [70] Fly Your Body, “S-FLY ACCESS,” <http://flyyourbody.com/en/8-s-fly-access>, June 2013.
- [71] Phoenix-Fly, “Prodigy 2,” .
- [72] Rail Corp, “RELIABILITY, AVAILABILITY AND MAINTAINABILITY (RAM),” .

Appendices

Part V

Project Deliverables

A

Project Log

In this appendix a short recap of what was presented in the previous reports is given. If one is familiar with the previous reports, only Section A.4 provides information which has not yet been covered. As previously mentioned, this is the fourth report of this DSE project. The previous reports were the project plan, the baseline review and the Mid-Term review. After the midterm review, the concept of a flying squirrel was investigated, the process and conclusion will be given at the end of this section.

A.1 Project Plan

In the project plan, all steps were presented that were necessary to get a good overview of the project. These include the team organization, work break down structure and a Gantt chart showing the different deadlines that need to be met. As this information is not important for the understanding of the current design, no further explanation is given in this report.

A.2 Baseline Review

The baseline review was the groundwork to develop a first conceptual design. This meant first analyzing the operation of a wingsuit in order to determine our requirements. A survey was held to get the necessary practical information. The results of this survey are presented in [9].

The first version of the functional flow diagram and function breakdown structure were given in this report. These parts continued to be further developed throughout the project and the final version of these parts are presented in this report. This holds for all the important parts of the baseline review: market analysis, resource allocation, technical risks, and sustainability. The only important part of the baseline review that is not represented in this report is the requirements discovery tree. However, an overview of the requirements can be seen in Chapter 17. This chapter presents a compliance matrix of our final detailed design in which it is investigated whether it meets the requirements.

A.3 Mid-Term Review

The third and last report before this final report, was the Mid-Term report. In the Mid-Term report all the design options that are obtained during a brainstorm are presented, analyzed and categorized by the different phases: Exit & Controllability, Aerodynamics, Structures, Emergency & Situational Awareness and Energy Disposal. For each function in each phase a trade-off is made to give insight into the advantages and disadvantages of the different design options and to see which design options are better than others. The best-scoring design options were used to set up three wingsuit designs, each with a different design goal, namely: performance, controllability and safety. Although wingsuits with increased controllability or performance could also enhance the safety, there is another 'safety' design. The focus of this design is to increase the safety and not to have a higher controllability or performance. However, these are only the principle focuses of the designs and some overlap is possible. Using a final design trade-off, the safety wingsuit was found to be the best according to our assigned criteria weights. The safety wingsuit was equipped with the following design options: anti-slip for the soles of the feet, quick-release for the arm wings, shoulder reinforcements, turbulator strips & vortex generators, passive flap & stall warning, a droop leading edge, air tunnels for flow re-energizing, wing connection, Swiss pouch and integrated GoPro. More information about these concepts can be found in Chapter 10 where they are explained in detail. For more information about the midterm review, the reader is advised to read the midterm review report.

A.4 Flying Squirrel concept

Optimally, all concepts should have been investigated before the midterm review and a final choice should have been made on the configuration. During the midterm review however, a new configuration came into view, which was not yet investigated and showed a few interesting characteristics: forward swept wings, comparable to flying squirrels. After some more research on the exact bone structures and flight principle of these animals a concept was developed [59][60][61]. The flight principle and the way the arms (also called the front legs) are bent are shown in Figures A.1 and A.2.

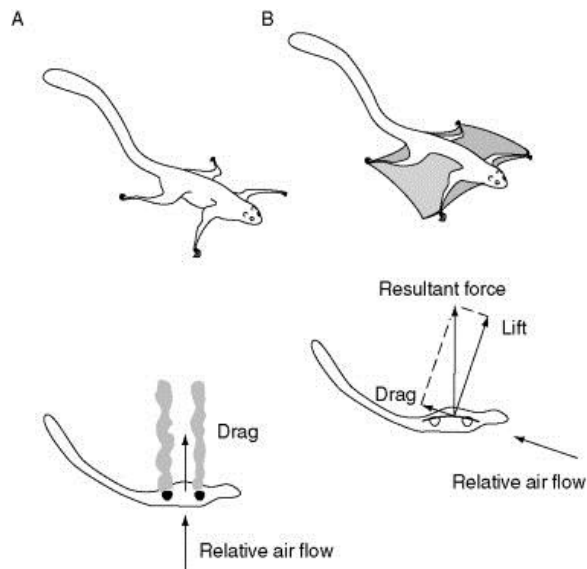


Figure A.1: Flight principle of flying squirrels [62]

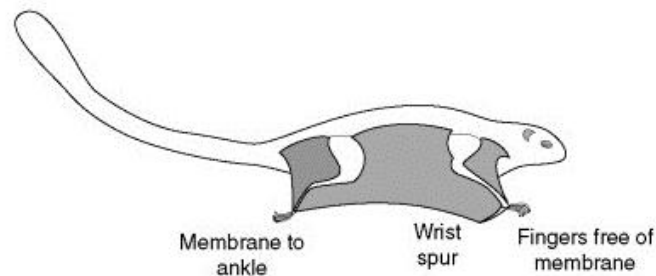


Figure A.2: Bone structures [62]

Because most of the times the best ideas are developed by copying nature, a wingsuit design based on the way flying squirrels fly and their bones are constructed was developed. A rough sketch is shown in Figure A.3. This concept, where the arms are swept forward, was further analyzed. Its advantages and disadvantages and the conclusion are described below.

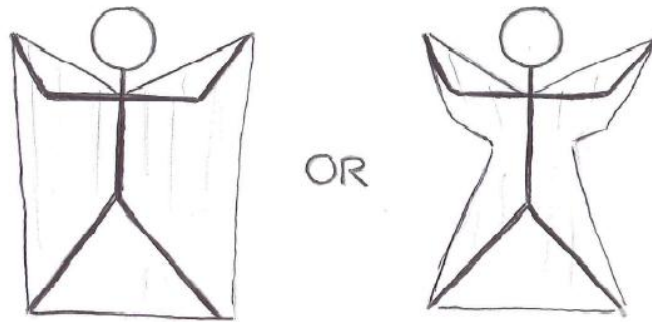


Figure A.3: Squirrel concepts

A.4.1 Pros

The advantages of the squirrel design option are first of all that it will have a slightly better performance. The same performance as with wingtips. However, the extra area will not have that much influence as this design will increase the area in rectangular shape instead of in square shape, the latter is better for the aspect ratio, since the aspect ratio is defined as $A = \frac{b^2}{S}$, where b is the span and S the surface. The forward swept wings have relative to the current backward swept wings less span, and thus a lower aspect ratio. Secondly, the maneuverability will be better and it has a smaller basic lift distribution.[63] Considering the pilot loads, it is not sure if this position will provide more comfortable pilot loads in all situations. Finally, this concept is based on biomimicry, which normally provides good results. Though, the position of the shoulders and joints of a squirrel are different. Therefore, it is debatable to what extent the wingsuiter can be compared with a flying squirrel.

A.4.2 Cons

The main disadvantage is that this design is more unstable in the yaw, this is due to the forward swept. Hence, a small yaw disturbance will lead to a bigger disturbance.[63] Furthermore, with this design, lots of adjustments to the current design need to be done, the leading edge and current idea for the droop need to be changed completely, location of zippers re-investigated and also this design will still need a quick-release. Also with the arms already bent forward, low performance flying will be more difficult. Currently when wingsuiters fly close to the ground, they fold their arms back to lower the performance and pilot loads. This way, they do not get very tired and in case of an emergency, they can increase their performance easily. However, with this design, this is not an option.

A.4.3 Conclusion

Concluded the advantages do not exceed the disadvantages. Moreover the new design does not yield enough profits for now to continue with it, compared to the one stated in the midterm review. Therefore, it was decided that the flying squirrel design will be rejected for now. Especially since this design requires a lot of adaptations to the current wingsuits and probably also raises unforeseen problems and complications. For example the leading edge will not be supported by the arms anymore, and so a different construction needs to be developed for this arm as the same support is needed. Also, a good leading edge for the aerodynamic shape is still desirable. Furthermore, this also implies that the zippers will need to be constructed differently. Hence, though it is a nice concept for further research, the flying squirrel concept will be rejected for the current project and the design, as stated in the midterm report, will be worked out further.

B

Functional Flow Diagram

The Functional Flow Diagram shows the logical order of activities to be executed by the wingsuit jumper in order to perform a proper wingsuit flight. This is put in the diagram to make sure that every possible function is incorporated in the wingsuit design.

The Functional Flow Diagram consists of one major flow line, which is divided into seven different sub flow lines. The seven sub flow lines describe: Preparation, Exit, Stable and Controllable flight, Canopy Deployment, Canopy Flying, Landing and Maintenance. Keep in mind that several activities may be performed in parallel and can come together. Take for example stability, control and steering, these are performed simultaneously.

The Preparation phase is an important part of the flight. Earth observation is used to determine the initial flight path/line. Observations from previous flights will be used to determine new (possibly more dangerous) flight lines until an optimal flight path has been found. Distinct landmarks are used for orientation during flight.

Next, the Exit procedure will be described. First, the jump from the Exit point is executed which immediately changes into falling. When one jumps with anti-slip, the jump will be more controllable. During the fall, correct attitude and speed should be gained, after which the wingsuit will start to inflate. Depending on the skill of the jumper, this procedure can be executed very quickly, and the jumper can start wingsuiting in a matter of seconds. Next to anti-slip, the wing connection will also increase the safety by inflating both wings simultaneously.

At this point, the wingsuiter is flying and will have to be able to perform a stable and controllable flight. During this phase, it is very important to keep a stiff posture at all times. This will help to maintain a stiff airfoil shape, which increases the wingsuit performance significantly by providing more lift. During the flight, the wingsuiter will continuously check his orientation and location and will adjust the heading and/or attitude in order to follow the predefined flight line. Using the stall warning the wingsuiter will know if he is approaching a stall. Simultaneously, the stability of the wingsuit will be checked and the wingsuiter will try to recover from an unstable situation if any instability should occur. If the wingsuiter will be in an emergency situation, the droop leading edge can be used to get out of this situation.

Once the wingsuiter arrives at the end of the flight line (or if the need should arrive), he/she will need to deploy his/her parachute. First, the orientation will be checked. When the wingsuiter has the correct orientation and location, the wingsuiter will deploy his parachute by activating the Swiss pouch while still flying. During the deployment of the parachute, the arms will be set free automatically due to the quick-release. If this system does not work correctly, the wingsuiter will still be able to free his arms by unzipping his arms using the conventional method.

The rest of the flight is continued by flying the canopy. The same control and stability process as during the wingsuit flight are applied here.

At the end of the flight, the Landing should be executed. First, the surroundings are checked. Then the flight speed is reduced. Lastly, the touch down is executed. The wingsuiter is now safely on the ground.

The flight is completed and now only the maintenance is left. The parachute is folded and the equipment is transported after which it is checked and, if necessary, repaired. The equipment is prepared for the next flight.

Functional Flow Diagram

Process

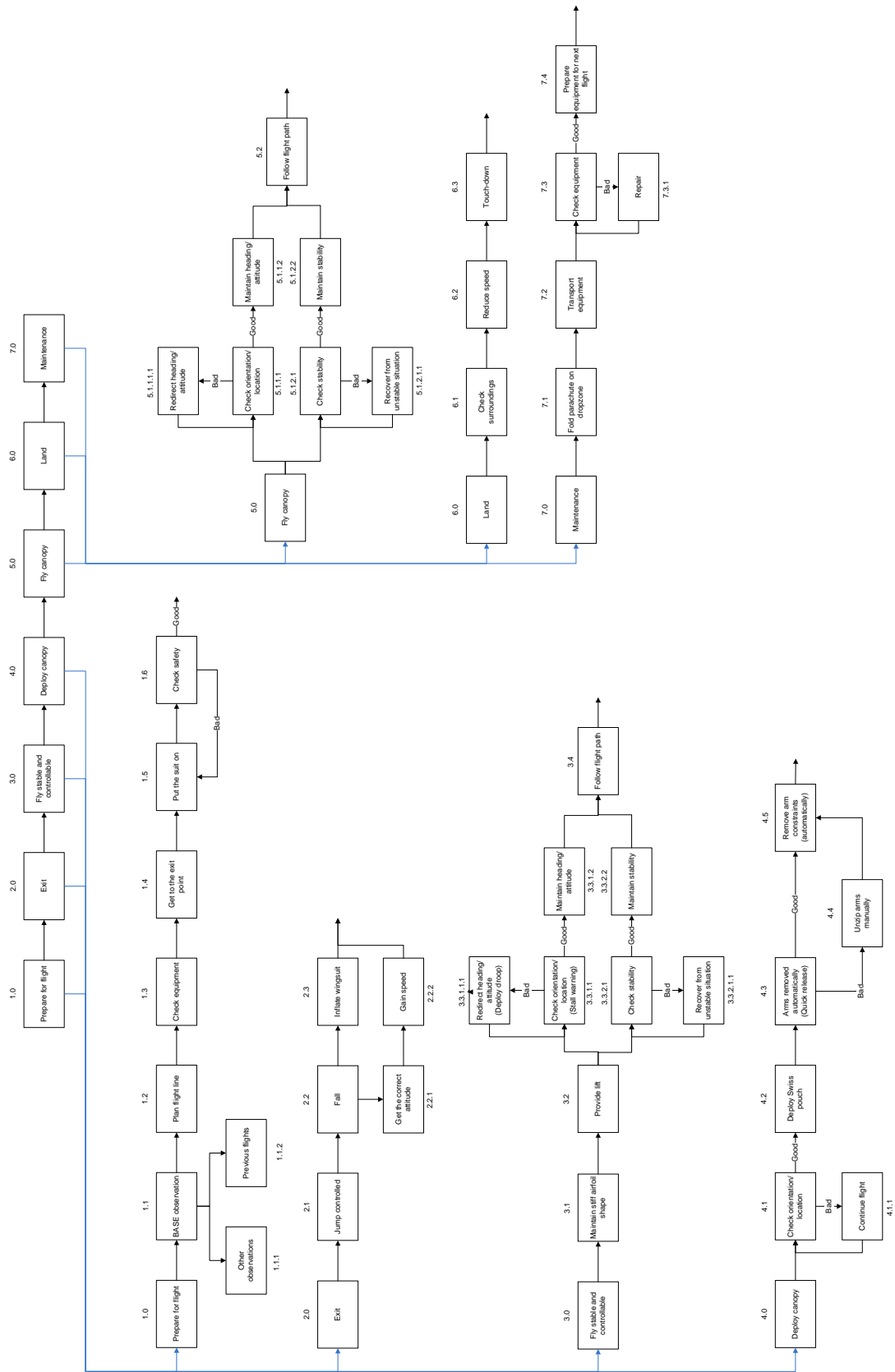


Figure B.1: The Functional Flow Diagram describes the wingsuit flying process.

C

Functional Breakdown Structure

In the functional breakdown structure (FBS) presented in figure C.1, the most important functions that the wingsuit must fulfill are presented. There are seven main phases in wingsuit flying, these are the main functions of the system. Each phase incorporates certain subfunctions that the wingsuit must fulfill. The relevant subfunctions are defined per flight phase in the same figure. As can be seen, the same elements as mentioned in the functional flow diagram are present. However, now sorted and presented by phase instead of in a time line construction.

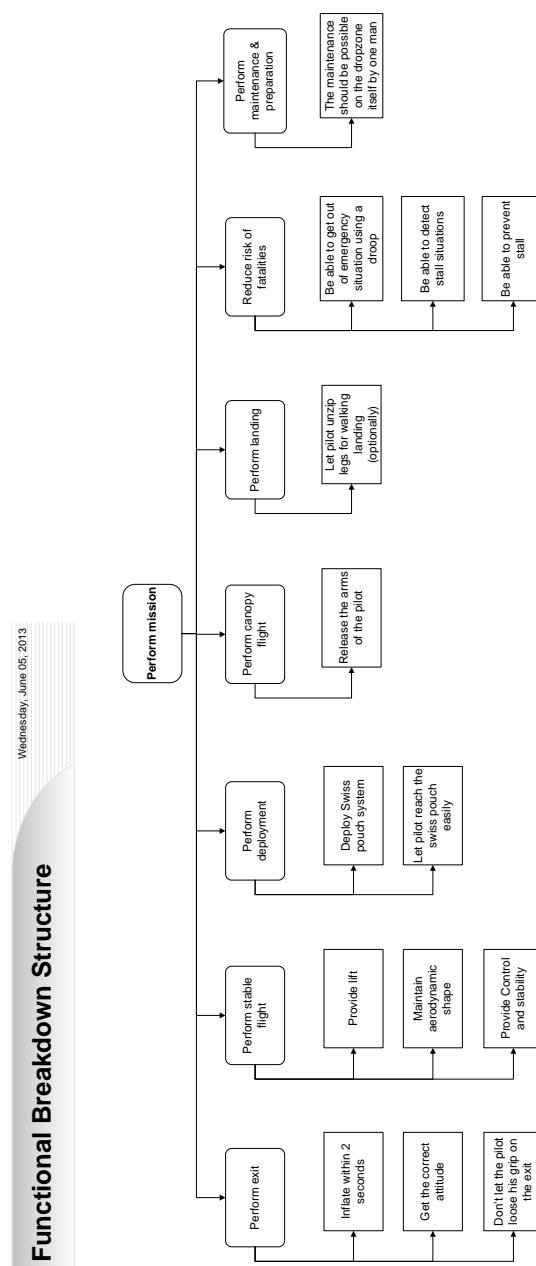


Figure C.1: The FBS represents hierarchically the functions that the product must perform.

D

Resource Allocation

To handle the design process of a wingsuit well, a clear resource allocation is needed. It makes sure that the team exactly knows which resources are available to design the final product. The resources can be split up in human resources and the technical resources. First, the human resources consist of the allocation of the team members to one of the aerospace fields. This can be found in the first section. Finally, the technical resources, which are presented in the last section, consist of the software that can be used, external sources and other resources.

D.1 Human resources

At the beginning of the project and design process, the main resources available are the team members involved. Every team member can be assumed to have a general knowledge about all Aerospace fields involved, as Aerodynamics and Structures. Also all team members know how to handle LaTeX and MATLAB and have other general usable skills. However, some are more specialized in certain topics or are more skilled in a particular area than others are. To make optimal use of all the knowledge available in the group, this is analyzed and the results can be found in table D.1.

Table D.1: Skills needed for the project and associated team members

Skill	Team member(s)
Aerodynamics	Matthijs, Kevin, Frank
Structures & Materials	Jetteke, Bram, Jef
Control, Flight & Performance	Thomas, Vera, Nigel, Mazin
MATLAB	Mazin
LaTeX	Mazin, Kevin
JavaFoil	Matthijs, Jef, Jetteke
XFLR5	Jetteke, Vera
CATIA	Nigel, Kevin

For the DSE only a limited amount of time is available. Therefore for optimal use of this time, the man hours available are allocated to the different phases of the project. This is presented in table D.2.

Table D.2: Man hours allocated per phase of the project

Main Phase	Man-hours expected	Man-hours completed
Project Set-Up	400	240
Project Definition	240	400
Conceptual Design	1200	1200
Testing	400	360
Detailed Design	1600	1800
Project Close-Out	560	480
Total hours	4400	4480

D.2 Technical resources

In this section the technical resources are explained which can be used to complete this project successfully.

D.2.1 Fellowship

Most of the time of the project will be spent in the Fellowship. The Fellowship has a couple of resources available that can contribute to a good working environment for the project.

Tables Table F in room 1.16 is permanently reserved for the group. In the Fellowship also some other tables are available. However, because their availability depends on a first come first serve basis this resource should not be count on too much.

Lockers Close to the group table there are some lockers available, two for each group, in which items of value can be stored. In this way, the risk that important material gets stolen is reduced.

D.2.2 Software

Software is very important for a smooth proceeding of the project. Especially for the analytical and numerical simulation of the project and to get well-founded results, it is crucial.

ShareLaTeX To be able to efficiently write reports with a group, ShareLaTeX can be used. ShareLaTeX is a word processing program that allows multiple people to work on the same text file at the same moment. Is free for single usage, however for a group project fifteen dollars a month is invested by the group. Because this can be split with ten people, it is a small investment that makes word processing with a group a lot easier.

CATIA When developing a new product it can be useful to sketch the product in a 3D program. Using a 3D program can be advantageous since the product can be seen as it would be in real life. Next to the real life view, the program is able to perform a stress analysis on the product. The TU Delft has the official license for the program from which the students are allowed to use this program for their project.

MATLAB To be able to do difficult calculations, mathematical packages can be used. Since MATLAB is provided by the TU Delft and is easy to use, MATLAB will be the mathematical program that will be used during this project.

JavaFoil In order to create and choose the correct airfoil shape for the analytical wingsuit model, JavaFoil can be used. This application can be found on the Internet and is free to use. The disadvantage is that the program is based on potential flow, assumes an infinite wingspan and has an incorrect stall modelling. Thus, it can only be used for 2D airfoil modelling.

XFLR5 For the analytical analysis of the wingsuit, XFLR5 is used. This program uses 2D and 3D panel methods for the analysis of the airfoil and wing. It has the capability to use (nonlinear) Lifting-line theory, Vortex Lattice Methods and 3D panel methods. XFLR5 can easily be found on the Internet and is free to download.

D.2.3 Tests

In this section the allocation of resources for tests are explained. Different resources are available for tests such as the wind tunnel and a flight test, but also measurement equipment, test pilots and other wingsuiters.

Wind tunnel TU Delft provides multiple test facilities that can be used. For this wingsuit project, only the OJF (Open Jet Facility) wind tunnel was large enough for a real life wingsuit. The OJF was only available at Thursday 24/05 and consequently the test had to be performed that day. Since this is a project from the TU Delft, the wind tunnel can be used free of charge.

Flight test Since Jarno Cordia performs many wingsuit jumps, he is a perfect fit for these flight tests in order to collect data. This can only be done at the specific dropzone, so the availability of the person to jump at that location is the main driver of this resource. Since Jarno has multiple wingsuits, only the aircraft flight has to be paid for to be able to perform a flight test.

Wingsuiters After contacting multiple wingsuiters, two wingsuiters, Jarno Cordia and Coen Disberg, were willing to perform tests for this project. The availability of the wingsuiter depends on their timetable.

Measurement equipment To get valuable data from the flight test, measurement equipment has to be used. This material will be provided by Ronald van Gent, which implies that it can be used free of charge for this project. The availability of this equipment depends on the time to prepare and deliver the equipment.

D.2.4 Wingsuit

Since the wingsuiters Jarno Cordia and Coen Disberg are willing to help for the project, their wingsuits can be used to get a better understanding of the aspects and aerodynamics of a wingsuit. Since the wingsuits are still used by their owners, the wingsuits can only be used for the project when they are not in wingsuit operation.

D.2.5 Knowledge from external sources

Due to the lack of knowledge, knowledge from external sources can be useful to complete the project. This knowledge can come from different parties, for instance wingsuiters, PhD students, other TU Delft staff members and wingsuit companies. The availability of the resource depends on the person providing the information. Because this is a TU Delft DSE project and most other third parties turned out to be very enthusiastic, these external sources do not have to be paid for their knowledge.

E

Technical Risk Assessment

In this appendix, the technical risks that may occur during the final stages of the project will be investigated. First, the different risks for the project will be determined. After which they will be analyzed further by grading them from unlikely to likely and from negligible to catastrophic.

E.1 Risks

Looking at the time remaining in the project, the following risks were determined.

1 Miscommunication

Miscommunication can lead to errors in design and inconsistency between parallel work in the numerical and analytical parts of the wingsuit evaluation. It can also lead to work done twice unnecessarily.

2 Lose focus and direction

The project at hand is clearer to the group at this moment than it was in the midterm reporting stage. Work division is clearer and so are the tasks to be performed. Care has to be taken in this stage that the numerical and analytical parts workloads are balanced correctly against the reporting workload.

3 Flight test conditions

In the event of bad weather, the flight test may not be conducted in time to finalize a comparison between outputs of the numerical, analytical and actual physical data. The conditions on the day itself could also be such that measuring flight performance is difficult or impossible.

4 Facility problems

Facility problems are a real risk, especially since the numerical calculations are performed on large time-scales. Computers will be running simulations for one or more days in a row. In the event of a power outage, these calculations will need to be redone. This may set the numerical part of the project back a number of days.

5 Disengagement of third parties

At this stage in the project, a disengagement of Phoenix-Fly, and especially Jarno Cordia would be disastrous. This would result in the flight test not being conducted, which means there is no validation data for any of the models and theories developed during the DSE. A solution could be to approach another wingsuit flyer to perform the test. However, this is not ideal as Jarno is fully briefed about the goals for measurements and design, and the new wingsuiter would need to be briefed from the start. In addition to that, the sheer amount of experience Jarno has, especially in the BASE jumping regime, has proved invaluable to the group. Such a resource will be sorely missed.

6 Technical setbacks

Technical setback risks are relevant for the numerical, analytical, flight test and design detailing. For example, the wind tunnel experiment did not go as planned. The construction supporting the wingsuiter in the tunnel had to be adjusted for increased stability. This unexpectedly used up valuable test time. A similar problem could occur during the setup or execution of the flight test.

7 Incomplete and/or incorrect trade-off

In parallel to the new wingsuit design the group is developing, a general wingsuit theory is also being formed. These two activities make the risk of an incorrect or incomplete trade-off smaller. If the trade-off for a novel wingsuit is performed incorrectly, it will not affect the theory. If the theory reasoning is incorrect, it will most likely not affect the validity of a solution in the new wingsuit.

8 Absence of group members

Time is short in this part of the project. Next to the required report deliverables, a flight test has to be conducted, CFD analysis performed, an analytical theory developed, design options physics worked out and sense has to be made of all the outcomes of these activities. Long-term absence of group members under pressure of these tasks is not desirable and can lead to significant delays or even a part being incomplete.

9 Usability of flight test data

Because the use of CFD and the analytical model needs to be validated by the flight test, the usability of the data of the flight test is a critical factor. In case the data is hard/impossible to filter, the valuable validation step of the models will be lost.

10 Outcomes numerical and analytical models unusable

Numerical and analytical models are developed to simulate the real behavior of wingsuits. The risk exists that the outcomes of these models do not at all resemble the actual flight performance characteristics of the wingsuit in the test. This problem is inherent to the development of these models, and cannot be dealt with by the group. Another iteration of these models will be needed to resemble this performance more closely. This would not be a problem by itself unless it is close to the deadline since it takes a long time to run the CFD simulations. Next to this problem it is also negative for group motivation, since it would be nice if these results were indeed verifiable.

11 Malfunction of flight test data recorder

Due to the cost and timing of the flight test, there exists only one opportunity to conduct the test. All equipment must be made functional before this test and it is critical that on the test day, this equipment will perform as expected. There is no margin for error. If a malfunction does occur, our models will go unvalidated.

12 Risk of accidents during flight test

Wingsuit flying in itself is an extreme sport, with certain risks attached to it. There is always the risk of injury or fatality when wingsuit jumping. This risk cannot go unnoticed.

E.2 Risk map

The different risks mentioned in the previous section are categorized in figure E.1. With this risk map it can be easily seen which risks need the most attention. As in the midterm period, a major point of attention is the communication. Too much miscommunication will lead to work done inefficiently and thus causes a critical loss of time. Also, the catastrophic nature of not being able to perform the physical wingsuit test makes that a special point of attention.

Catastrophic	12		3	
Critical	4	2, 5, 8, 9, 11, 10	1	
Marginal			6, 7	
Negligible				
	Very Unlikely	Unlikely	Likely	Very Likely

Figure E.1: Risk map displaying the chance of an event to happen, and its impact

F

Market Analysis and Product Introduction

For any engineered product to be successful, a solid design is necessary. However, this is not the only factor that determines its success. An analysis of the market needs to be made as a preparation to the SWOT analysis. Subsequently, this SWOT analysis will aid in selecting an adequate business strategy for introducing the new product. The market introduction is planned by setting a market share target for the newly founded wingsuit producing company. Subsequently, the market for wingsuits is estimated in three scenarios, namely a smaller, same and larger than expected market. From these market estimates and the target market share, the number of wingsuits to be produced in the predefined number of years can be determined for different scenarios.

Summarizing, the planning of the introduction of a new wingsuit looks like this:

- Market analysis
- Determine market share target
- Set up three scenarios for market size
- Determine number of wingsuits to be produced after introductory period
- Determine buildup of production in introductory period

F.1 Market analysis

The following parts of the market analysis for wingsuits can be identified:

- An overview of wingsuit sales will be compiled. Ideally, a geographic distribution and time varying volume of total sales will be determined. It is of importance to predict sales growth for the coming years.
- An indicative market price is necessary to determine pricing for the newly designed wingsuit.
- Target groups should be identified, clearly making a distinction between BASE jumpers and skydivers. Also, the distribution channels through which to reach these target groups have to be identified.
- Finally, an overview of the various wingsuit manufacturers as competitors for the wingsuit design will be made.

F.1.1 Wingsuit Sales

The amount of wingsuits sold on a yearly basis is hard to determine. This is mainly due to a number of unknown factors:

- The number of regular users of wingsuits is not known.
- The number of wingsuits owned by regular wingsuit users varies significantly (between one and five models per user is not uncommon).

- Sales figures for the various large manufacturers (listed in Section F.1.4) are difficult to obtain.

An extremely rough estimate of sales could be deduced using some assumptions and from estimates given by members of the wingsuiting community. These numbers should be regarded as purely indicative, and further research should be conducted if decisions were to be based on these numbers.

It is estimated that the number of regular wingsuit flyers in the United States lies between 500 and 1000.[64] Worldwide, the number of wingsuiters is deemed to be about 4000.[64] Assuming a purchase rate per wingsuiter of approximately one per year, and half the wingsuits operated by skydiving/BASE schools the total amount of wingsuits sold would total 6000 per year.

F.1.2 Pricing

It is important to know the price ranges of different wingsuits, so the newly designed wingsuit can be priced appropriately. Luckily, composing a pricing overview for the main manufacturers is quite easy to make. Each manufacturer has a set of models available, suited for beginner to expert level wingsuiters. These differences in models, priced low to high respectively, account for the main variations in pricing between different wingsuits individually. Below a summary graph is presented with the total number of wingsuits divided into pricing categories, accompanied by a graph on the number of models each manufacturer has in a specific pricing category[65][4][5][66].

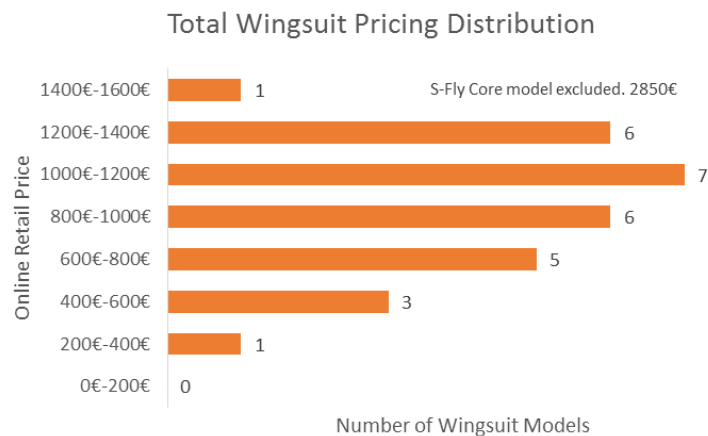


Figure F.1: Number of wingsuit models in certain pricing categories of all manufacturers combined



Figure F.2: Number of models in certain price categories per wingsuit manufacturer

The wingsuit to be designed will be a high-end new wingsuit. Most high-end wingsuits are found in the €1400 - €1600 price range, with one outlier: the S-Fly Core model from Fly Your Body. Therefore the decision was made to price the wingsuit at €1500. This lies nicely in line with what customers today are willing to pay for high end wingsuits. Also, the newer, more expensive wingsuits currently available have an added value for their new technology which accounts for about €100-€200. The benefit of the wingsuit to be designed will lie within this range.

F.1.3 Customer

There are four clearly identifiable target groups. The first is the most obvious one; these are the current BASE wingsuiters. The main problem will be convincing them of the advantages of our new safer suit because they will be reluctant to change their old habits. Also in case of great structural changes, they might think the original bird-like experience is corrupted.

The second group consists of skydive wingsuiters who would consider BASE wingsuiting with our safer advanced wingsuit. Since their main interest is the increase in safety when performing a BASE wingsuit jump.

The third group consists of people who will use the suit for skydiving. This might not be possible as there are different regulations for both disciplines. However, for now this group is also considered.

The final group that has to be considered is the group of people who will start skydiving and in time wingsuiting with our safer suit in mind. For these people it is important to keep wingsuiting extremely fun and hence attractive, but greatly increasing the safety.

The best method for delivery is at home delivery. This is because the number of wingsuit flyers is too small to open a shop at a fixed location. There are however a few companies who open shops next to their research/production facilities, also including tour guides.

F.1.4 Competitors

In order to further extent the insight in the current market, the different competitors will now briefly be discussed

Phoenix-fly Phoenix-Fly is one of the larger suit manufacturers. It has one of the most diverse catalogue offering a variety of eight wingsuits, with several additional features like back inlets and BASE pouches. Due to the wide variety of suits, they are able to focus on all aspects of BASE jumping and skydiving. These include endurance flight, performance flight, high maneuverability and easy flyable suits for beginners. For development, a lot of test flying is used. Airfoils are chosen using 2D simulation software. Their suits are manufactured by Atair.

Tony Suits Creating suits for over twenty years, Tony Suits is also one of the older manufactures of wingsuits. Tony Suits has a smaller catalogue compared to Phoenix-fly offering a variety of six suits. However, Tony Suits has a lot more track suits and other skydiving operations compared to Phoenix-fly. The suits are mainly designed for endurance flight. Regarding development, it is mentioned on their site they have the most active research and development program due to the fact they are located next to a good skydive dropzone. This implies that a great part of their development is through test flights.

Squirrel Having started from 2012, they are one of the newer companies producing wingsuits. At the moment, they only have one wingsuit, which is a suit optimized for glide performance and aimed at advanced wingsuit flyers. Their design philosophy is safety. On their site, it is mentioned they use real aerodynamics for development. Their suits are produced by Ozon.

Fly Your Body A French company that was created in 2003 by Loic Jean Albert. Loic is one of the pioneers of modern wingsuit flying. He played a major role in the large progress that has been made in the design of wingsuit these recent years. They have nine wingsuit models, the S-FLY series, but the models resemble each other a lot. They are not very present on the internet.

Intrudair A skydive suit manufactures that created three suits, one for glide performance, one for flight time and one for beginners.

Birdman One of the older companies, and the first commercial wingsuit manufacturer, expected to release three new wingsuits this year.

Jii-Wings Jii-Wings has one all-round wingsuit, which was designed inspired by looking at the flow around birds.

Nitro-Riggings Nitro Rigging is a company constructing canopies, track suits and wingsuits. It started building wingsuits in 2004 and has six different wingsuits. All their suits are handmade in the USA in which they take great pride. However, due to this, their delivery times are increased up to six weeks.

F.2 Market scenarios

It is estimated that Phoenix-Fly manufactures and sells approximately 1500 wingsuits per year. It is impossible to determine exactly how large the market share of Phoenix-Fly is in the worldwide sales of wingsuits, so an assumption has to be made that is consistent with our previous wingsuit sales estimate. It is assumed that Phoenix-Fly sales account for a quarter of all wingsuits sold, bringing the grand total of wingsuits sold worldwide to 6000. This is in line with the previous estimate. The total value of the market then is approximately 5.8 million euros at an average wingsuit price of about 960 euros.[65][4][5][66]

To account for uncertainties in these numbers, a number of market size scenarios will be introduced. An overview of these is given in table F.1. The scenarios in this table are accompanied by the number of wingsuits the new company would have to sell for a market share of 10%.

Table F.1: Overview of different wingsuit market scenarios

Type of market	Worldwide Sales	Target Sales
Small Market	4500	450
Midsized market	6000	600
Large Market	7500	750

F.3 Production target and buildup strategy

The amount of annual production increase that needs to be realized by the newly founded wingsuit manufacturer is graphically presented in table F.2. This follows the market scenarios from table F.1. The target sales number is assumed to be reached in five years.

Table F.2: Required annual production growth for new wingsuit company per scenario

Type of market	Required Growth	
Small Market	90	★ ★ ★ ★ ★ ★ ★ ★ ★ ★
Midsized market	120	★ ★ ★ ★ ★ ★ ★ ★ ★ ★ ★ ★ ★ ★
Large Market	150	★ ★ ★ ★ ★ ★ ★ ★ ★ ★ ★ ★ ★ ★ ★ ★

G

H/W - S/W block diagram

The H/W-S/W block diagram shows the interactions and mutual relations between the hardware components and the software components in the design. The rectangular blocks resemble the hardware parts and the oval shaped blocks resemble the software. The lines between the blocks resemble the interactions and relations. The diagram can be seen in Figure G.1.

The wingsuit is the product that combines everything. All the systems in the second row are part of the wingsuit. First off, there are the vortex generators on the wingsuit. Because they are placed on the same spanwise location as the passive flap, only in upstream direction, the vortices induced by them travel directly over the passive flap. This interaction is one of utmost importance, since it determines how well the passive flap works.

The passive flap also affects the vortex generators but in a lesser extent than the other way around. If the passive flap is pitched up entirely, the wires of the passive flap put a tension force on the ODT. The software of this ODT then sends a voltage to the headset that turns into a sound signal at the headset, which alerts the wingsuiter of the near stall situation. If the wingsuiter wants to deploy his canopy, he/she pulls his Swiss pouch. This Swiss pouch opens the canopy bag, after which the canopy deploys. Due to the opening of the canopy the quick-release system frees the arms of the wingsuiter so that he/she is able to fly the canopy.

The anti-slip is a part of the wingsuit, but does not interact much with the other systems of the wingsuit. At last, the wing connection and the air tunnels are placed on the same location on the wingsuit, the wing connection will serve as housing for the air tunnels. Therefore a mutual interaction exists between the two systems.

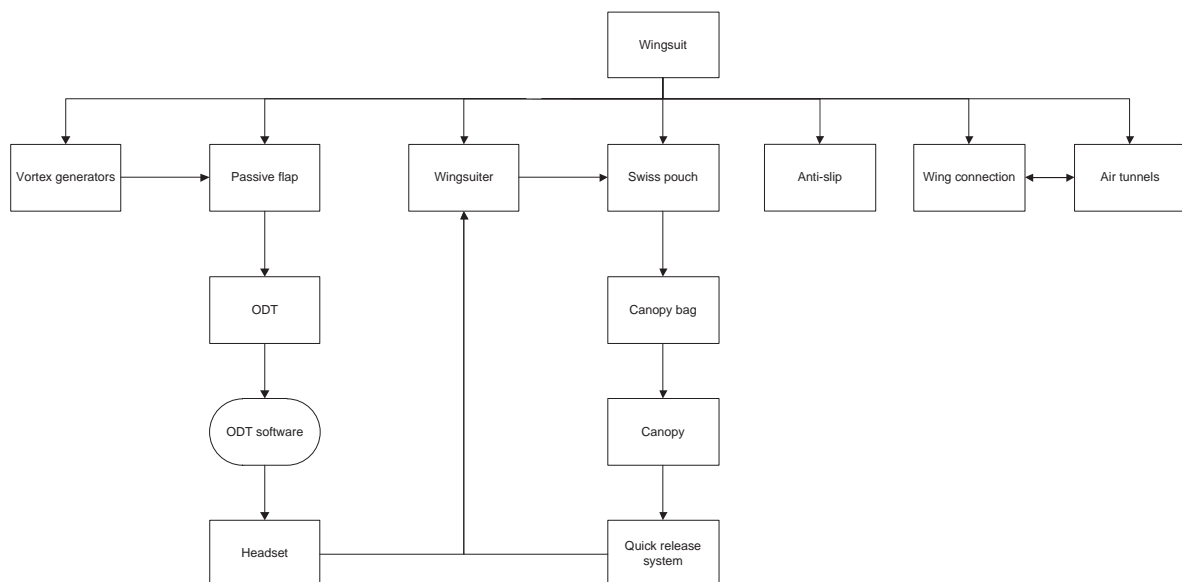


Figure G.1: The HWSW block diagram showing the interaction and relations between different systems of the wingsuit design.

H

Electrical block diagram

There is only one system of the wingsuit that consumes electricity, namely the stall warning. The ODT provides its own energy and only uses energy when sending the near-stall signal. The FlySight, who receives the signal and sends it to the headset, needs batteries to be able to function. The FlySight system that is used by many wingsuiters has a built-in rechargeable lithium-polymer battery [46]. Since every used device has an internal battery for itself, there is no harnessing in the wingsuit. This makes the use of the electrical block diagram obsolete.

I

Data Handling Block Diagram

Similar to the electrical block diagram, the data handling block diagram will be limited since the only system that uses data handling is the stall warning system (the GPS logging that some wingsuiters do is not seen as part of the wingsuit design). The data handling block diagram can be seen in Figure I.1



Figure I.1: The data handling block diagram showing the data handling between different systems of the wingsuit design.

The passive flap sends a signal to the ODT in means of tensile force. The signal that is send by the ODT is handled by the FlySight (which need to be slightly modified), which on his turn sends a signal to the headset of the wingsuiter. The FlySight has a standard plug-in for headsets [46]. The wingsuiter is then alerted by a sound from the headset.

J

Manufacturing & Production

The wingsuit that is designed in this DSE project has as major goal: the safety of the pilot. This safety increase can be obtained by technical improvements, such as aerodynamics and structures. Although this concept suit can become a mass series product, this is not the main goal of the project. It is also expected that the main parts of the production of the wingsuit will be the same as current wingsuits. Therefore, no flow diagram of the manufacturing activities of the product plan will be created.

K

Sustainable Development Strategy

During a design process, the sustainability of the project is very important to keep in mind. In the sustainability discussion, two main aspects are addressed:

1. Design sustainability: how sustainable is the manufacturing process? How durable is the design (what is the lifetime of the product)? Is it possible to recycle after the product is taken out of service?
2. Contribution to sustainable environment: what is the environmental impact of the product in operation?

First the sustainability of the current wingsuit design is thoroughly investigated, after which the possible sustainability improvements of the new design are discussed.

K.1 Sustainability of wingsuit design

In this section the sustainability of the current wingsuit design is discussed. Section K.1.1 deals with the design sustainability, while Section K.1.2 covers the environmental impact during operation.

K.1.1 Sustainability in the Design

Before the actual wingsuit performs its maiden flight, several processes have taken place which could influence the sustainability of the entire project. The manufacturing process as well as the materials, durability and recyclability are discussed in this section.

Manufacturing Process

Phoenix Fly, one of the biggest manufacturers of wingsuits, uses several materials for their wingsuits. Certain areas, where substantial wear occurs, are reinforced with more sturdy fabric. The fabric is hand cut and also tailored by hand. This is all done according to the wingsuiters measurements. The cutting happens using heated knives in order to 'sing the edges of the seams'. This make sure the seams stay intact and the fabric will not fray. After the pieces of fabric are hand cut, it is just a matter of sewing and stitching the fabric together. The whole process uses quite some manual labor and is fairly energy efficient.

Materials

Most wingsuits are made from either F-111 or Para-pak fabric. The F-111 fabric is a zero porosity, lighter, thinner and less sturdy material, whereas the Para-pak on the other hand is heavier, thicker and a more sturdy and durable material. The Para-pak wingsuits weigh roughly 400 grams more than the F-111 wingsuits. "Especially for skydiving, this is a recommendable option to deal with the additional wear and tear of airplane floors and repeated packing." [67] Unfortunately, it has slightly worse drag characteristics. The manufacturer Phoenix Fly is now working on a new fabric, called Cameroon Ultra-Light. Phoenix-Fly: 'For BASE jumping we now also offer the new Cameroon Ultra-Light fabric. This slick fabric has good low drag characteristics and is 25% lighter than normal Zero-P. The fabric also is more durable and sturdy.' [67] It would therefore be most logical to pick the Cameroon Ultra-Light fabric as the main material for the design.

Durability

Due to the nature of wingsuiting, the suits sometimes tear and stitches can get loose. Also deficiencies in rigging lines can occur sporadically. In this case the material will need to be repaired or replaced. The ZeroP is less durable and will thus need more repairs. Repairs are most of the time performed by the manufacturers and sometimes by private riggers. The repair is usually not complicated and does not need much new material. It is mostly sewing up tears in the fabric. All in all, the wingsuit requires very low maintenance and is very durable.

A wingsuiter will most likely 'outgrow' his/her suit before the wingsuit is completely worn out, especially with the Para-pak and Cameroon Ultra materials which are most durable (such a suit can last for 10+ years, or at least 800 jumps). Therefore the replacement of a wingsuit is more dependent on the development of the skill of the wingsuiter and the development of new wingsuits. Durability is therefore not the most important part of the sustainability.

Recycling

The re-usability of a wingsuit is limited. Usually the wingsuit is discarded, due to the need for a new model. The fabric of the wingsuit is light and strong and would therefore be very suitable for a range of applications, but due to the aerodynamic requirements of the construction, the wingsuit has only small patches of fabric without stitches, reinforcements or other modifications. This makes it harder to recycle the wingsuit to for example bags or other clothes. According to CES EduPack [57], the material, mostly Nylon, can be recycled, downcycled, combusted for energy recovery and used for landfill. Since the last two options, combustion and landfill both create a quit high environmental burden, these two options are avoided as much as possible. Mylar, used in some conventional wingsuits, can not be recycled, but it can be downcycled, combusted and used for landfill.

K.1.2 Contribution to sustainable environment

Wingsuit flying is both performed in skydives and BASE jumps. Since our project focuses on a new design for BASE activity, the sustainability of this operation has been looked into in this section.

The operation of a wingsuit during BASE jumping is a very green activity.

Arriving at the exit point

The first stage of operation deals with the transportation towards the exit point which most wingsuiters do by foot. The hike through the mountains forms a significant part of the entire BASE experience [6]. Furthermore ski lifts are used and occasionally a helicopter is used to bring the wingsuiters to the right spot. Generally, the transport phase can thus be considered very sustainable.

Smoke canisters

Sometimes smoke canisters, attached to the legs of the wingsuiter, are used to make the flight even more visually attractive. Most smoke pods use the same mixture for smoke creation[68], the chemical reaction is shown in equation K.1:



Table K.1: Components of smoke creation

Input		Output	
sugar	$C_{12}H_{22}O_{11}$	Potassium carbonate	K_2CO_3
potassium nitrate / saltpeter	KNO_3	Carbon-dioxide	CO_2
		Water vapor	H_2O
		Nitrogen gas	N_2

Input components:

The input components are safe and non-poisonous. Both sugar and saltpeter are used in cooking and saltpeter is also widely used as fertilizer.

Output components/reaction products:

Potassium carbonate is safe and non-poisonous and is often used to 'soften' water. Carbon-dioxide and water vapor are greenhouse gasses and the creation of these gasses should therefore be minimized. Nitrogen gas is the most abundant component of the earth's atmosphere and is one of the building blocks of organic material.

K.2 Sustainability of the advanced wingsuit design

The design of the advanced wingsuit should obviously consider the sustainability aspect. The following sections address the topics which are most influential on the sustainability of the new design.

Manufacturing

Due to the nature of the wingsuit sport, the demand for wingsuits is not very high. At this moment the manufacturing process is mainly done by hand (as stated in Section K.1.1). This way of processing is feasible for low demand, however, should the demand increase in the future, a better manufacturing process should be looked into. Until that time, the manufacturing process is quite energy efficient.

Material

Over the years many different materials have been used for wingsuits and many improvements of materials have been made. At this point in time, the best material available for wingsuits is Cameroon Ultra-Light fabric. The durability of this fabric is very high and thus greatly helps the sustainability of the wingsuit. This type of material will be used for the advanced wingsuit. The advanced wingsuit does not defer much from conventional wingsuits material wise. Most concepts use the same fabric and foam as is used at the moment in wingsuiting. The shoulder reinforcements however use aluminum, which is in these quantities a new material in the wingsuit. Aluminum can be recycled, downcycled, and eventually used for landfill.

Arriving at the exit/jumping point

The biggest advantage of current BASE wingsuit operation is the flexibility of transportation and ability to hike towards the exit point. During the design phase, portability was therefore be an important requirement. This aspect of the sport also has its charm, unlike skydivers, wingsuiters make long hikes

Summary of design considerations regarding sustainability

The following considerations were taken into account during the design phase in order to maintain sustainability:

- The primary material used for design is be Cameroon Ultra-Light (durable fabric)
- Manufacturing process is kept the same
- The wingsuit is light, and thus easy to handle and transport.

L Project Design & Development Logic

While the DSE is finished after ten weeks, the project itself is certainly not. In order to really design a fully producible wingsuit that fulfills the requirements and the mission need statement a lot more work needs to be covered. This appendix describes the work that still needs to be done after the DSE. The work flow diagram can be seen in Figure L.1.

In the diagram, three main lines can be seen; the detailed design, the prototype testing and the manufacturing line. It must be stated that there are no tools to be designed, since a lot of work is done by hand and the only tooling machines that are used are already available. Also in this diagram (compared to the WFD during the DSE), the iterating aspect of a design process is very clear.

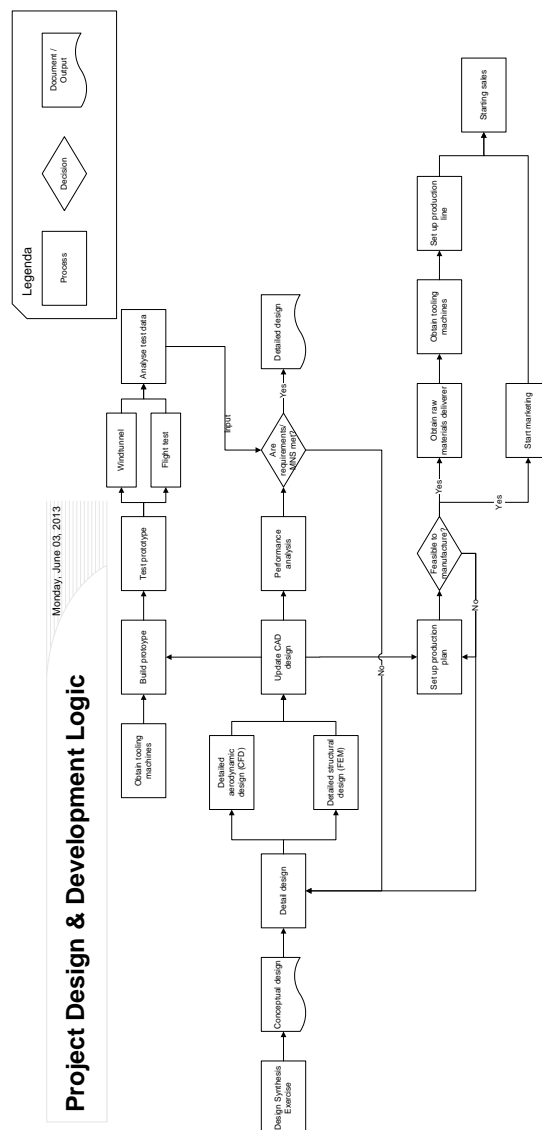


Figure L.1: The project design & development diagram

M

Project Gantt Chart

The project Gantt chart gives an overview of all the post-DSE activities and the allocation of time duration as well as a start and end date. The Gantt chart can be seen in Figure M.1.

It could be noted that there is a lot of time between the performance analysis and the requirements check to finish the detailed design. This is to grant extra time to the engineers, because certainly some design iterations will be needed after both the performance analysis and the analysis of the prototype tests.

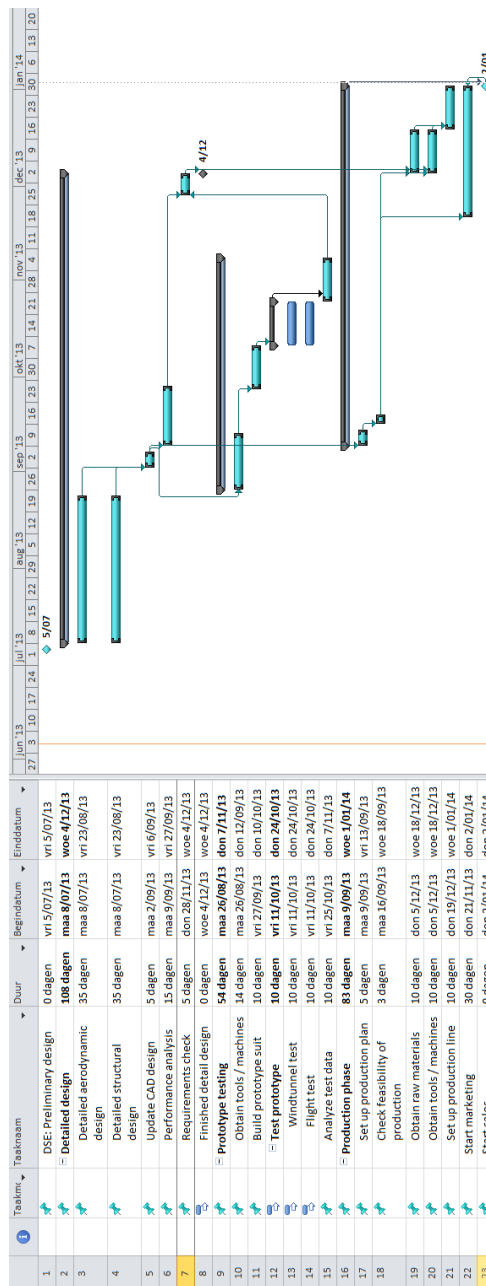


Figure M.1: The project Gantt chart depicting the post-DSE activities

N

Cost Breakdown Structure

The cost breakdown structure describes the costs of the post-DSE project activities. It consists of the activities that were defined in the project design & development logic with all the according costs. The scheduled time, 6 months, was defined in the Gantt chart, M. The cost breakdown structure is the basis of the cost estimate for the product of the system. The cost breakdown is shown in Table N.1, where it is divided in three main parts. Each of those parts resembles a line of activities in the project design & development logic.

It is assumed that all employees are students and very enthusiastic about this project. Their salary will therefore be higher than the average student salary, and set at €15 per hour. The material costs are the costs for the final product. Other direct cost covers the costs not directly related to the final product, such as software and marketing costs.

N.1 Material cost

The production cost of one advanced wingsuit is hard to determine. Here one has to include both the material costs and the manufacturing costs. The material cost of the wingsuit was determined based on the estimated material cost of concurrent wingsuit manufactures. From a well established wingsuit manufacturer [69], the extra cost for using Cameroon Ultra Light was €70. In Appendix F, it was found that a low experience wingsuit model costs about €300 - €500 and a medium experience model costs approximately €700 - €1000. Because very little garment is used in the low experience models. One could compare the wingsuit manufacturers selling low experience models by comparing their respective areas and prices, making the large assumption that both wingsuit manufacturers use the same margins on their wingsuits. From this information one could assume a material cost. The chosen wingsuits are the ACCESS (€285, [70]) and the Prodigy 2 (€515, [71]). The Prodigy 2 has approximately twice as much fabric as the ACCESS, see Figure N.1, as the Prodigy 2 has an inflatable leg wing, unlike the ACCESS.



Figure N.1: The left picture is the Prodigy 2, the right picture the ACCESS, which is a simpler model.

Assuming the garment costs of the ACCESS are about €85, the material cost of the Prodigy 2 would be €170. Since the Prodigy 2 uses more stitching and has a more complicated design, this could help explain the price difference. This is also extrapolated to the Vampire 5 (€1300), which has a larger, more complicated, wing. The Prodigy 2 has a wing area of $0.80m^2$. This leads to a $\frac{cost}{area}$, of $\frac{170}{0.80} = 212.5 \frac{€}{m^2}$. Applying these cost estimations to the Vampire 5, which has a wing area of $1.73m^2$, this leads to a material cost of €367.6. The Cameroon Ultra Light material will most likely be roughly €70 for the whole suit [69]. Since Cameroon Ultra Light ultra light will be used, this will be approximately $40.5 \frac{€}{m^2}$.

This will lead to a total of $408.1 \frac{\text{€}}{\text{m}^2}$, since the planform and wing area of the advanced wingsuit will be the same as the Vampire 5. Adding at margin for passive flaps and air tunnels and anti-slip soles, the material cost per suit is set at €440. In the Production Phase, raw materials are obtained for the production of 5 wingsuits, (€2200). Start marketing also contains some material cost, in the form of printing business cards and promotional posters.

N.2 Other direct cost

If this project would continue with the complex software, it using now, such as CATIA, the prices of licenses would lead to too expensive wingsuits. Therefore open source software will be used, such as FreeCAD for the wingsuit design. For the CFD analysis, open source software such as OpenFOAM, might be useful. For both the aerodynamic and the structural design software, learning to work with this software might take more time than working with the commercial software used now. During the check on the feasibility of the production, looking for an office is also taken into account. The rent of this office, or workshop, will cost money. This will be scheduled under obtain tooling machines. The rent of the workshop will be €800 a month, for a start up time of 6 months, with an surety of an €800, leading to a total of €4800.

Table N.1: The cost breakdown structure depicting the costs for the post-DSE activity.

Activity	Labor [hrs]	Labor [€]	Material [€]	ODC [€]	Total [€]
Detailed aerodynamic design	1120	16800			16800
Detailed structural design	630	9450			9450
Update CAD design	88	1320			1320
Performance analysis	180	2700			2700
Requirement check	60	900			900
Obtain tooling machines	168	2520	700		3320
Build prototype	240	3600	440		4040
Test prototype: wind tunnel	240	3600			3600
Test prototype: flight test	240	3600			3600
Analyze test data	320	4800			4800
Set up production plan	40	600			600
Check feasibility of production	24	360			360
Obtain raw materials	80	1200	2200		3400
Obtain tooling machines	80	1200		4800	6000
Set up production line	160	2400			2400
Start marketing	240	3600	20	1500	5120
Total	3910	58650	3360	6300	68310

O

Return On Investment

Developing and producing a new design of a wingsuit is a costly investment. This investment will only be feasible if the sales are sufficient to get a profit. To make sure the investment is feasible and to find out what the profit might be, an analysis will be conducted to establish the return on investment (ROI). To establish this ROI, several data should be known. This market data will be described in Section O.1. The next section, (O.2), will evaluate the balances of sales and costs, and will conclude with the final ROI.

O.1 Market data

The most important data to establish the ROI of the advanced wingsuit are the following numbers:

- Market price
- Market volume
- Achievable market share
- Development cost
- Production cost
- Direct operational cost

O.1.1 Market price

The wingsuit market is a relatively small market, with a range of different wingsuits. The market price of the current wingsuits lies between the €750 and €1600. The advanced wingsuit will be most likely around the upper limit of the current market price.

O.1.2 Market volume

The market volume is most easily measured in the quantity of wingsuits sold. Due to the small number of wingsuiters in the world, this number is relatively low. As described in Section F.2, the current market volume worldwide is 6000 wingsuits.

O.1.3 Achievable market share

It was explained in Appendix F, a new company it is desirable to obtain a market share of at least 10% of the worldwide sales. So to calculate the ROI this number will be used. Phoenix-Fly manufactures and sells approximately 1500 wingsuits per year. To achieve this in a 5 year period, an annual production growth of 120 wingsuits is required. See Section F.2 for a more detailed description of the market share.

O.1.4 Development cost

The advanced wingsuit design is in development for the whole duration of the DSE, by ten people. As seen in Table N.1, the DSE labor hours time comes down to a total of 3910 labor hours. At this point, the salary of these students is around €15 per hour. This sums up the development cost to €58650, this includes testing costs, prototypes and other used equipment. For machinery, an initial investment of €700 is necessary. This adds to the development cost, and gives a total of €68310.

O.1.5 Production cost

The production cost of one advanced wingsuit is hard to determine. Here one has to include both the material costs and the manufacturing costs. As can be seen in Table N.1, the material cost for one wingsuit is €440.

The wingsuit is hand cut and tailored, which will take roughly half a week, i.e. 20 man hours. Some machinery is used for this. An estimate of the total manufacturing costs of the advanced wingsuit would be €200. This brings the total production cost per wingsuit to €640.

O.1.6 Direct operational cost

The great thing about BASE jumping with a wingsuit, is that it requires nothing else than the wingsuit and a jumping spot to execute. Therefore there exists no direct operational cost for wingsuits. Note that for skydiving with a wingsuit, an aircraft travel fee is required, however this will not be included in this evaluation as the advanced wingsuit is designed for wingsuit BASE.

O.2 Cost and sales balances

The Return on Investment is established at the end of the project. It is by definition:

$$RoI = \frac{Product\ sales - Total\ cost}{Total\ cost} \quad (O.1)$$

In the previous sections, O.1.1 to O.1.6, the costs and sales have been determined. The product sales is the share in the market volume (600) times the market price (€1500). The total cost is the share in market volume times production cost (€640 plus the development cost for a whole year (€213420). From these values the ROI is found to be: $ROI = 0.73$. However it is not very likely that during the first year, 10% of the market will be flying this wingsuit. To break even, 160 wingsuits have to be sold. The first year, it is expected that about 120 wingsuits will be sold, the ROI will therefore be negative $ROI = -0.16$.

P

Operations and Logistic Concept Description

This appendix will give the operational and logistical concept descriptions. Therefore first the mission statement is repeated: increase the safety, while keeping the fun. The "keeping the fun" is in fact a limiting requirement with regard to the operational aspect of wingsuit flying. It means that increasing the safety should not take away the adrenaline rush or 'flying like a bird' feeling. Restricting the sport with too much regulations is not an option to obtain safety. That is why the overall operational concept description, which will be given first, will not vary much compared to the old one. After the operational concept description is presented the logistical concept description will be given.

P.1 Operational concept description

The current as well as the new concept description are given in figure P.1 (current left, advanced right). As mentioned before both the current and the new OCD look similar. Only the 'open arm zippers' segment is left out as a quick-release will be used. This does not mean that the changes between both wingsuits are minor, rather the use of the system remains. The flight and parachute deployment are in fact quite different. As a final remark, it is noted that in case one of the checks with regard to the wingsuit is negative, it is recommended that the wingsuit is sent back to the manufacturer.

P.2 Logistic concept description

When the design of the wingsuit is completed, the production phase can start. In this phase logistical lines have to be set up.

Since the wingsuit has to fit the person perfectly, the wingsuits tailor made. This means that the major production of the suit can only start once the order is in. Also the amount of orders is quite small and irregular. Therefore it is concluded that it is best to work with a subcontractor to produce the suits. The materials to produce the wingsuit are quite basic and can be bought easily from fabric suppliers.

To get the suit to the buyer, mailing will be used. The numbers of sales are too small to open an actual shop or to sell wingsuits at current existing shops specialized in sportswear. A special courier could be used and, if possible, the time of the process should be reduced. This however, would increase the cost.

At this moment the wingsuit is in the hands of the customer. This however, is not enough to do a successful BASE jump. Other equipment will have to be purchased separately, like a parachute rig and a backpack to carry it. Also the logistics of getting to and from the exit will not be provided by the producing company. Some will require a long hike in the mountains, while others will be reachable by car. In case some part of the suit breaks or tears apart and needs a repair, the suit will have to be sent back to the manufacturer.

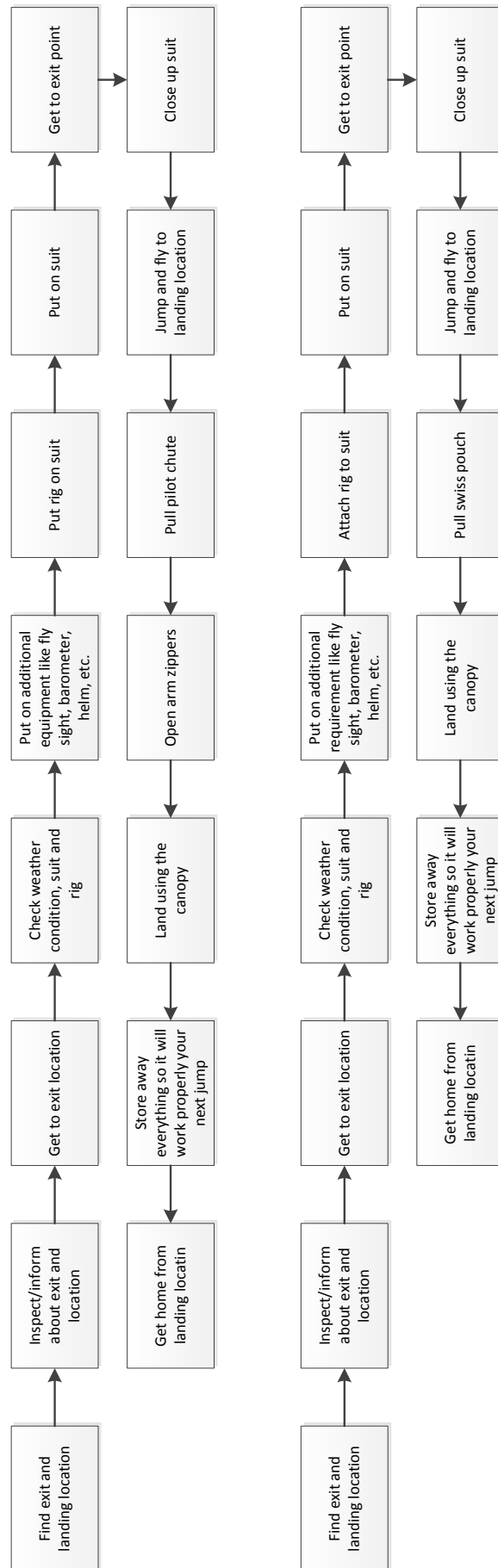


Figure P.1: Current & new operational concept description

Q

RAMS

The goal is to design a product that rarely fails, available when needed, easy repairable and safe. These characteristics translate into four important parameters: reliability, availability, maintainability and safety or RAMS. These four elements will be discussed in this appendix.

Starting off with the reliability of the new wingsuit. Reliability is defined as the probability that a specified item will perform a specified function within a defined environment, for a specified length of time [72]. In this case if the environment is defined as in flight and the item considered is providing lift, the reliability for this critical requirement should be and is equal to 100. The wingsuit should inflate and not tear apart during 100 percent of the flights. This of course assuming a suit is checked for obvious tears and malfunction before flight. However when the item considered is for example the stall warning system, the reliability will be much lower because it is a less critical and more complex component. So the reliability of the critical items is increased (ex. wing connection), however the reliability of the less critical components is decreased. This mainly because a lot of new features like the stall warning system are implemented. So concluding the overall mean time between failures (MTBF) will increase, but the MTBF of the critical parts will be reduced. Up to zero percent if in flight is considered to be the environment.

Availability of an item/system is the probability that this item/system will be in a state to perform a required function under given conditions, at a given instant in time or over a time interval, assuming that the given external resources are provided [72]. The availability of our wingsuit will be very high, up to 99%. Only when the wingsuit needs to be repaired, a certain amount of downtime presents itself. Folding the wingsuit and the Swiss pouch, replacing the quick release will also increase the downtime. Putting this into a formula, the following equation is obtained:

$$Availability = \frac{Mean\ up\ time}{(Mean\ up\ time + Mean\ down\ time)} \quad (Q.1)$$

Compared to the old system, the availability will decrease, because of the new additional systems that increase the down time.

Maintainability is basically the ease with which the system can be repaired. Due to safety issues it is recommended that in case the wingsuit is damaged, it is sent back to the manufacturer. This means it can take a few weeks to get your wingsuit repaired. However there are seldom any impairments that can not be repaired fairly easy. The main question with wingsuits is mostly if it is still worth the cost.

The last item considered in a RAMS analysis is safety. Since the goal of our project was to keep the fun while increasing the safety, a lot of effort has been put into safety throughout the project. The requirements are based on this goal. More about which requirements are actually met, can be found in the requirements compliance matrix and feasibility analysis, Chapter 17. Also, all design concept were implemented with the idea of increasing the safety. So this parameter is certainly thoroughly researched. However if the ultimate design goal of increasing the safety with factor ten is actually met, only time can tell. But the safety of this new suit is certainly higher compared to the old one.

Part VI
Results

R

Analytical Simulation - 2D results

In this appendix the results of the 2D simulations with both JavaFoil and XFLR5 can be found.

R.1 JavaFoil

The following graphs, visible in figure R.1, show respectively $C_l-\alpha$, $C_d-\alpha$ and $\frac{C_l}{C_d}-\alpha$ graphs constructed with JavaFoil.

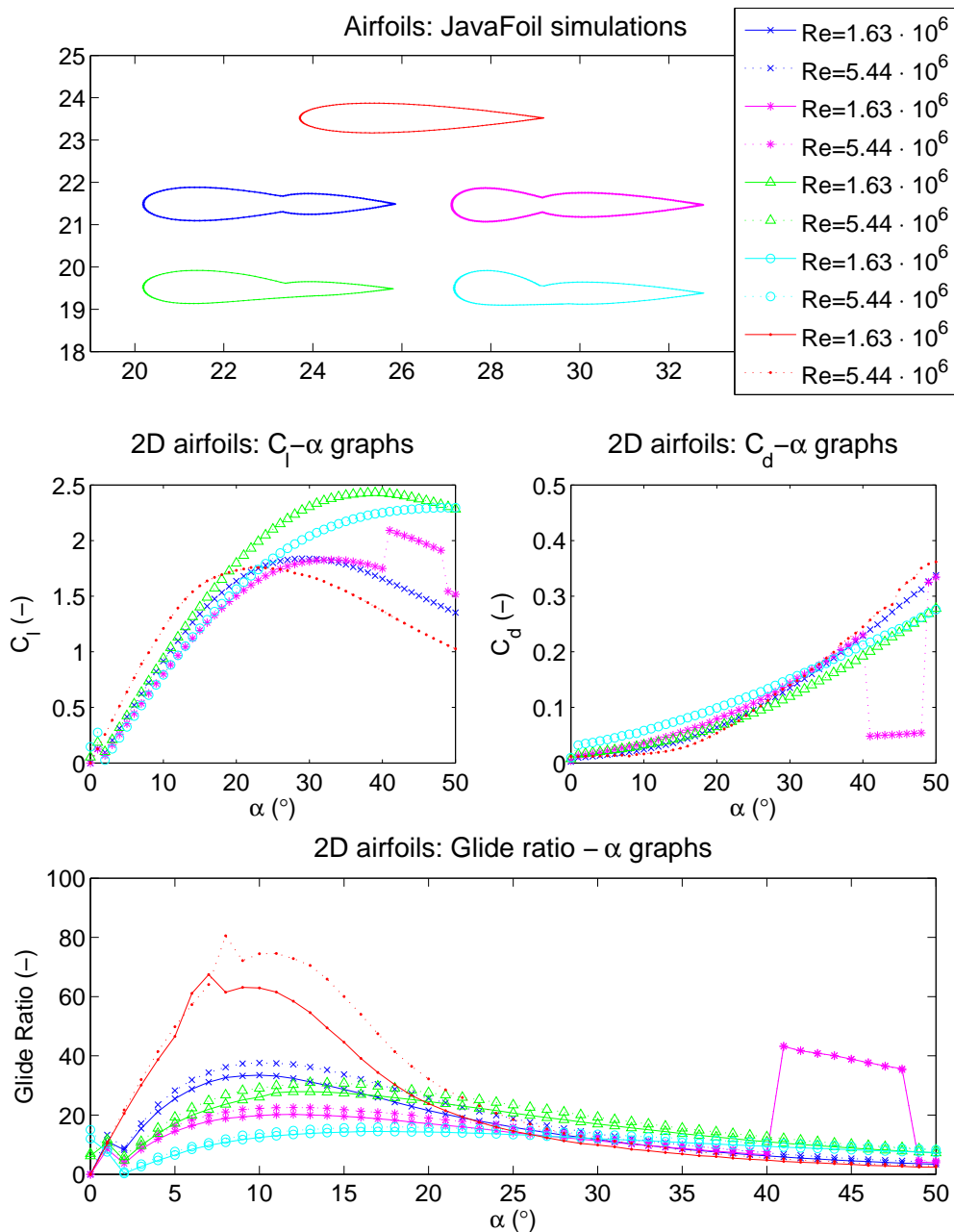


Figure R.1: JavaFoil results for the 2D airfoil models

R.2 XFLR5

The following graphs, visible in figure R.2, show respectively $C_l-\alpha$, $C_d-\alpha$ and $\frac{C_l}{C_d}-\alpha$ graphs constructed with XFLR5.

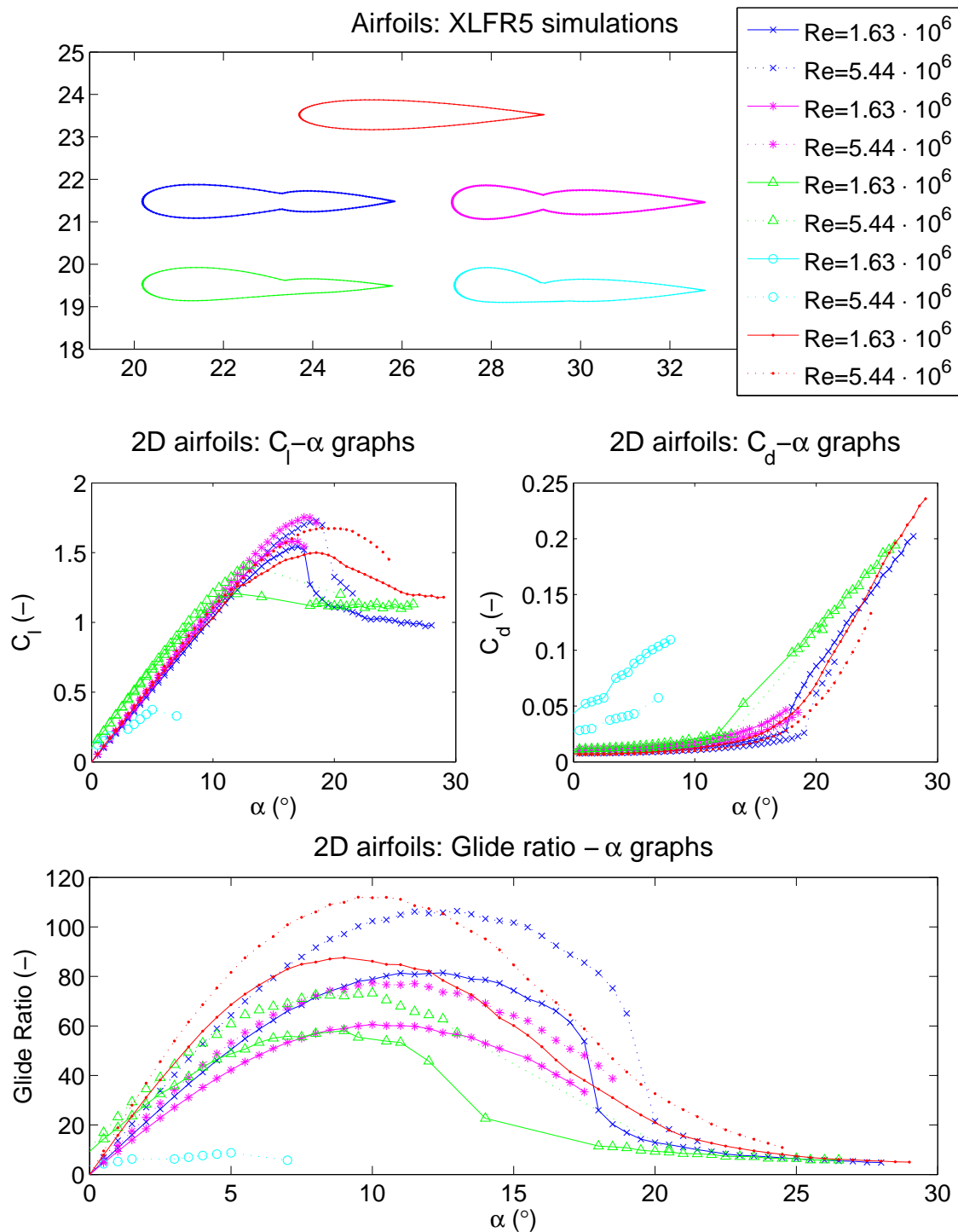


Figure R.2: XFLR5 results for the 2D airfoil models

S

Analytical Simulation - 3D results

In this appendix the results of the 3D simulations with both JavaFoil and XFLR5 can be found. As well as the effects of the concepts on the results.

S.1 JavaFoil

The following graphs, as shown in figure S.1, show respectively $C_L - \alpha$, $C_D - \alpha$ and $\frac{C_L}{C_D} - \alpha$ graphs constructed with JavaFoil.

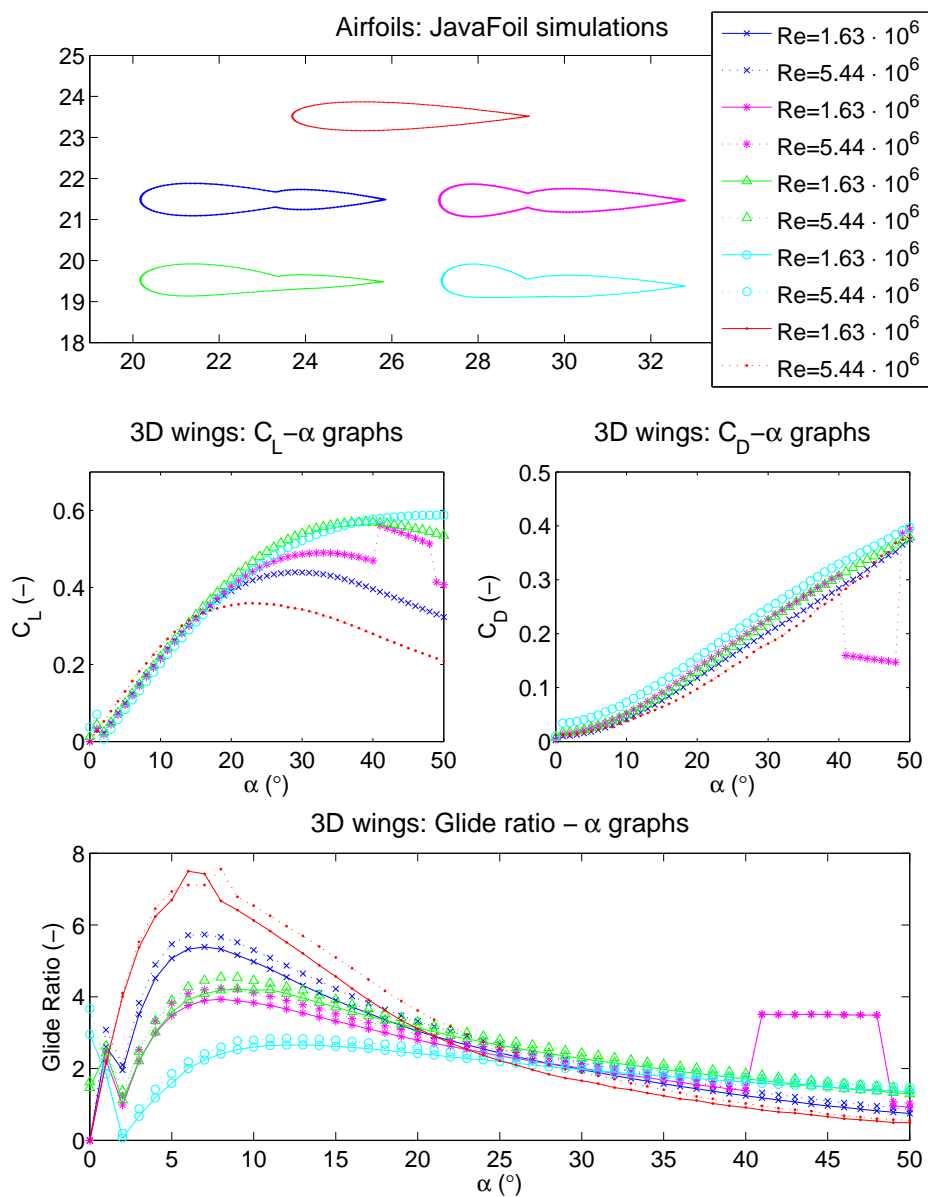


Figure S.1: JavaFoil results for the 3D wingsuit models

S.2 XFLR5

The following graphs, as shown in figure S.2, show respectively $C_L - \alpha$, $C_D - \alpha$ and $\frac{C_L}{C_D} - \alpha$ graphs constructed with XFLR5.

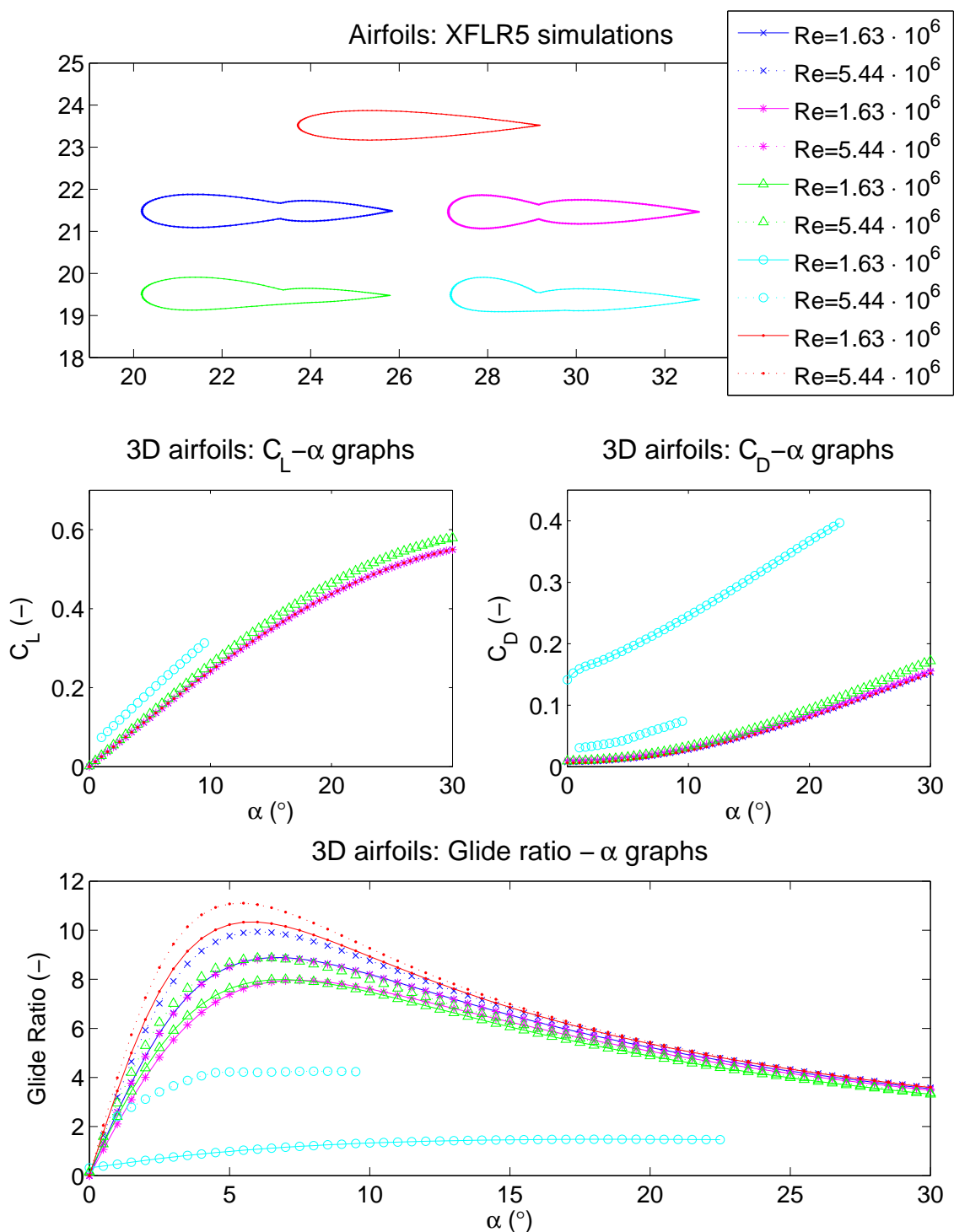


Figure S.2: XFLR5 results for the 3D wingsuit models

S.3 Impact of droop concept

In this appendix the results of the analytical analysis for the design concepts are presented. Only one concept is evaluated analytically, namely the droop leading edge. The effect of the droop leading edge is simulated with JavaFoil.

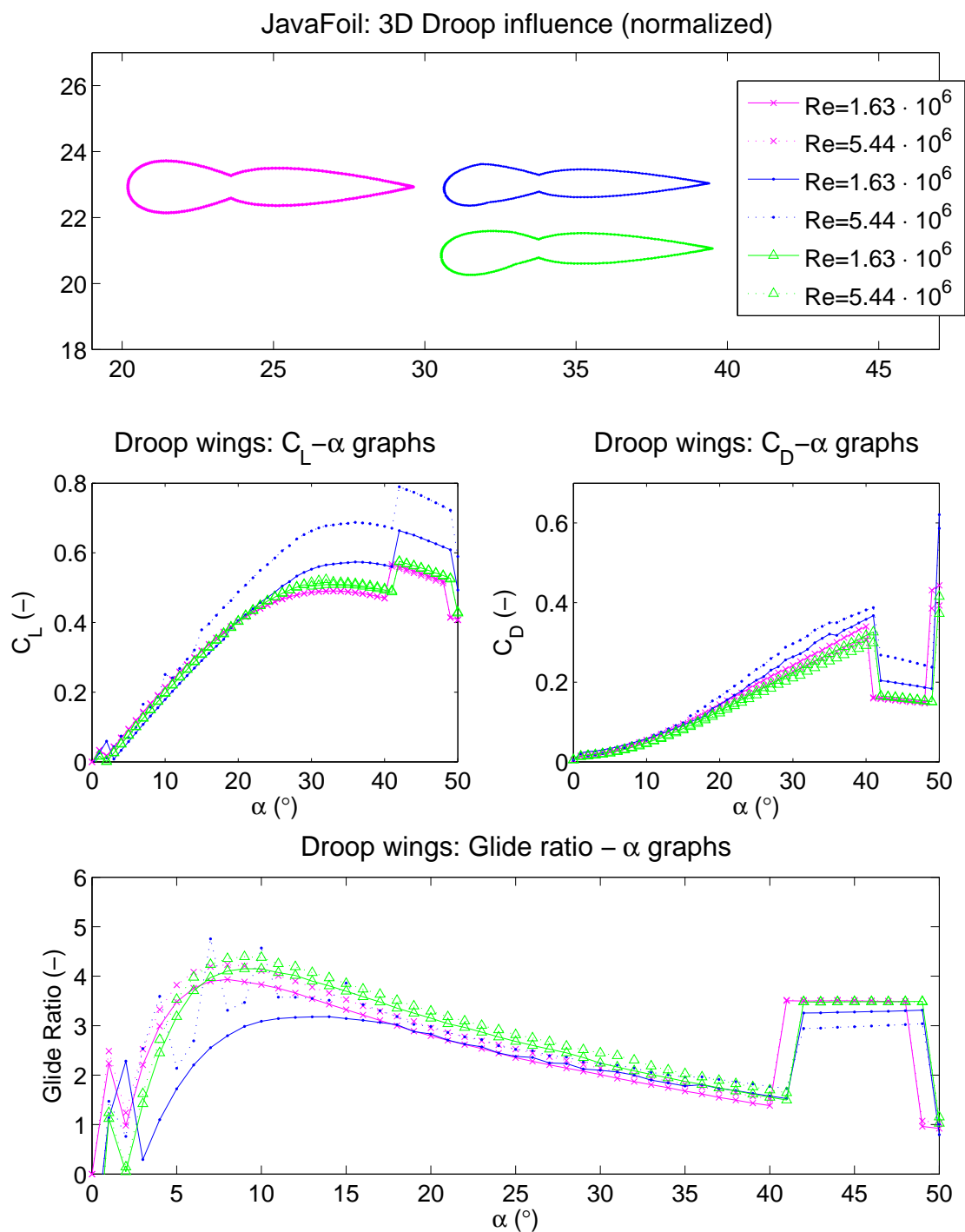


Figure S.3: JavaFoil 3D results for an airfoil with and without droop

The purple airfoil (left in the upper picture) is the basic airfoil shape without droop. The blue airfoil shape has a droop angle of 10° and a hinge point at $0.25c$. The green airfoil shape has a droop angle of 20° and a hinge point at $0.15c$.

T

Validation

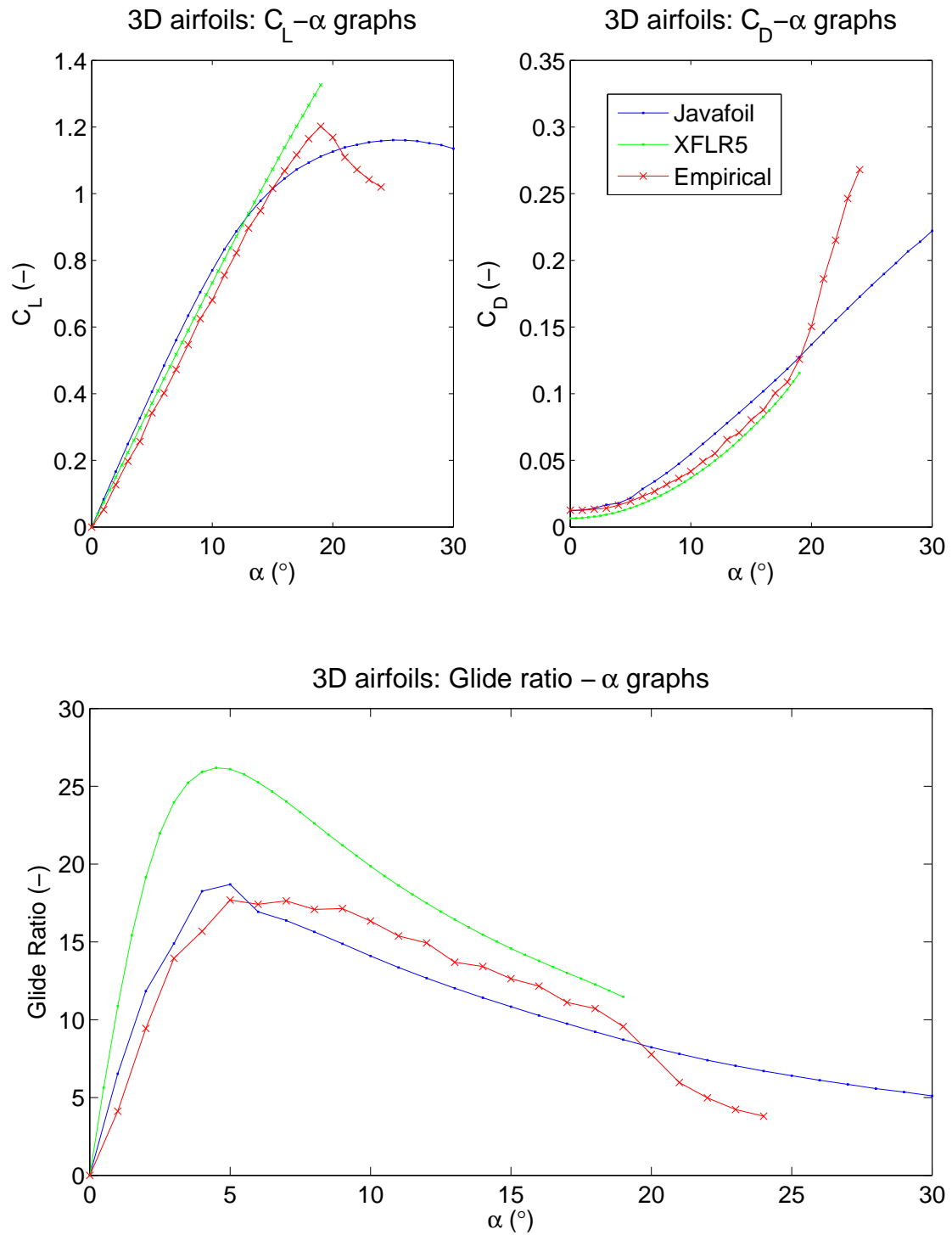


Figure T.1: Validation of JavaFoil and XFLR5 using experimental data on NACA0021 wing

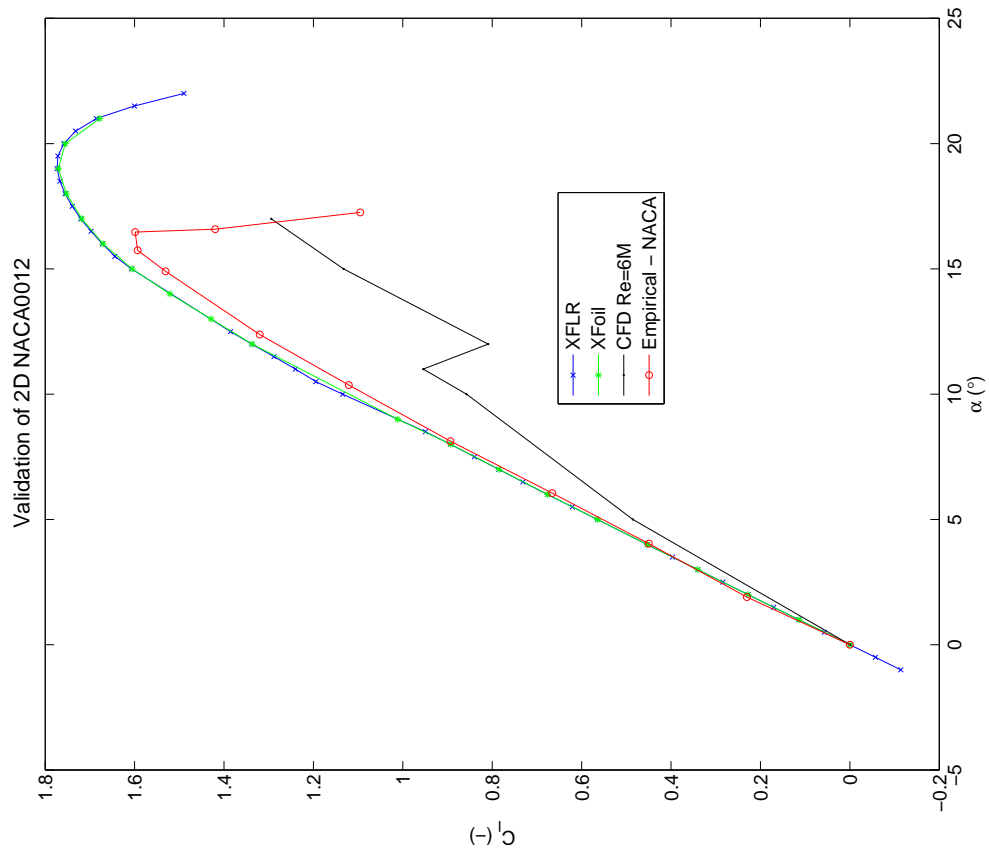


Figure T.2: Validation of the CFD program using experimental data on NACA0012 airfoil

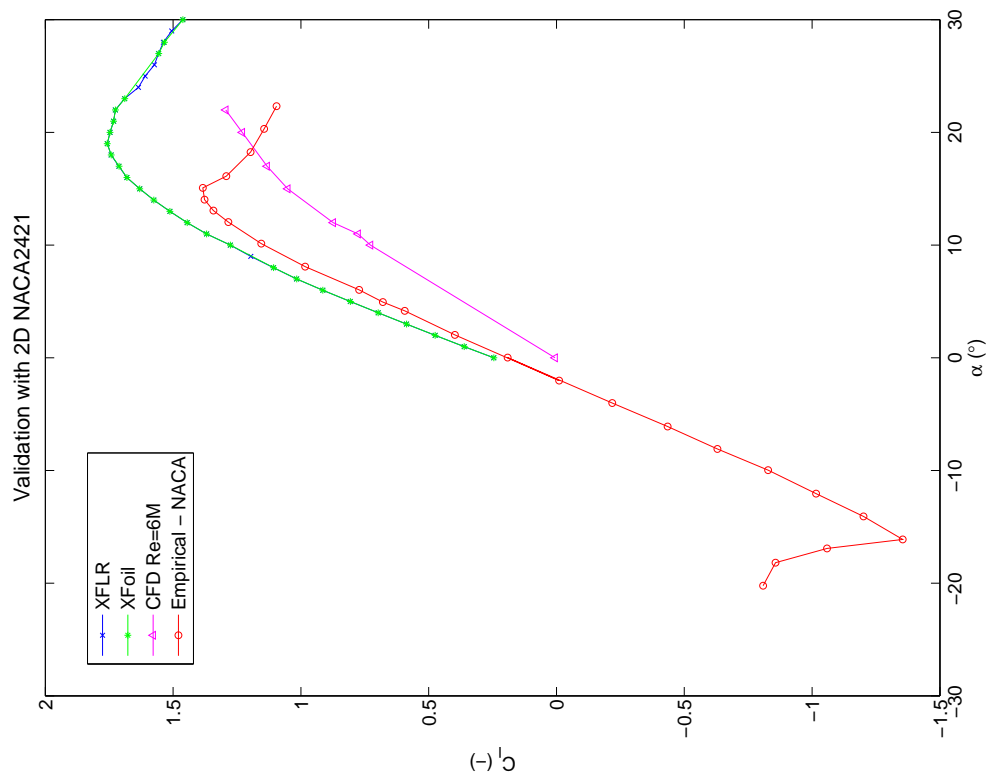


Figure T.3: Validation of the CFD program using experimental data on NACA2421 airfoil

U

Numerical Analysis - Results

In this appendix, the results of the numerical analysis with the CFD program are shown.

U.1 Basic wingsuit - 2D results

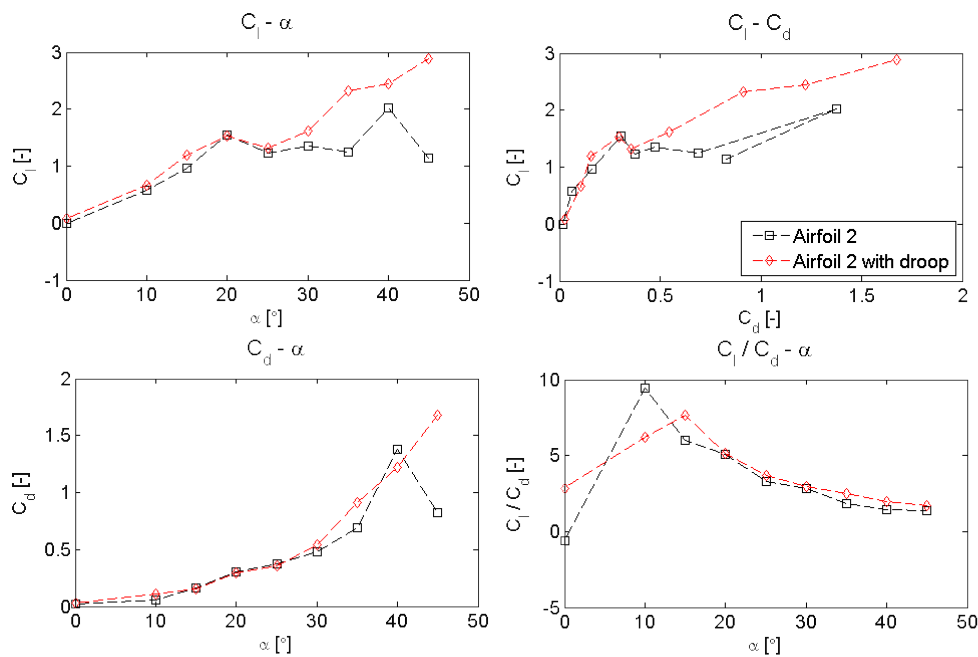


Figure U.1: Results for the different airfoils

For the 2D simulations, only one concept was simulated. The droop leading edge was simulated. The results can be found in Section U.1.1

U.1.1 Droop leading edge

The effect of the droop leading edge is simulated in 2D. Some data points of the 2D simulation and comparison can be found in Table U.1. The configuration is simulated at different angles of attack with a droop angle of $\delta = 20^\circ$.

Table U.1: Some of the data points of the 2D analysis of the leading edge droop for different angles of attack.

Configuration	10°			20°			30°			40°		
	C_l [-]	C_d [-]	$\frac{L}{D}$ [-]	C_l [-]	C_d [-]	$\frac{L}{D}$ [-]	C_l [-]	C_d [-]	$\frac{L}{D}$ [-]	C_l [-]	C_d [-]	$\frac{L}{D}$ [-]
Original	0.57	0.06	9.4	1.55	0.30	5.16	1.35	0.48	2.8	2.02	1.37	1.47
Drooped	0.66	0.11	6.18	1.52	0.29	5.13	1.62	0.55	2.97	2.44	1.22	2

All the results were plotted and can be seen in Figure U.2

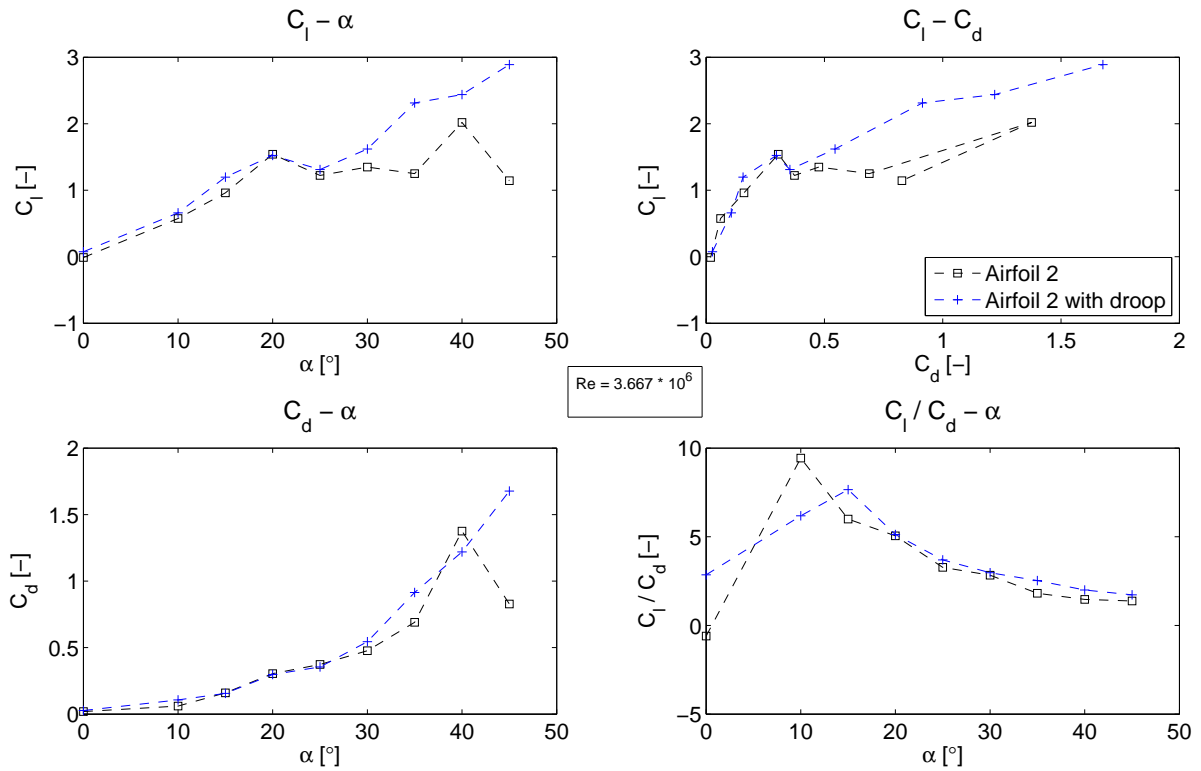


Figure U.2: Comparison of the airfoil shape with and without the droop.

U.2 Basic wingsuit - 3D CFD results

The following graphs, as shown in figure U.3, show respectively $C_L - \alpha$, $C_D - \alpha$ and $\frac{C_L}{C_D} - \alpha$ graphs constructed with the CFD program.

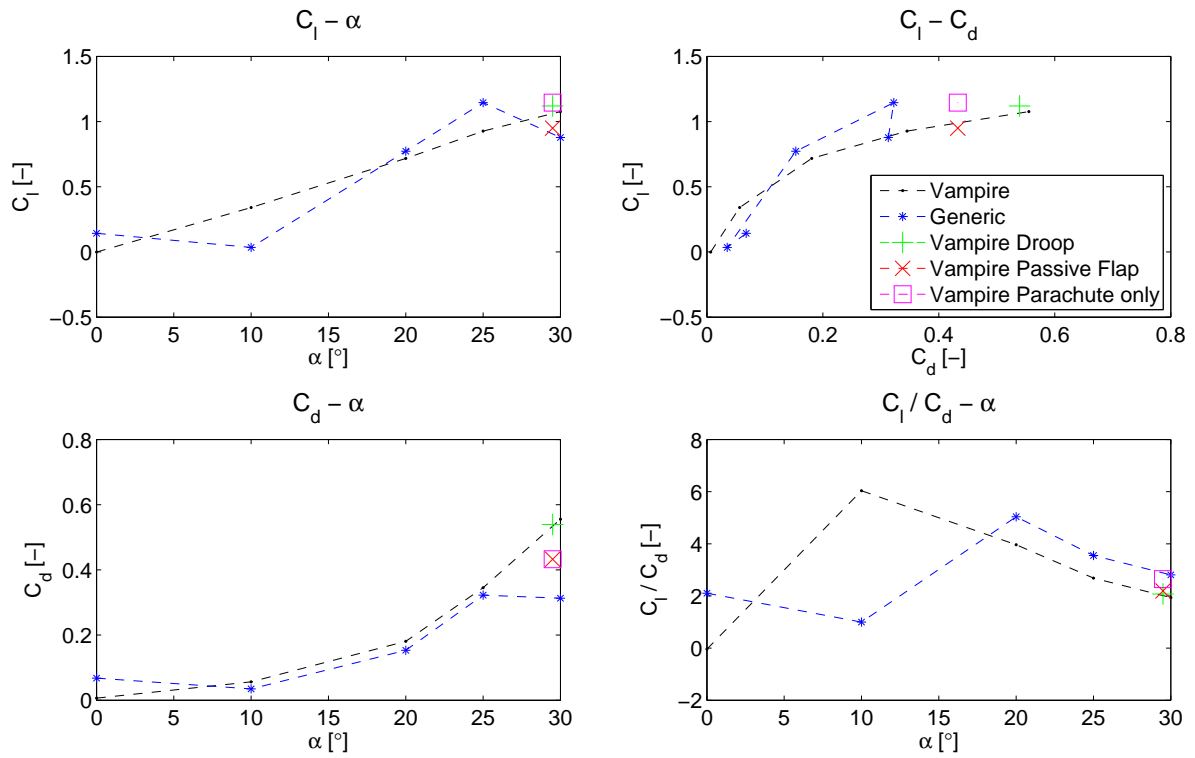


Figure U.3: $C_L - \alpha$, $C_D - \alpha$, $C_L - C_D$ and $C_L/C_D - \alpha$ curves of 3D wingsuit

U.2.1 Effect of concepts

The effects of some of the concepts on the wingsuit were also investigated using numerical simulations. The results of these simulations can be found in Figure U.3 of this section. Unfortunately, only one data point could be simulated for the droop concept and passive flap.

V

Numerical verification

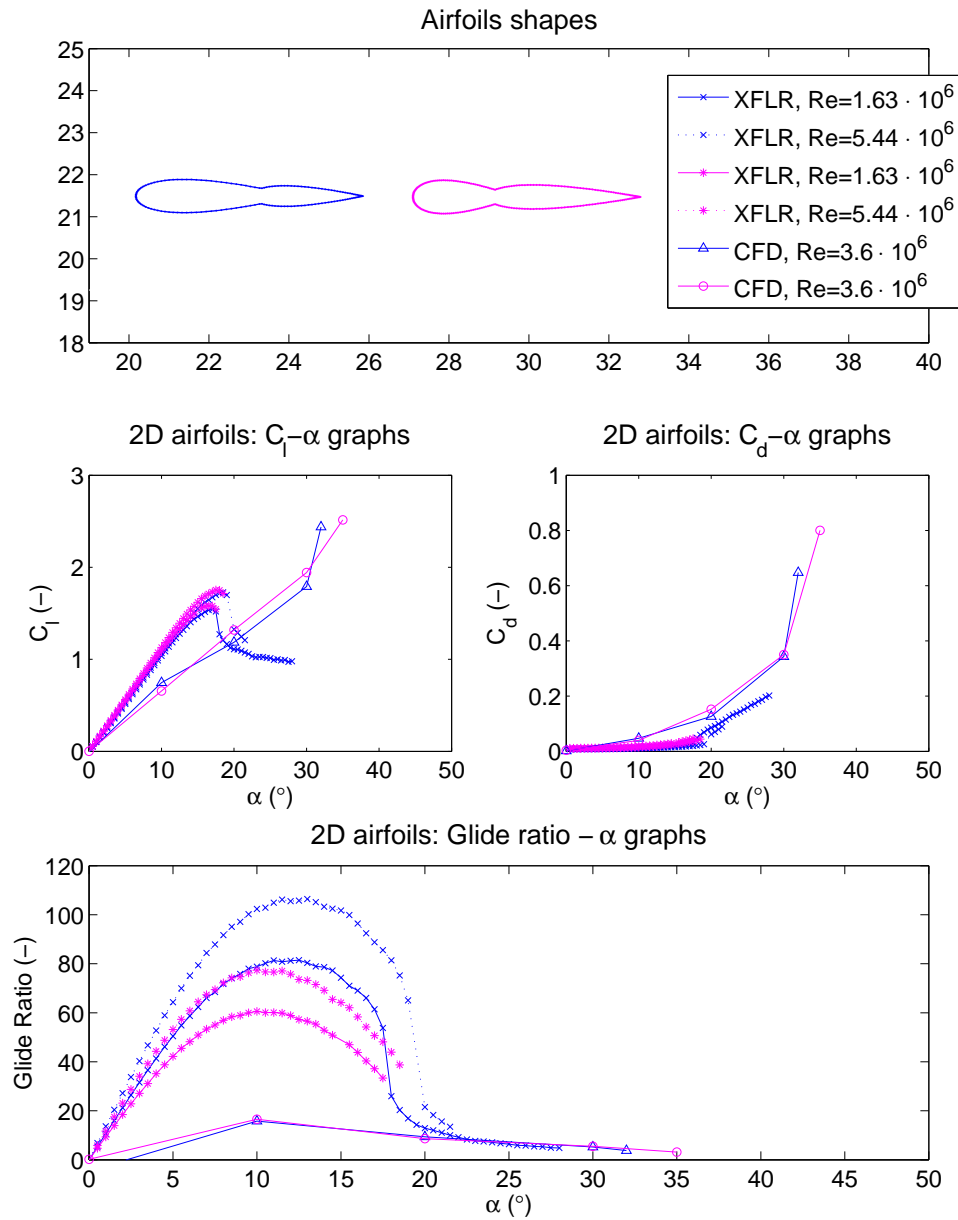


Figure V.1: Verification of the numerical simulation with the calculations from XFLR5 - first run

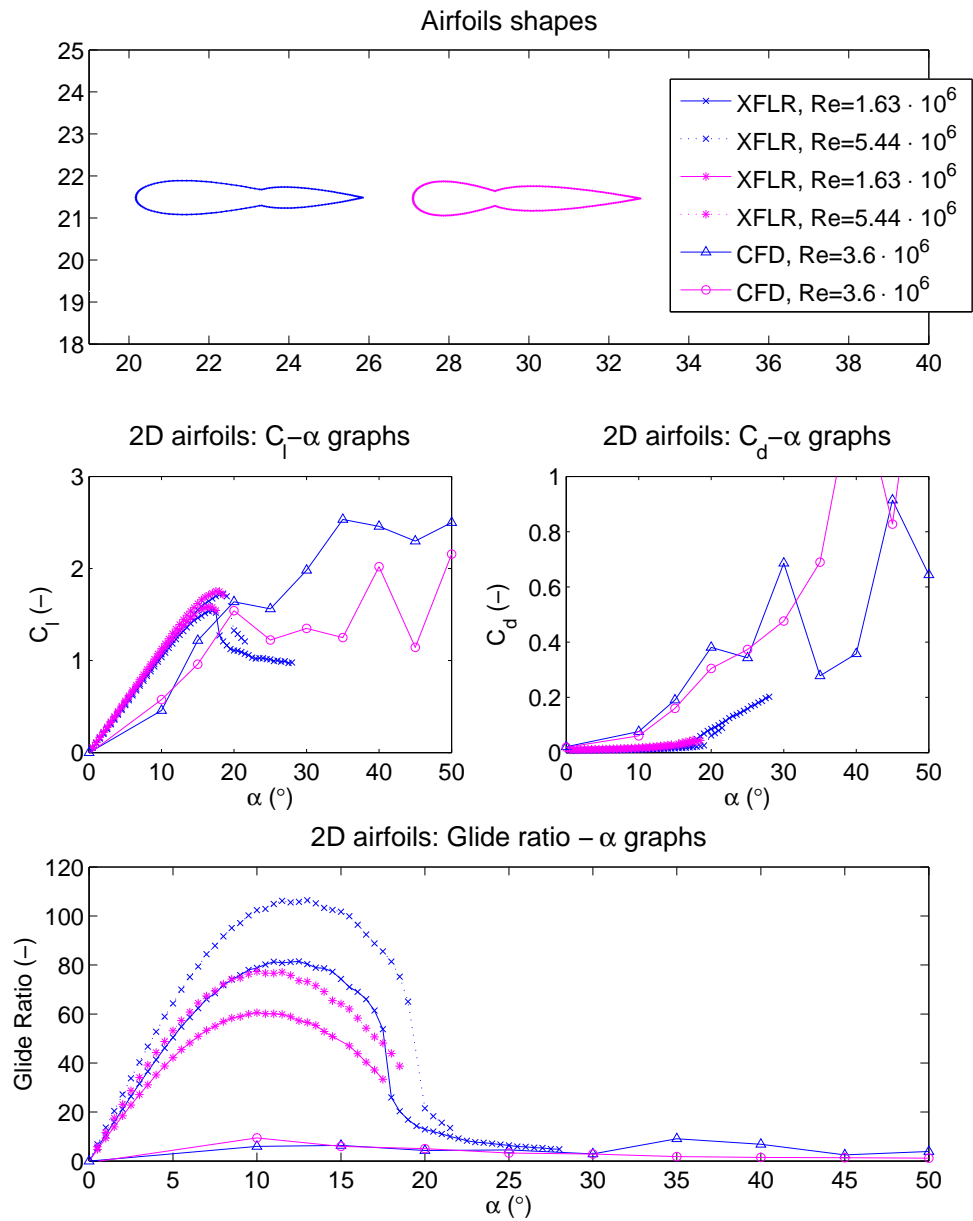


Figure V.2: Verification of the numerical simulation with the calculations from XFLR5

W

MATLAB CODE

W.1 Shoulder reinforcement

```
1 %% stress calculations in critical section shoulder reinforcement
2
3 clc
4 clear all
5
6 %% declare variables critical section 1 (joint connection)
7
8 F=100; % backward force in Newton
9 A=43.34*10^(6); % Area critical section 1 (m^2)
10 x.F = 0.150/2; % x distance to calculate joint (m)
11 y.F = 0.1275; % y distance to calculate joint (m)
12
13 %% calculation critical section 1
14
15 F_joint = (F * x.F)/y.F; % F in joint
16 shear_joint.conection = F/A; % shear stresses in backward direction
17 tensile_joint.conection = F_joint/A; % tensile stresses on critical section 1
18
19 %% declare variables critical section 2 (ball on socket joint)
20
21 R=0.0075; % radius ball(m)
22 depth = 0.003; %depth ball in socket joint
23 c.angle = sin(depth/R); % angle in radians
24 R1 = cos(c.angle)*R; % height start socket on ball
25 stress = F_joint/(R^(2)*pi R1^(2)*pi); % average stress an joint
26
27 %% calculation critical section 2
28
29 heigth = (R1+0.0001):0.0000001:R;
30 heigth2 = 0:0.00001:0.0075;
31
32 test = sqrt(R^(2) (heigth).^ (2))+R (R depth);
33
34
35 f_force.height = stress * (1)*(R1^(2)*pi heigth.^ (2)*pi); % accumulated force as ...
    function of heigth
36 A2 = (2*pi*heigth).*( sqrt(R^(2) (heigth).^ (2))+R (R depth)); % accumulated area for ...
    shear calculation
37
38 f_shear.heigth1= (stress * (1)*(R1^(2)*pi ...
    heigth.^ (2)*pi))./((2*pi*heigth).*( sqrt(R^(2) (heigth).^ (2))+R (R depth))); % ...
    find max shear and its lacion through vector
39 [max_shear2,i] = max(f_shear.heigth1);
40 max_shear3 = f_shear.heigth1(i);
41 location = heigth(i);
42
43 f_shear.heigth = @(h) (stress * (1)*(R1^(2)*pi ...
    h.^ (2)*pi))./((2*pi*h).*( sqrt(R^(2) (h).^ (2))+R (R depth))); % find max shear and ...
    its lacion using equations
44 max_shear = fminbnd(@(h) f_shear.heigth(h),R1,R);
45
46 plot(f_shear.heigth1,heigth); % plot
47 xlabel('Shear stress (Pa)');
48 ylabel('height (m)');
```